Quantum Hall Effects 量子 **Hall** 效应

Mark O. Goerbig
Laboratoire de Physique des Solides, CNRS UMR 8502
Université Paris-Sud, France

Revised & Translated by Laserdog
Chaoli Translation Group

October 27, 2016

目录

Chapter 1

Introduction
简介

量子 Hall 效应——二维 (2D) 电子在强磁场下的研究 [见图. 1.1(a)] 在过去的几十年里成为了一个非常重要的研究课题。对于量子 Hall 问题的兴趣源于其处于低维量子系统和强关联电子系统 (或许是无尽的凝聚态物理中最主要的问题) 的交合处。理论角度上说，学习量子 Hall 系统需要详尽阐述一系列新概念，其中很多是在高能物理的量子场论中而不是凝聚态物理中熟知的，比如电荷分数化，非对易几何，拓扑场论等。

这个讲义是出于提供一个量子 Hall 物理的基本知识的合集，从而使得有兴趣的研究生能够获得他/她自己在这方面学习的能力。我们由此努力的完成了这个讲义，不可避免的舍去了一些我们认为超出这个讲义应有的介绍性的内容——这些在我们给出的参考文献或者详细的教科书中有讲述。

1.1 History of the (Quantum) Hall Effect
(量子)Hall 效应的历史

1.1.1 The physical system
研究的系统

我们的主要的关于量子 Hall 系统——在垂直磁场下的 2D 电子系统——的知识，源自于对电输运的测量。我们驱动电流 I 通过样品，并测量纵向和横向的电阻 (也叫 Hall 电阻)。这两种电阻的不同是至关重要的，而且可以拓扑的来定义：考虑通过样品流经任意两个接触点 [图. 1.1(a) 的 C1 和 C4] 的电流，并在你心中画一条连接着两个接触点的线。纵向电阻就是你测了两个连线不会穿过 C1 和 C4 连线的点之间的电阻。在图. 1.1(a) 中，我们选 C5 和 C6 作为纵向电阻的测量。横向电阻则是通过连接两端的先必然会穿过连接 C1 和 C4 的线 [比如图. 1.1(b) 中的 C3 和 C5]。

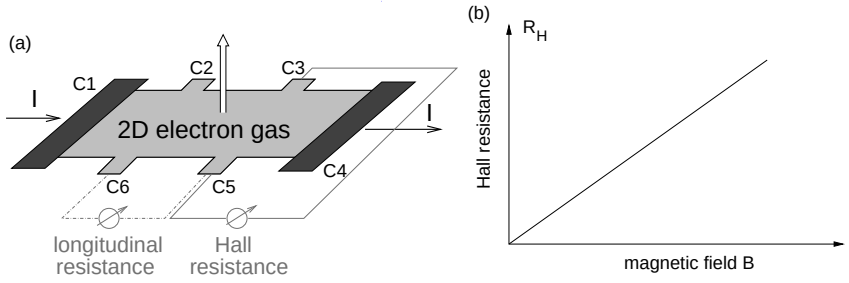

图 1.1: *(a)* 处在垂直磁场中的 2D 电子 (量子 Hall 系统)。在传统的输运测量中，在 C1 和 C4 之间施加电流 I。纵向电阻可以是 C5 和 C6 之间 (或者 C2 和 C3 之间) 的测量。横向 (或 Hall) 电阻是通过比如说 C3 和 C5 中间测量得到的。*(b)* 经典 Hall 电阻关于磁场的函数。

1.1.2 Classical Hall effect
经典 Hall 效应

显然的，如果有量子Hall 效应，我们自然会期望有经典Hall 效应。事实上就是这样，而且历史可以追溯到 1879 年 Hall 展示薄金属片的横向电阻 R_H 随垂直磁场强度 B 线性变化 [图. 1.1(b)] 那时去。

$$R_H = \frac{B}{qn_{el}} \ , \tag{1.1}$$

其中，q 是载流子的电量 (电子导电时 $q=-e$，其中 e 在本讲义此后的地方被规定为正数。)，而 n_{el} 是 2D 的载流子密度。大家可以简单地想成是 Lorentz 力导致带电粒子运动的转向，从而形成样品由 C1 和 C4 分割的两端的密度梯度的堆积。值得注意的是经典 Hall 电阻在现在仍然被广泛的用来判定导电材料的带电粒子的电荷以及密度。 定量的讲，经典 Hall 效应可以用 Drude 模型在金属中的扩散输运来理解。在这个模型中，我们可以考虑一个载流子，携带动量 $\mathbf{p}$，由运动方程

$$\frac{d\mathbf{p}}{dt} = -e\left(\mathbf{E} + \frac{\mathbf{p}}{m_b}\times\mathbf{B}\right) - \frac{\mathbf{p}}{\tau},$$

来描述，其中 $\mathbf{E}$ 和 $\mathbf{B}$ 分别是是电场和磁场。这里我们考虑了带负电荷的粒子 (比如，电子 $q=-e$)，而其有效质量[†]m_b。最后一项解释了由杂质带来的耗散和弛豫。从运动方程的稳态解 $d\mathbf{p}/dt = 0$ 可以得到宏观的输运性质，比如说系统的电阻率或电导率，而对于 2D 电子来说 $\mathbf{p} = (p_x, p_y)$

$$\begin{aligned} eE_x &= -\frac{eB}{m_b}p_y - \frac{p_x}{\tau}, \\ eE_y &= \frac{eB}{m_b}p_x - \frac{p_y}{\tau} \ , \end{aligned}$$

其中我们设磁场在 z-方向。上面的式子中，自然地出现了特征频率

$$\omega_C = \frac{eB}{m_b} \ , \tag{1.2}$$

我们称为回转频率，因为它标志着带电粒子在磁场中的回旋运动。通过 Drude 电导率，

$$\sigma_0 = \frac{n_{el}e^2\tau}{m_b} \ , \tag{1.3}$$

我们可以把方程重写为

$$\begin{aligned} \sigma_0 E_x &= -en_{el}\frac{p_x}{m_b} - en_{el}\frac{p_y}{m_b}(\omega_C\tau), \\ \sigma_0 E_y &= en_{el}\frac{p_x}{m_b}(\omega_C\tau) - en_{el}\frac{p_y}{m_b}, \end{aligned}$$

或者用电流密度来表示，

$$\mathbf{j} = -en_{el}\frac{\mathbf{p}}{m_b} \ , \tag{1.4}$$

如果用矩阵形式来写的话，$\mathbf{E} = \rho\mathbf{j}$，电阻率张量为

$$\rho = \sigma^{-1} = \frac{1}{\sigma_0}\begin{pmatrix} 1 & \omega_C\tau \\ -\omega_C\tau & 1 \end{pmatrix} = \frac{1}{\sigma_0}\begin{pmatrix} 1 & \mu B \\ -\mu B & 1 \end{pmatrix}, \tag{1.5}$$

最后一步中，像前面讲过的，将迁移率定义为

$$\mu = \frac{e\tau}{m_b} \ . \tag{1.6}$$

[†]由能带决定

从前面的式子中，我们可以很快地得到 Hall 电阻 (电阻率矩阵 ρ 的非对角元)

$$\rho_H = \frac{\omega_C \tau}{\sigma_0} = \frac{eB}{m_b}\tau \times \frac{m_b}{n_{el}e^2\tau} = \frac{B}{en_{el}} \,. \tag{1.7}$$

而类似的，从(1.5)中，通过矩阵求逆，电导率矩阵为

$$\sigma = \rho^{-1} = \begin{pmatrix} \sigma_L & -\sigma_H \\ \sigma_H & \sigma_L \end{pmatrix}, \tag{1.8}$$

其中 $\sigma_L = \sigma_0/(1+\omega_C^2\tau^2)$，而 $\sigma_H = \sigma_0\omega_C\tau/(1+\omega_C^2\tau^2)$。值得讨论的是，在理论上没有杂质的极限下，即 $\omega_C\tau \to \infty$ 这种非常长的散射时间下电阻率和电导率的矩阵分别为

$$\rho = \begin{pmatrix} 0 & \frac{B}{en_{el}} \\ -\frac{B}{en_{el}} & 0 \end{pmatrix} \qquad \text{以及} \qquad \sigma = \begin{pmatrix} 0 & -\frac{en_{el}}{B} \\ \frac{en_{el}}{B} & 0 \end{pmatrix}, \tag{1.9}$$

注意到，如果我们只关注纵向电阻率的话，我们会得到非常反直觉的结论，即 (纵向) 电阻率会和 (纵向) 电导率同时趋于零。在干净的样品的极限 $\omega_C\tau \to \infty$ 下，存在磁场的系统的输运性质完全由非对角元，即横向电阻率/电导率成分来描述。我们会在量子 Hall 系统中讨论整数量子 Hall 效应时再来看这一点。

Resistivity and resistance
电阻率与电阻

上面对于电子输运的处理都是用 Drude 模型来计算有磁场下的经典耗散 2D 电子系统的电导率或电阻率的。然而，实验上并不能测量理论上很好计算的电导率或者电阻率，而是测量电导或者电阻。通常来说，这些量彼此之间是相关的，但是这取决于导体的几何形状——电阻 R 与电阻率 ρ 的关系为 $R = (L/A)\rho$，其中 L 是导体的长度，而 A 是截面大小。从尺度变换的角度来说，一个 d-维的导体，截面大小按照 L^{d-1} 变换，所以电阻和电阻率的尺度变换行为是

$$R \sim \rho L^{2-d}, \tag{1.10}$$

从中可以立刻发现 2D 导体是很特殊的。从量纲的角度来说，2D 的电阻和电阻率是一样的，而且电阻是尺度不变的。这种尺度缩放的观点忽略了长度 L 和宽度 W(2D 的散射截面大小) 并不非要一样：事实上，2D 导体的电阻取决于所谓的长宽比L/W，前面有一个系数 $f(L/W)$ [8]。然而，对于横向 Hall 电阻来说，长度反而是一个散射截面大小的作用，因此 Hall 电阻率和 Hall 电阻确实是一样的，即 $f = 1$。我们在第3章中会看到，这样的结论不仅仅在经典层面，对量子 Hall 效应也成立。不仅如此，量子 Hall 效应更不要求输运的样品有特定的几何性质，所以 Hall 电阻的测量十分精准 (准确到 10^{-9})。量子 Hall 效应如今被用来给电阻定标。

1.1.3 Shubnikov-de Haas effect
Shubnikov-de Haas 效应

首先在强磁场下的 2D 电子输运实验中与量子现象相关的是 1930 年发现的 Shubnikov-de Haas 效应 [9]。经典的电阻率张量的结果(1.5)规定纵向电阻率 $\rho_L = 1/\sigma_0$(纵向电阻类似)，与磁场无关，然而 Shubnikov 和 de Haas 发现超过某些特定的磁场强度之后纵向电阻关于磁场发生振荡，如图. 1.2(a)；而 Hall 电阻不像纵向电阻那样振荡，仍然是 B 的线性关系，与经典 Drude 模型一致(1.7)。Landau 很快的解释了 Shubnikov-de Haas 效应是有 2D 电子在强磁场下能量量子化导致的。这即为*Landau* 量子化，我们在第2节会讲解。通俗的说，Landau 量子化相当于对回转半径的量子化，即电子在磁场中做圆周运动的量子化。这就导致了其动能量子化为所谓的 Landau 能级 (LLs)，$\epsilon_n = \hbar\omega_C(n+1/2)$，其中 n 是整数。为了使这个量子化有效，磁场必须强到使得电子的一个完整的圆周运动周期中不会发生碰撞，即 $\omega_C\tau > 1$。这个条件定义了临界磁场 $B_c \simeq m_b/e\tau = \mu^{-1}$(其取决于迁移率)，超过它纵向电阻就开始振荡。注意当今的样品最高的迁移率可以达到 $\mu \sim 10^7$ cm^2/Vs $= 10^3$ m^2/Vs，从而只需要 $B_c \sim 1$ mT 就可以观察到 Shubnikov-de Haas 振荡。

这种效应可以用比 Drude 模型更精确一些的描述电子输运的理论模型 (比如说，Boltzman 输运方程) 来理解。其得到电导率和扩散方程的 Einstein 关系，以及纵向电阻率

$$\sigma_L = e^2 D\rho(E_F) \tag{1.11}$$

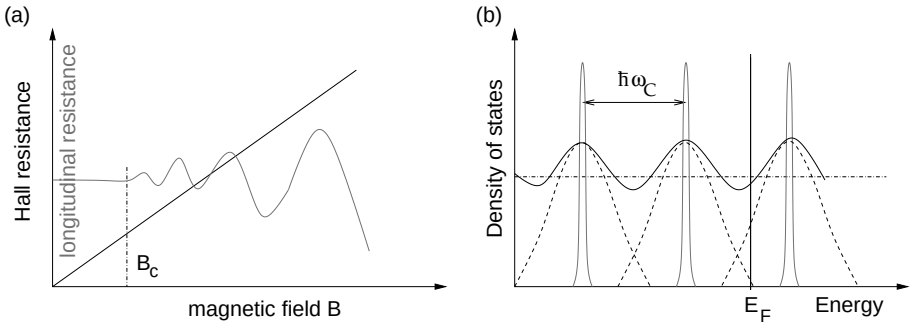

图 1.2: *(a)* the Shubnikov-de Haas 效应草图。超过临界磁场 B_c 之后，纵向电阻 (灰色) 关于磁场强度开始震荡。Hall 电阻仍然是 B 的线性关系。*(b)* 态密度 (Density of states, DOS)。在干净的系统中，DOS 包含等距分布的处于能量为 $\epsilon_n = \hbar\omega_C(n+1/2)$ 的峰 (灰色)，而在有高浓度的杂质的样品中，峰会被展宽 (dashed 线)。连续的黑线表示对峰包括交叠部分的和，E_F 表示费米能。

表明会正比于在费米能 E_F 的态密度 (DOS) $\rho(E_F)$，而不是电子密度[1] 。根据 Landau 量子化，洁净系统的 DOS 在能量处于 $\epsilon_n = \hbar\omega_C(n+1/2)$ 时包含一系列 delta 峰

$$\rho(\epsilon) = \sum_n g_n \delta(\epsilon - \epsilon_n),$$

其中 g_n 则是考虑了能级简并的结果。这些峰由于真实样品的杂质而被展宽 [见图. 1.2(b)]，从而 DOS 在能级 ϵ_n 处达到能量最大值。考虑样品内电子数恒定，由零场的费米能位置决定而不与 B 相关[2]。 当扫动磁场强度[†]时，LLs 的能级间距发生变化，DOS 在 E_F 恰好扫过一个 LL 的能量的时候最大，而在 E_F 处于两个紧邻的 LLs 之间的时候最小。这种 DOS 关于磁场的振荡从(1.11)中可以得到纵向电导率 (或电阻率)，这是 Shubnikov-de Haas 效应的核心。

1.1.4 Integer quantum Hall effect 整数量子 Hall 效应

50 年后，v. Klitzing，Dorda，和 Pepper 在 1980 年发现了量子力学在磁场下的 2D 电子输运性质中有一个更有力的证据：整数量子 Hall 效应 (IQHE)[10]。1985 年的诺贝尔奖就因为 v. Klitzing 的这项极为重要的发现而授予了他。

IQHE 的发现与材料科学的突破密切相关，直接导致了制备高品质的场效应管，从而实现了 2D 电子气。这些技术会在后面的一节中做简单的综述 (第1.2节)。

IQHE 在极低的温度下实现，其能量尺度 k_BT 比 LL 的间距 $\hbar\omega_C$ 要小得多。这个图中 Hall 电阻量子化了，从而不再是经典中的那种与 B 的线性关系，反而展现出了在某些特定磁场下的平台 (见图. 1.3)。在平台处，Hall 电阻是一个常数——实际上是 e^2/h 的整数分之一

$$R_H = \left(\frac{h}{e^2}\right)\frac{1}{n}\,, \tag{1.12}$$

其中 n 是整数。 Hall 电阻的平台伴随着纵向电阻为零。这使得我们回想起 Shubnikov-de Haas 效应，纵向电阻同样会趋于极小值，尽管不是零。Shubnikov-de Haas 最小值点的纵向电阻的趋零确实可以用来决定从 Shubnikov-de Haas 到 IQHE 的 crossover[‡]。

[1]然而，需要注意费米能和 DOS 都是电子密度的函数。不仅如此，考虑到更多的细节之后，扩散系数 D 同样取决于态密度，从而取决于外磁场。这影响到了振荡的具体形式，但是并不会影响振荡的周期。

[2]实际上这是一个很粗糙的假定，因为如果态密度是磁场的函数 $\rho(\epsilon, B)$，费米能则有关系式

$$\int_0^{E_F} d\epsilon\, \rho(\epsilon, B) = n_{el}.$$

然而，Shubnikov-de Haas 振荡的基本形式可以在假定费米能恒定的前提下理解

[†]译者注：扫动——和扫频一个用法的 “扫”

[‡]译者注：有的时候会被翻译为渡越

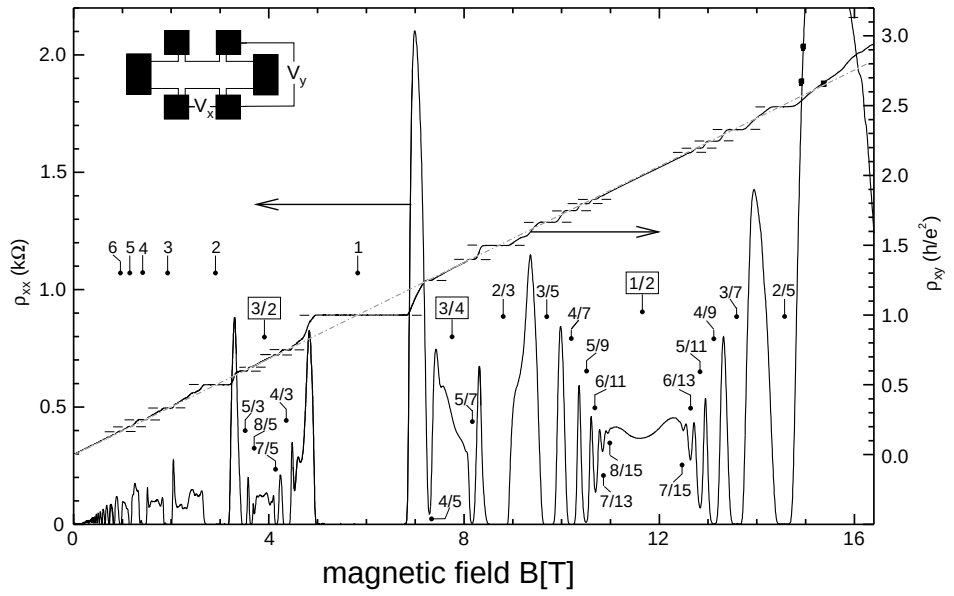

图 1.3: 量子 Hall 效应的通常样子 (由 J. Smet, MPI-Stuttgart 测量)。每一个 Hall 电阻的平台伴随着零纵向电阻。经典 Hall 电阻由 dashed-dotted 线表示。数字标识了平台：整数 n 表示 IQHE；而 $n = p/q$，其中 p 和 q 是整数，则标志了 FQHE。

值得说明的是，Hall 电阻的量子化(1.12)是普遍现象，即与样品的特性，比如几何尺寸啊，制备 2D 电子气的衬底啊，甚至杂质的浓度和分布啊都无关。这种普遍性是导致 Hall 电阻量子化的高精确性 (通常 $\sim 10^{-9}$) 的原因，而且如今——自从 1990 年——被用来做电阻标准[3]

$$R_{K-90} = h/e^2 = 25\,812.807\,\Omega, \tag{1.13}$$

也被称为 Klitzing 常数 [11, 12]。而且，在第1.1.2节中已经提到的，纵向电阻趋零标志的散射时间趋于无穷 [见 (1.9) 式]。这是另一个标志着这个效应的普适性的现象，即 IQHE 并不取决于特定的杂质（或者散射体）的排列特性。

对于 IQHE 的详细讨论，以及杂质的贡献，请见第3章。

1.1.5 Fractional quantum Hall effect
分数量子 Hall 效应

在发现了 IQHE 的三年之后，在更高品质，即更高迁移率的 2D 电子系统中发现了更意想不到的现象：分数量子 Hall 效应 (FQHE)。这个现象的名字就是被设立来与 IQHE，即 (1.12) 式中的 n 是整数，相对的。Tsui, Störmer 和 Gossard 发现了 $n = 1/3$[13] 的 Hall 量子化电阻。从唯象的角度来说，这种现象十分容易令人联想到 IQHE：量子化的电阻平台，以及趋零的纵向电阻 (见图. 1.3，其中可以同事看到 IQHE 和 FQHE)。1998 年的诺贝尔奖授予了 Tsui, Störmer 和 Laughlin，由于他们对于 FQHE 的实验发现和理论。

在发现了 $n = 1/3$ 的 FQHE 之后[4]，物理学家们发现了大量的不同形式的 FQHE，和各种理论描述。首先是 2/5 和 3/7 态 (即 $n = 2/5$ 和 $n = 3/7$) 这种 $p/(2sp \pm 1)$ 系列，其中 s 和 p 是整数。这个系列建立了一个很有趣的解释，把 *F*QHE 看成有电子 "捕获" 了偶数个磁通量子的特殊的准粒子的 *I*QHE，被称为复合费米子(CF) 理论 [15, 16]。这种理论的基础我们在第4.4节讲述。1987 年，Willet *et al.* 发现了另一种有趣的 FQHE：$n = 5/2$ 和 $7/2$[17]——它之所以有趣是因为那时之前只有 $n = p/q$ 中奇数分母的态才在单层系统中观测到了。从理论的角度，1991 年 Moore 和 Read[18]，以及 Greiter, Wilczek 和 Wen [19] 表明 FQHE 可

[3]角标 K 致敬 v. Klitzing，而 90 表示开始使用 IQHE 作为电阻的单位的时间。

[4]n 代表着 LLs 的占据数，通常有希腊字母 ν 表示，在第2节将会讨论到

能由一类非常特殊的，称为 *Pfaffian* 的波函数来描述，其包含粒子配对和非 Abel 统计的任意子型激发。这些粒子由于其潜在的量子计算价值，在当今被充分的研究。任意子有关的物理性质我们在第4.3节简要介绍。最后，我们会对 2003 年 Pan *et al.*[20] 的 $n = 4/11$FQHE 做简要 (而且不完全的) 回顾：它不符合上述 CF 序列，但是却属于 FQHE 的一种生成 CF 序列而不是 IQHE 的 CF 序列。

1.1.6 Relativistic quantum Hall effect in graphene
石墨烯中的相对论性量子 Hall 效应

最近，量子 Hall 物理经历了另一件意料之外的事情的推导：在石墨烯——一种单原子厚的石墨层——中发现了“相对论性”量子 Hall 效应 [6, 7]。石墨烯中的电子表现的好像相对论性无质量粒子一样。形式上，它们的量子力学性质不再由 (非相对论性的)Schrödinger 方程描述，而是由 2D 相对论性 Dirac 方程 [21] 描述。而其导致的就是，对石墨烯的电子动能的 Landau 量子化和常规的 (非相对论性的)2D 电子系统不一样，我们会在第2节讨论。这种“相对论性”量子 Hall 效应有不一样的 Hall 平台，其 Hall 电阻 $R_H = h/e^2n$ 中，不再是 n 为整数，而是 $n = \pm 2(2n' + 1)$ 其中 n' 为整数，即 $n = \pm 2, \pm 6, \pm 10, \ldots$。序列中的正负号 (±) 代表石墨烯中有两种对量子 Hall 效应载流子，电子在导带而空穴在价带。我们会在第1.2节简要讨论，通过场效应，我们可以很容易的改变石墨烯中的载流子特性。

相互作用有的时候会影响到其他整数 Hall 平台的形成，比如 $n = 0$ 和 $n = \pm 1$ [22]，就不会自然地出现在 $n = \pm 2(2n' + 1)$ 的相对论性量子 Hall 效应序列里面。此外，最近还观察到了 $n = 1/3$ 的 FQHE，尽管是在比图. 1.1(a) 更为简单的几何 (二端) 构型中 [23, 24]。

1.2 Two-Dimensional Electron Systems
二维电子系统

上面已经提到过，量子 Hall 效应的历史与制备高迁移率的 2D 电子系统的技术进步是密切相关的。更高的迁移率使得人们可以去探测 Hall 曲线的精细结构，从而看到那些不容易观察到的量子 Hall 态，比如奇异 FQHE 态 (比如 $5/2, 7/2$ 或 $4/11$ 态)。这与光学里面追求更高的分辨率是一个意思：更高的光学分辨率就可以去观察更微小的物体。类似的，电子迁移率就相当于分辨率，微小的物体就是量子 Hall 态。数量级上，现今最好的 2D 电子气 (在 GaAs/AlGaAs 异质结中) 的特征迁移率为 $\mu \sim 10^7$ cm^2/Vs。

1.2.1 Field-effect transistors
场效应管

首个发现 IQHE 的样品被称为金属-氧化物-半导体场效应管(MOSFET)。金属层和半导体层 (通常为掺杂的硅) 中间放了绝缘的氧化物 (比如 SiO_2) 层 (见图. 1.4的内插图 *I*)。金属层的化学势可以通过栅极电压[†]V_G 来调节。当 $V_G = 0$ 时，费米能在半导体中的位置处于能隙中，且在掺杂的受主能级之下 [图. 1.4(a)]。利用正栅极电压 $V_G > 0$ 调低金属中的化学势，金属中就会流入空穴，从而通过场效应将电子从半导体中吸到半导体-绝缘体界面。这些电子占据受主能级，从而半导体靠近界面的部分的能带向下弯曲，填充的受主能级就会低于费米能 [图. 1.4(b)]。

栅极电压超过某一阈值之后，半导体能带的弯曲强烈到不仅是受主能级，就连靠近界面的导带都低于费米能了，从而有一些电子填充到了上面 [图. 1.4(c)]。因此我们就有了通过这种三角形的结构来获得导带中的电子的束缚势的办法，而且其动力学行为被量子化为 z-方向的离散能级子带 (见图. 1.4的内插图 *II*)。电子波函数在 z-方向延展，但是通常来说 MOSFETs 只在最低的子带 E_0 上填充[‡]，从而电子就是纯粹的 2D 行为，没有在 z-方向上的运动。

通常这些系统中的 2D 电子密度都在 $n_{el} \sim 10^{11}$ cm^{-2} 量级，即远低于正常的金属。这实际上对于学习 IQHE 和 FQHE 很重要，因为当 2D 电子密度在穿过系统的磁通密度 (以磁通量子 h/e 作单位) 的量级 $n_B = B/(h/e)$ 的时候，这些现象才会显著。而金属表面电子密度在 10^{14} cm^{-2} 量级，这需要非常高的磁场 (1000T 的量级) 来实现 $n_{el} \sim n_B$。

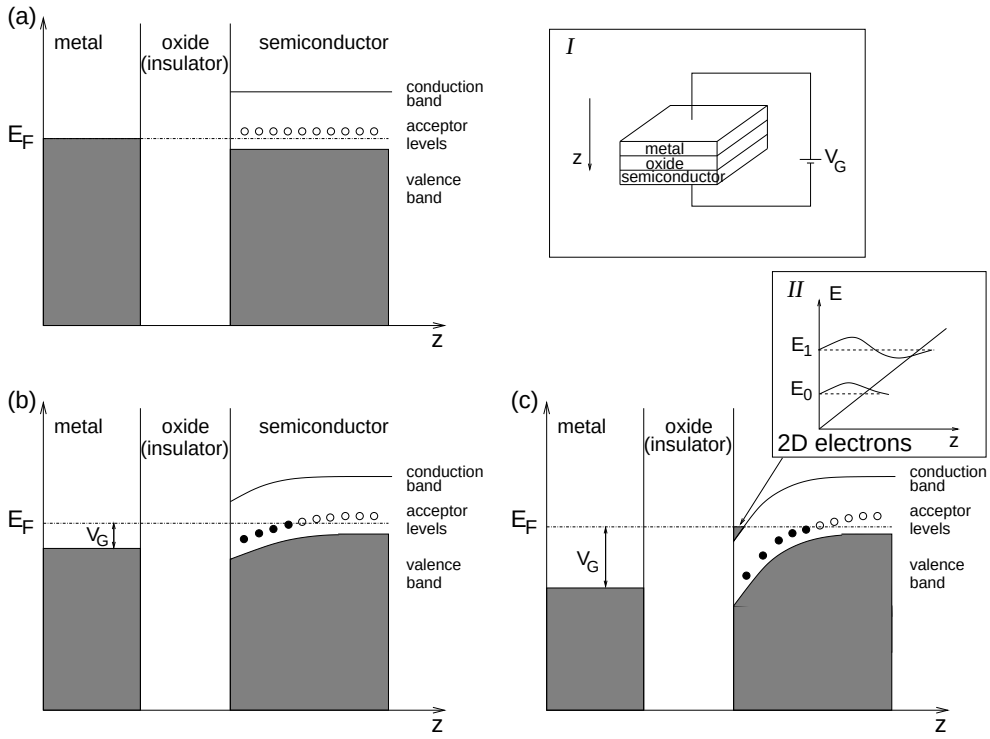

图 1.4: MOSFET(金属-氧化物-半导体场效应管)。内插图 I 为 MOSFET 的图示。*(a)* $V_G = 0$ 时的能级结构。金属部分，能带填充到费米能级 E_F，氧化物部分绝缘。半导体部分，费米能处在能带的带隙上 (价带和导带中间)。接近价带的地方，尽管比 E_F 高，仍然是受主能级 (acceptor levels)。*(b)* 金属部分的化学势仍然由栅极电压 V_G 通过场效应来控制。其结果是半导体中被引入空穴，且能带向下弯曲但仍高于阈值电压。*(c)*，在绝缘体界面附近的导带也被占据，从而得到了 2D 电子气。这种束缚势得到的是三角形结构；能级 (电子的子能带) 见内插图 II。

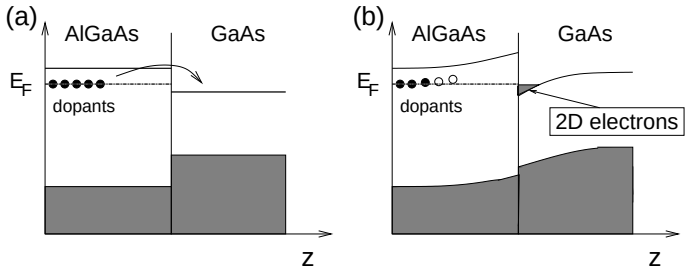

图 1.5: 半导体异质结 (GaAs/AlGaAs). *(a)* 距离表面一定距离处引入 AlGaAs 层的掺杂。费米能在能隙处，位于掺杂能级处。GaAs 导带比掺杂能级要低，因此掺杂层靠近界面的电子倾向于进入 GaAs 的导带。*(b)* 这种极化会弯曲两个半导体边界附近的能带，从而在 GaAs 一边形成 2D 电子气。

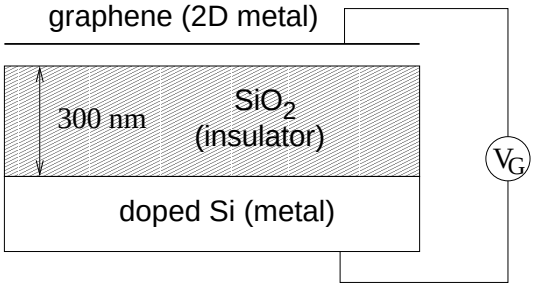

图 1.6: SiO_2 衬底上的石墨烯示意图，背栅极用金属性掺杂的硅。石墨烯-SiO_2-背栅极系统可以看成由栅极电压 V_G 控制电荷密度的电容器。

1.2.2 Semiconductor heterostructures 半导体异质结

MOSFETs 的迁移率通常在 $\mu \sim 10^6$ cm^2/Vs 的量级，其主要受限于氧化物-半导体界面的品质，而利用分子束外延生长 (MBE) 的半导体异质结——最主流的是 GaAs/AlGaAs 异质结——则克服了这项技术的困难，实现了原子精度的界面，而迁移率也达到了 $\mu \sim 10^7$ cm^2/Vs 的量级。这是实现 FQHE 所必要的迁移率，也确实在 GaAs/AlGaAs 样品中第一次观察到 [13]。

在 (一般的)GaAs/AlGaAs 中，两种半导体并没有相同的能隙：GaAs 的能隙比被施主离子在距离界面一定距离处掺杂的 AlGaAs 小 [图. 1.5(a)]。费米能因此被钉在那些 AlGaAs 的施主能级上，从而可能会比那些没被占据的 GaAs 中的导带能级更高，从而能量的角度上来讲，施主能级上的电子会倾向于去占据靠近界面处的 GaAs 的导带能级。从而，AlGaAs 的能带就会向上弯曲，GaAs 的则向下弯曲。类似于之前说过的 MOSFET，这样就可以用三角约束势在 GaAs 侧获得 2D 电子气了。

1.2.3 Graphene 石墨烯

石墨烯——一种单原子厚的石墨层——是一种非常新奇的 2D 电子系统，它可以看成是零交叠的半金属，或者零能隙的半导体，其导带和价带之间没有能隙。而如果没有掺杂的情况下，费米能就恰好处在价带导带接触的位置，其态密度线性的趋于零。

为了调制石墨烯中的费米能，通常来说会把石墨烯薄片放在 300nm 厚的 SiO_2 层上，而这 SiO_2 层又放在正掺杂的硅衬底上 (见图. 1.6)。这种三明治结构可以看成一个电容，其中硅层用来做背栅极 (图. 1.6)，电容量为

$$C = \frac{Q}{V_G} = \frac{\epsilon_0 \epsilon A}{d}, \tag{1.14}$$

其中 $Q = en_{2D}A$ 是电容的电荷量，总电压 A，栅极电压 V_G，SiO_2 厚度 $d = 300$，相对介电常数 $\epsilon = 3.7$。从而，场效应导致的 2D 载流子密度为

$$n_{2D} = \alpha V_G \qquad \text{with} \qquad \alpha \equiv \frac{\epsilon_0 \epsilon}{ed} \simeq 7.2 \times 10^{10} \frac{\text{cm}^{-2}}{\text{V}}. \tag{1.15}$$

栅极电压大概在 -100 到 100 V 之间，因此最大的载流子密度大概在 10^{12} cm^{-2} 量级，而石墨烯自己的载流子密度是零，下一章会讲到这点。栅极电压超过 ± 100 V 之后，电容会被击穿。

不同于半导体异质结中的 2D 电子气，石墨烯中的迁移率很低：通常在 $\mu \sim 10^4 - 10^5$ cm^2/Vs 这个数量级。然而，石墨烯样品是通过表皮剥离技术来实现的，即将石墨晶体从周围的环境下剥离下来，而最高迁移率的 GaAs/AlGaAs 的样品则是由非常高级的技术才能制备的。石墨烯样品的迁移率与商用的硅基元件相当。

---

†译者注：也叫门极电压，或门电压

‡译者注：因为 z-方向长度很短，其对应的能级间隔就很高，从而任一激发能级都在费米能之上

Chapter 2

Landau Quantisation
Landau 量子化

最基本的了解 IQHE 和 FQHE 的出发点是 Landau 量子化，即自由带电 2D 粒子在垂直磁场中动能的量子化。本章中，我们将会对不同形式的 Landau 量子化做详细介绍。我们选择了这种量子化的最一般的形式，从而能够解释非相对论性和相对论性 2D 粒子的诸多性质，比如能级简并和全同性。在第2.1节中，我们介绍没有磁场情况下的 2D 粒子的 Hamiltonians，并讨论 Schrödinger 型和 Dirac 型粒子，进而在第2.2节讨论非零磁场。第2.3节则讨论非相对论性和相对论性粒子的 LL 结构。

2.1 Basic One-Particle Hamiltonians for $B = 0$
$B = 0$ 下的单粒子 Hamiltonian 原型

在本节中，我们介绍接下来要使用的最基本的量子力学中处理方法。一般的，我们考虑平移不变的 2D 粒子的 Hamiltonian[1]，即动量 $\mathbf{p} = (p_x, p_y)$ 在没有磁场下是一个运动常数。在量子力学中，这代表动量算符与 Hamiltonian 对易，$[\mathbf{p}, H] = 0$，并且动量算符提供一个好量子数。

2.1.1 Hamiltonian of a free particle
自由粒子的 Hamiltonian

自由粒子的情况下，我们有非相对论形式

$$H = \frac{\mathbf{p}^2}{2m}, \tag{2.1}$$

其中粒子质量 m。[2]然而我们感兴趣的是电子在某些材料 (金属中，或者在半导体界面上) 中的运动。粗看起来，用自由空间来描述晶体环境中的电子的运动是非常粗糙的假设。实际上，粒子在晶格中的行为并非由 (2.1) 中的 Hamiltonian 来描述，而是由

$$H = \frac{\mathbf{p}^2}{2m} + \sum_i^N V(\mathbf{r} - \mathbf{r}_i), \tag{2.2}$$

描述，其中最后一项表示格点 $\mathbf{r}_i$ 上的离子实带来的静电能。显然，Hamiltonian 现在是关于粒子距离粒子实位置 $\mathbf{r}$ 的函数，而动量 $\mathbf{p}$ 也不再是运动常数或好量子数了。

通过 Bloch 定理可以解决这个问题：尽管一般的空间平移并不像自由粒子 (2.1) 的情况一样是对称性算符了，在晶格无限延展的情况下 (我们这里做这种假定[3])，任意格矢的平移仍然使得系统不变。类似于自由粒子的时候我们定义了动量为空间平移的生成元，现在可以定义晶格平移的生成元。这种生成元被称为晶格动

[1]所有的矢量 (包括量子力学中的算符)$\mathbf{v} = (v_x, v_y)$ 除非特别说明，都是 2D 的。

[2]$\mathbf{p}$ 是常数的结论即使在相对论性粒子中都是对的。不同的是，Hamiltonian 描述是取决于参考系的，因为能量并不是 Lorentz 不变的，即换到另一个匀速平动参考系将会使得能量变化。这使得相对论性量子力学更倾向使用 Lagrangian 而不是 Hamiltonian。

[3]尽管这看起来是标准的 “理论学家的假定”，当晶体尺寸比其它任何尺寸，比如晶格距离，或者费米波长都要大时，它实际上是一个非常好的近似。

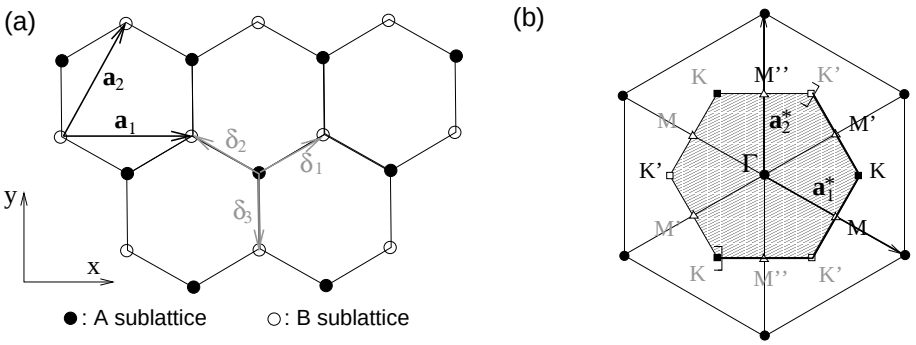

图 2.1: *(a)* 蜂巢晶格。三个矢量 $\boldsymbol{\delta}_1$，$\boldsymbol{\delta}_2$，和 $\boldsymbol{\delta}_3$ 将*nn*碳原子连在一起，间隔 $a = 0.142$。三角形 Bravais 格子的基矢为 $\mathbf{a}_1$ 和 $\mathbf{a}_2$。*(b)* 倒格子为三角形晶格。原胞的格矢为 $\mathbf{a}_1^*$ 和 $\mathbf{a}_2^*$。阴影区域代表第一 Brillouin 区 (BZ)，中心为 Γ 点，两个不等价的角落 K(黑色方块) 和 K'(白色方块)。第一 BZ 的深色边界表示定义中包含的部分，从而没有点被重复计算两次。从而，第一 BZ 的严格定义是阴影区假设深色的边界。为了完整性，我们同样展示了三个不等价的格点 M，M' 和 M''(白色三角)。

量，或者准动量。这种晶格平移的离散性的结果就是，不是所有的晶格动量都是物理的，只有那些在第一布里渊区 (Brillouin zone, BZ) 才是：任何的振动模式，无论是晶格振动或是电子波，波矢超出第一 BZ 的都可以用第一 BZ 内的某个波矢的某个模式描述。这份讲义不可能包含完整的固体物理课程，我们推荐读者关于这部分参考标准的固体物理教科书 [25, 26]。

对于 (完美) 晶体来说也是这样的，如果一直记得 $\mathbf{p}$ 是第一 BZ 种的晶格动量的话，我们可以把 Hamiltonian 用 $H(p_x, p_y)$ 来表示。注意到，尽管最后的 Hamiltonian 经常会写成 (2.1) 的形式，其质量往往不是自由电子质量而是有效质量m_b，其由能带的特殊性质决定[4]——不仅如此，质量通常还依赖传播方向，因此一般的 Hamiltonian 应该写为

$$H = \frac{p_x^2}{2m_x} + \frac{p_y^2}{2m_y} \ .$$

2.1.2 Dirac Hamiltonian in graphene
石墨烯中的 Dirac Hamiltonian

上面考虑的 2D 晶格中的电子行为只在*Bravais*晶格，即所有的格点从晶体学的角度来说都是等价的，下才成立。然而，有些晶格，比如石墨烯中碳原子的蜂巢晶格，由于价带电子的 sp^2 杂化，并不是 Bravais 晶格。这种时候，人们就会考虑用 Bravais 晶格再加上一种特定的 N_s 个格点 (被称为基元) 的形式来刻画这种晶格。如图. 2.1(a) 所示为蜂巢晶格的情况。比较格点 A(实心圆) 和格点 B(空心圆) 的时候，我们注意到这两者周围的原子的不同：A 的最近邻是在东北，西北和南向的，而 B 的最近邻则是在北，西南和东南向。准确的说，晶体学上这两种格点并不等价——尽管它们化学上来说是等价的，即由同种原子或离子占据。每一个晶格的子集构成了两种子晶格，蜂巢晶格因此可以看出三角形的 Bravais 晶格和一个两原子基元 (即由 $\boldsymbol{\delta}_3$ 连接的 A 和 B 格点) 的组合物。

为了计算有 N_s 个 Bravais 子格子——即 N_s 个格点的基元——的电子能带结构，必须要把一般的电子波函数用 N_s 个不同的波函数的叠加态来描述，而且要对每个子晶格满足 Bloch 定理 [25, 26]。严格地讲，它得用 $N_s \times N_s$ 的矩阵来描述，而其产生 N_s 个不同的能带。有 N_s 个子晶格的晶格里面，实际上每一个子晶格都 (数量上对应) 有一个能带，而石墨烯的话就是有两个带，分别对应导带和价带。

倒空间中低能电子的 Hamiltonian 即为

$$H(\mathbf{k}) = t \begin{pmatrix} 0 & \gamma_{\mathbf{k}}^* \\ \gamma_{\mathbf{k}} & 0 \end{pmatrix}, \tag{2.3}$$

这是用考虑最近邻 hopping 的紧束缚模型计算得到的，其中 hopping 强度为 t。由于 A 格点的最近邻就是 B 格点，而且反之亦然，所以 Hamiltonian 是非对角的，而由于时间反演对称性 $[H(-\mathbf{k})^* = H(\mathbf{k})]$，非对角元彼此复共轭。前面讲到，在第一 BZ，即图. 2.1(b) 中那个六角型的区域，中的晶格动量 $\mathbf{k}$ 已然完备，而函数

[4]比如在 GaAs 中，有效质量是 $m_b = 0.068m_0$，其中电子自由质量 m_0。

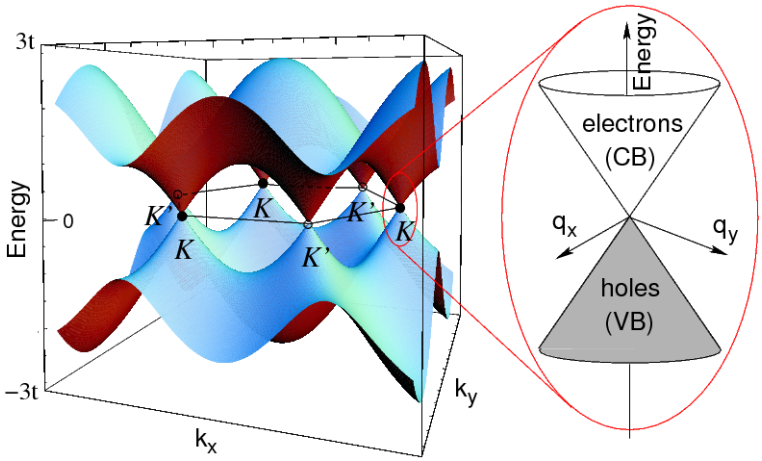

图 2.2: 石墨烯的能带。价带和导带在两个不等价的 BZ 角落 K 和 K' 处相交。非掺杂的石墨烯的费米能就在这两个接触点处，在其附近能带的色散行为是圆锥形的。

$\gamma_{\mathbf{k}}$ 的准确形式会在附录A中作解释 [(A.9)]。通过把 Hamiltonian 进行对角化，我们可以得到如图. 2.2所示的两条能带，标记为 $\lambda = \pm$。价带 ($\lambda = -$) 与导带 ($\lambda = +$) 在第一 BZ 中的不等价的两个角会接触。由于石墨烯决定低能导电性的 π-轨道的电子数量和格点数量一样多，所以总的能带结构是半满的。这半满性来自于电子的自旋取向，使得 π-轨道被两个电子占据。而其结果就是，除非如上一章第1.2节来用场效应进行掺杂，否则费米能就会与两条能带在 K and K' 处相接。

图. 2.2的内插图表明了石墨烯能带的接触点 K 和 K' 附近能带色散为线性的，而这个区间足以描述关心的能量尺度[5]。两个能带的圆锥形状令人想到相对论性粒子，其色散为 $E = \pm\sqrt{m^2c^4 + \mathbf{p}^2c^2}$，其中光速 c，粒子质量 m。如果后者是零，我们就有 $E = \pm c|\mathbf{p}|$，与低能石墨烯的情况十分接近 (图. 2.2的内插图)，因此可以处理为*无质量 Dirac 费米子*。对石墨烯中的电子的描述我们这里取得是连续极限，但是要注意到我们实际上有两种粒子——一种 K 附近的，而一种 K' 附近的。这带来了我们称之为*谷简并*的二重简并。

石墨烯中的电子和无质量的相对论性粒子是通过相接触点 K 和 K' 附近把 Hamiltonian 做低能展开 (2.3) 得到的；两个接触点的动量为 $\mathbf{K}$ 和 $\mathbf{K}' = -\mathbf{K}$[见图. 2.1(a)]，我们关心的动量 $\mathbf{k} = \pm\mathbf{K} + \mathbf{p}/\hbar$，其中 $|\mathbf{p}/\hbar| \ll |\mathbf{K}|$。通过把函数 $\gamma_{\pm\mathbf{K}+\mathbf{p}/\hbar}$ 展开到一阶，就得到了如下形式[6]

$$H = t\begin{pmatrix} 0 & \nabla\gamma^*_{\mathbf{K}}\cdot\mathbf{p} \\ \nabla\gamma_{\mathbf{K}}\cdot\mathbf{p} & 0 \end{pmatrix} = v\begin{pmatrix} 0 & p_x - ip_y \\ p_x + ip_y & 0 \end{pmatrix} = v\mathbf{p}\cdot\boldsymbol{\sigma}$$

其中 $\boldsymbol{\sigma} = (\sigma^x, \sigma^y)$ 为 Pauli 矩阵。

$$\sigma^x = \begin{pmatrix} 0 & 1 \\ 1 & 0 \end{pmatrix}, \qquad \sigma^y = \begin{pmatrix} 0 & -i \\ i & 0 \end{pmatrix} \qquad \text{以及} \qquad \sigma^z = \begin{pmatrix} 1 & 0 \\ 0 & -1 \end{pmatrix}$$

而我们把 Hamiltonian(2.3) 在 K 点附近展开[7] 。费米速度 v 实际上就相当于光速 c，只不过小了三百倍 $c \simeq 300v$。这部分的具体细节看附录A。上面的 Hamiltonian 就是标准的无质量 2D 粒子的形式，有的时候也被称为 Weyl 或 Dirac Hamiltonian。

本章的剩下部分会讨论两种分别对应非相对论性和相对论性粒子的 Hamiltonian

$$H_S = \frac{\mathbf{p}^2}{2m_b} \qquad \text{和} \qquad H_D = v\mathbf{p}\cdot\boldsymbol{\sigma}\ , \tag{2.4}$$

在非零磁场下是如何进行描述的。

[5]实际上，石墨烯的低能区间大概处于 $10 - 100$meV 区，而非线性的修正则在 eV 区才会显著。
[6]其中，对称性要求 $\gamma_{\pm\mathbf{K}} = 0$
[7]在 K' 点可以得到类似的结果，见附录A的 (A.15) 式。

2.2 Hamiltonians for Non-Zero B Fields 非零磁场的 Hamiltonian

2.2.1 Minimal coupling and Peierls substitution Peierls 替换与最小耦合

为了描述磁场中的电子，需要用规范不变的动量形式 [27]

$$\mathbf{p} \to \mathbf{\Pi} = \mathbf{p} + e\mathbf{A}(\mathbf{r}), \tag{2.5}$$

其中 $\mathbf{A}(\mathbf{r})$ 是磁场产生的磁矢势 $\mathbf{B} = \nabla \times \mathbf{A}(\mathbf{r})$。这种规范不变的动量正比于电子速度 $\mathbf{v}$，而电子速度是一个物理量从而自然是规范不变的。由于磁矢势 $\mathbf{A}(\mathbf{r})$ 不是规范不变的，所以动量 $\mathbf{p}$ 也不是。对磁矢势加一个任意的函数 $\lambda(\mathbf{r})$ 的梯度 $\mathbf{A}(\mathbf{r}) \to \mathbf{A}(\mathbf{r}) + \nabla\lambda(\mathbf{r})$ 并不会改变磁场，因为梯度的旋度是零。而动量在规范变换下需要按照 $\mathbf{p} \to \mathbf{p} - e\nabla\lambda(\mathbf{r})$ 变换，来弥补差的磁矢势而保证 $\mathbf{\Pi}$ 是规范不变的。这种替换 (2.5) 也被叫为*最小替换*。

当我们用格点来考虑电子的位置的时候，由于多条能带的存在，这种替换就更加微妙了。磁矢势会变得无界，即使是有限的磁场。当我们选取某个特定的规范，比如 Landau 规范 $\mathbf{A}_L(\mathbf{r}) = B(-y, 0, 0)$ 的时候，着看的更加清楚，磁矢势会大到 $B \times L_y$，而 L_y 是系统在 y-方向的宏观延展程度。然而，(2.5) 这种替换在晶格间距 a 仍然远小于*磁场尺度*

$$l_B = \sqrt{\frac{\hbar}{eB}}\,, \tag{2.6}$$

的时候仍然正确。此时我们称它为*Peierls 替换*。磁场尺寸是存在磁场时一个很自然的基本长度尺度。a 大概是原子尺度 (~ 0.1 to 10 nm)，而 $l_B \simeq 26\,\mathrm{nm}/\sqrt{B[\mathrm{T}]}$，这种条件，在如今的高场实验室中 (连续区域 ~ 45 T，脉冲区域 ~ 80T)，对所有的原子晶格中都成立[8]。

利用 (Peierls) 替换 (2.5)，由于我们已经知道没有磁场的情况，存在磁场中的带电粒子的 Hamiltonian 就很显然了

$$H(\mathbf{p}) \to H(\mathbf{\Pi}) = H(\mathbf{p} + e\mathbf{A}) = H^B(\mathbf{p}, \mathbf{r}).$$

注意由于磁矢势的空间分布，我们得到的 Hamiltonian 不再是平移不变的，而 (规范相关的) 动量 $\mathbf{p}$ 也不是一个守恒量了。我们在 Hamiltonian(2.4) 的基础下做推广，得到对于非相对论性情况

$$H_S^B = \frac{[\mathbf{p} + e\mathbf{A}(\mathbf{r})]^2}{2m_b} \tag{2.7}$$

而对相对论性情况

$$H_D^B = v[\mathbf{p} + e\mathbf{A}(\mathbf{r})] \cdot \boldsymbol{\sigma} \tag{2.8}$$

2.2.2 Quantum mechanical treatment 量子力学处理

为了在量子力学框架下分析单电子 Hamiltonian(2.7) 和 (2.8)，我们用标准的*正则量子化*[28] 来处理，即把物理量用作用在 Hilbert 空间中的态矢量的算符来表示。这些算符彼此不对易，也就是说他们作用在态矢量上的顺序影响对系统的描述。形式上，在两个算符 $\mathcal{O}_1$ 和 $\mathcal{O}_2$ 中引入*对易关系* $[\mathcal{O}_1, \mathcal{O}_2] \equiv \mathcal{O}_1\mathcal{O}_2 - \mathcal{O}_2\mathcal{O}_1$。如果 $[\mathcal{O}_1, \mathcal{O}_2] = 0$ 则二者对易，反之不对易。Hamiltonian 中最基本的物理量是 2D 坐标 $\mathbf{r} = (x, y)$ 及其对应的正则动量 $\mathbf{p} = (p_x, p_y)$，其满足对易关系

$$[x, p_x] = i\hbar, \qquad [y, p_y] = i\hbar \qquad \text{以及} \qquad [x, y] = [p_x, p_y] = [x, p_y] = [y, p_x] = 0, \tag{2.9}$$

即坐标和其对应方向的动量不对易。这种不对易性导致了 Heisenberg 不等式，即人们没办法同时知道量子型粒子的坐标和动量 $\Delta x \Delta p_x \gtrsim h$ 以及 $\Delta y \Delta p_y \gtrsim h$。

对易关系 (2.9) 导致了规范不变的动量算符的各个分量不再对易

$$\begin{aligned}[\Pi_x, \Pi_y] &= [p_x + eA_x(\mathbf{r}), p_y + eA_y(\mathbf{r})] = e\left([p_x, A_y] - [p_y, A_x]\right) \\ &= e\left(\frac{\partial A_y}{\partial x}[p_x, x] + \frac{\partial A_y}{\partial y}[p_x, y] - \frac{\partial A_x}{\partial x}[p_y, x] - \frac{\partial A_x}{\partial y}[p_y, y]\right),\end{aligned}$$

[8] 高磁场只能够通过半损毁实验 *(semi-destructive experiments)* 实现，里面的样品仍能保持使用，但是产生磁场的线圈需要替换

其中我们用到了在两个算符的对易式是个复常数，或者某个算符自己与 $\mathcal{O}_1$ 和 $\mathcal{O}_2$ 都对易 [28] 时的如下关系[9]

$$[\mathcal{O}_1, f(\mathcal{O}_2)] = \frac{df}{d\mathcal{O}_2}[\mathcal{O}_1, \mathcal{O}_2] \tag{2.10}$$

利用对易关系 (2.9)，可以看到

$$[\Pi_x, \Pi_y] = -ie\hbar\left(\frac{\partial A_y}{\partial x} - \frac{\partial A_x}{\partial y}\right) = -ie\hbar\left(\nabla \times \mathbf{A}\right)_z = -ie\hbar B,$$

用磁场尺度表示出来 (2.6)，

$$[\Pi_x, \Pi_y] = -i\frac{\hbar^2}{l_B^2}\,. \tag{2.11}$$

这个式子是这一章的最基本的结论，值得我们对它进行更多的讨论。

- 如我们所料，规范不变量 ($\mathbf{\Pi}$ 的两个分量) 之间的对易式也是规范不变的。它只取决于普适的常数和磁场强度 B，而与矢势 $\mathbf{A}$ 无关。
- 规范不变的动量 $\mathbf{\Pi}$ 的分量互相共轭，就像 x 与 p_x，或者 y 与 p_y 那样。而 p_x 作为生成元生成了沿着 x-方向的平移操作 (p_y 生成 y-方向的)。这里是一样的：Π_x 生成了一个对规范不变动量的沿着 y-方向的推动，而 Π_y 则生成了 x-方向的。
- 其结果就是无法同时将 Π_x 和 Π_y 对角化，而不像 p_x 和 p_y 对易的零磁场中那样。

为了解 Hamiltonians (2.7) 和 (2.8)，像量子力学里面的一维谐振子一样，通常使用共轭算符对 Π_x 和 Π_y 引入阶梯算符。量子力学课上会讲，阶梯算符就像取一维谐振子相空间的值一样，可以用位置 (x-轴) 和动量 (y-轴) 来表示

$$\tilde{a} = \frac{1}{\sqrt{2}}\left(\frac{x}{x_0} - i\frac{p}{p_0}\right) \qquad \text{以及} \qquad \tilde{a}^\dagger = \frac{1}{\sqrt{2}}\left(\frac{x}{x_0} + i\frac{p}{p_0}\right),$$

其中 $x_0 = \sqrt{\hbar/m_b\omega}$，$p_0 = \sqrt{\hbar m_b\omega}$ 是谐振子频率 ω 下的归一化系数 [28]。由于位置 x 与动量 p 彼此是共轭变量，以及精心选取的归一化系数，我们得到了非常棒的阶梯算符对易关系 $[\tilde{a}, \tilde{a}^\dagger] = 1$。

对于磁场中的 2D 电子气，阶梯算符实际上起到了一种复规范不变动量 (或速度) 的作用，即

$$a = \frac{l_B}{\sqrt{2}\hbar}\left(\Pi_x - i\Pi_y\right) \qquad \text{以及} \qquad a^\dagger = \frac{l_B}{\sqrt{2}\hbar}\left(\Pi_x + i\Pi_y\right), \tag{2.12}$$

其中我们同样精心选取了恰当的归一化系数从而

$$[a, a^\dagger] = 1. \tag{2.13}$$

同样可以将算符用阶梯算符 (2.12) 展开，这在后面会极大地方便运算

$$\Pi_x = \frac{\hbar}{\sqrt{2}l_B}\left(a^\dagger + a\right) \qquad \text{以及} \qquad \Pi_y = \frac{\hbar}{i\sqrt{2}l_B}\left(a^\dagger - a\right). \tag{2.14}$$

2.3 Landau Levels
Landau 能级

在之前的章节里面所讨论的内容将会对计算非相对论性的 (2.7) 和相对论性的 (2.8)Hamiltonian 的能谱有很大帮助。而本节则着重于理解这种能谱。考虑到电子不仅携带电荷还携带自旋，每一个能级都会因此劈裂成能级差为 $\Delta_Z\epsilon = g\mu_B B$ 的两个能级，g 是 landég-因子，$\mu_B = e\hbar/2m_0$ 是 Bohr 磁子。我们忽略自旋自由度从而简化量子力学的形式以及能级结构，也就是说我们相当于在处理无自旋费米子。然而，自旋自由度实际上会带来很多有趣的物理问题，这值得我们特别留意。这些问题我们在第5章详述。

[9] 更严格的说，我们利用了多元函数的梯度在算符函数中的推广

$$[\mathcal{O}_0, f(\mathcal{O}_1, ..., \mathcal{O}_J)] = \sum_{j=1}^{J}\frac{\partial f}{\partial \mathcal{O}_j}[\mathcal{O}_0, \mathcal{O}_j]$$

只要 $[[\mathcal{O}_0, \mathcal{O}_j], \mathcal{O}_0] = [[\mathcal{O}_0, \mathcal{O}_j], \mathcal{O}_j] = 0$ 其中 $j = 1, ..., N$ 满足，这个关系就是正确的。

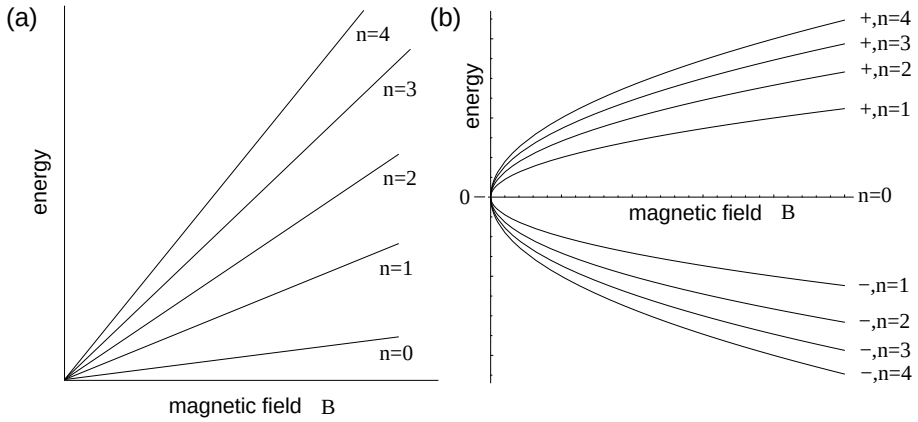

图 2.3: Landau 能级作为磁场的函数*(a)* 非相对论性，$\epsilon_n = \hbar\omega_C(n+1/2) \propto B(n+1/2)$. *(b)* 相对论性，$\epsilon_{\lambda,n} = \lambda(\hbar v/l_B)\sqrt{2n} \propto \lambda\sqrt{Bn}$.

2.3.1 Non-relativistic Landau levels 非相对论性 Landau 能级

非相对论性电子的 Hamiltonian (2.7) 用规范不变动量写出来有下面的形式：

$$H_S^B = \frac{1}{2m_b}\left(\Pi_x^2 + \Pi_y^2\right).$$

很自然的可以把它与一维谐振子类比，因为 Π_x 与 Π_y 彼此共轭，且都以二次形式出现在 Hamiltonian 里面。如果用阶梯算符 (2.14) 和对易关系 (2.13) 来描述的话，很容易就得到

$$\begin{aligned} H_S^B &= \frac{\hbar^2}{4ml_B^2}\left[a^{\dagger 2} + a^\dagger a + aa^\dagger + a^2 - \left(a^{\dagger 2} - a^\dagger a - aa^\dagger + a^2\right)\right] \\ &= \frac{\hbar^2}{2ml_B^2}\left(a^\dagger a + aa^\dagger\right) = \frac{\hbar^2}{ml_B^2}\left(a^\dagger a + \frac{1}{2}\right) \\ &= \hbar\omega_C\left(a^\dagger a + \frac{1}{2}\right), \end{aligned} \tag{2.15}$$

其中最后一步利用了电子回转频率 (1.2) 和磁场特征尺度 (2.6) 的关系 $\omega_c = \hbar/m_b l_B^2$。

就像一维谐振子那样，Hamiltonian(2.15) 的本征值和本征态即由占据数算符$a^\dagger a$ 的本征值本征态 $a^\dagger a|n\rangle = n|n\rangle$ 来完备描述。阶梯算符作用在这些态上得到如下行为 [28]

$$a^\dagger|n\rangle = \sqrt{n+1}|n+1\rangle \qquad \text{以及} \qquad a|n\rangle = \sqrt{n}|n-1\rangle, \tag{2.16}$$

其中最后一步仅对于 $n > 0$ 成立——a 作用在基态 $|0\rangle$ 上得零，

$$a|0\rangle = 0. \tag{2.17}$$

这个式子能帮助我们计算最低能量本征态和构造高能量 n 的态 (见第2.4.1节)

$$|n\rangle = \frac{\left(a^\dagger\right)^n}{\sqrt{n!}}|0\rangle. \tag{2.18}$$

2D 带电非相对论性粒子的能级由分立的整数 n 标志，

$$\epsilon_n = \hbar\omega_C\left(n + \frac{1}{2}\right). \tag{2.19}$$

这些能级我们叫他*Landau* 能级(LL) 如图. 2.3(a) 所示，显然是磁场的函数。由于回转频率与磁场强度成线性，LL 自然也就与磁场强度成线性了。

2.3.2 Relativistic Landau levels
相对论性 Landau 能级

我们用与处理非相对论性电子完全一样的办法来处理石墨烯中相对论性电子 (2.8) 的行为。用阶梯算符 (2.12) 表示，Hamiltonian 为

$$H_D^B = v\begin{pmatrix} 0 & \Pi_x - i\Pi_y \\ \Pi_x + i\Pi_y & 0 \end{pmatrix} = \sqrt{2}\frac{\hbar v}{l_B}\begin{pmatrix} 0 & a \\ a^\dagger & 0 \end{pmatrix}. \tag{2.20}$$

注意到特征频率 $\omega' = \sqrt{2}v/l_B$ 在这里就起到和回转频率相类似的效果。然而，这次特征频率没办法写成 eB/m_b 的样子了——对于石墨烯来说，有效质量就是零，回转频率发散[10]。

求解 Hamiltonian(2.20) 的本征值和本征态，首先写出本征值方程 $H_D^B\psi_n = \epsilon_n\psi_n$。由于 Hamiltonian 是 2×2 矩阵，所以本征态是一个 2-旋量，

$$\psi_n = \begin{pmatrix} u_n \\ v_n \end{pmatrix},$$

从而我们需要解方程组

$$\hbar\omega' a\, v_n = \epsilon_n\, u_n \qquad 以及 \qquad \hbar\omega' a^\dagger\, u_n = \epsilon_n\, v_n\ , \tag{2.21}$$

对旋量的第二个分量有

$$a^\dagger a\, v_n = \left(\frac{\epsilon_n}{\hbar\omega'}\right)^2 v_n \tag{2.22}$$

注意到这个分量是占据数算符的本征态 $n = a^\dagger a$，我们在前面的小节里面已经见过了。从而我们可以得到旋量第二分量 v_n 与非相对论性Hamiltonian(2.15) 的本征态 $|n\rangle$ 最多差一个归一化系数：$v_n \sim |n\rangle$。此外还可以看到能量的平方正比于量子数 $\epsilon_n^2 = (\hbar\omega')^2 n$。这个方程有正负两个解，从而得要引入另一个量子数 $\lambda = \pm$ 来标记正负能的解。这个量子数其实也起到了在第2.1节中零磁场时标记能带的作用 (导带 $\lambda = +$，价带 $\lambda = -$)。总之我们有了能谱 [29]

$$\epsilon_{\lambda,n} = \lambda\frac{\hbar v}{l_B}\sqrt{2n} \tag{2.23}$$

能级如图. 2.3(b) 所示。这种相对论性 *Landau* 能级的色散关于磁场有 $\lambda\sqrt{Bn}$ 形式。

我们知道旋量第二分量的时候，利用 (2.21) 其实也同时得到了第一分量 $u_n \propto a\, v_n \sim a|n\rangle \sim |n-1\rangle$。得注意的是把零能 LL($n=0$) 与其他能级区分开。对于 $n=0$，从 (2.17) 看出第一分量为零，从而旋量为

$$\psi_{n=0} = \begin{pmatrix} 0 \\ |n=0\rangle \end{pmatrix}. \tag{2.24}$$

而对于其它情况 ($n \neq 0$)，有正负能两个解，其本征态的两个分量有一个会差负号。通常来说会使用这种旋量的表示方法

$$\psi_{\lambda,n\neq 0} = \frac{1}{\sqrt{2}}\begin{pmatrix} |n-1\rangle \\ \lambda|n\rangle \end{pmatrix}. \tag{2.25}$$

Experimental observation of relativistic Landau levels
相对论性 Landau 能级的实验观测

相对论性 LL 可以通过传输谱的测量来发现，即我们给样品打光上去，并测量光的透过率。实验用的石墨烯是通过外延生长得到的[11][31]，并随后进行了对衬底的剥离 [32]。如果单色光的频率和 (部分) 填充的 LL(λ, n) 与未被占据的 LL($\lambda', n\pm 1$) 之间偶极跃迁频率共振了的话，光子就会被吸收，并形成两个能级之间的电磁激发 [见图. 2.4(a)]。而注意到非相对论性 2D 电子气中，只有与最末的 LLn 与第一个未被占据的 LL$n+1$ 之间存在偶极跃迁，跃迁能量为 $\hbar\omega_C$，与 n 无关，因此只能观测到回转频率处单个吸收峰 (回转共振)。在石墨烯中，由于导带价带两条电子能带的存在，会出现多种可能的跃迁，其能量为

$$\Delta_{n,\xi} = \frac{\hbar v}{l_B}\left[\sqrt{2(n+1)} - \xi\sqrt{2n}\right],$$

其中 $\xi = +$ 表示同属一种能带，而 $\xi = -$ 则反之。因此我们得到一系列共振能级，其色散关系为 $\Delta_{n,\xi} \propto \sqrt{B}$，并且可以从试验中得到 [见图. 2.4(c)，结果取自 Sadowski *et al.* [31]]。注意到图. 2.4(c) 中的虚线是根据一个拟合参数 (费米 v) 得到的，与各个 n 的实验数据都吻合的很好。

[10] 有时会认为引入一个回转质量m_C，其引入的办法是令 $\omega' \equiv eB/m_C$。然而这种质量是人为引入的，从而与载流子密度相关。本讲义中不引入这个概念。

[11] 外延生长的石墨烯通过在 SiC 晶体上通过热石墨堆积而形成石墨烯 [30]

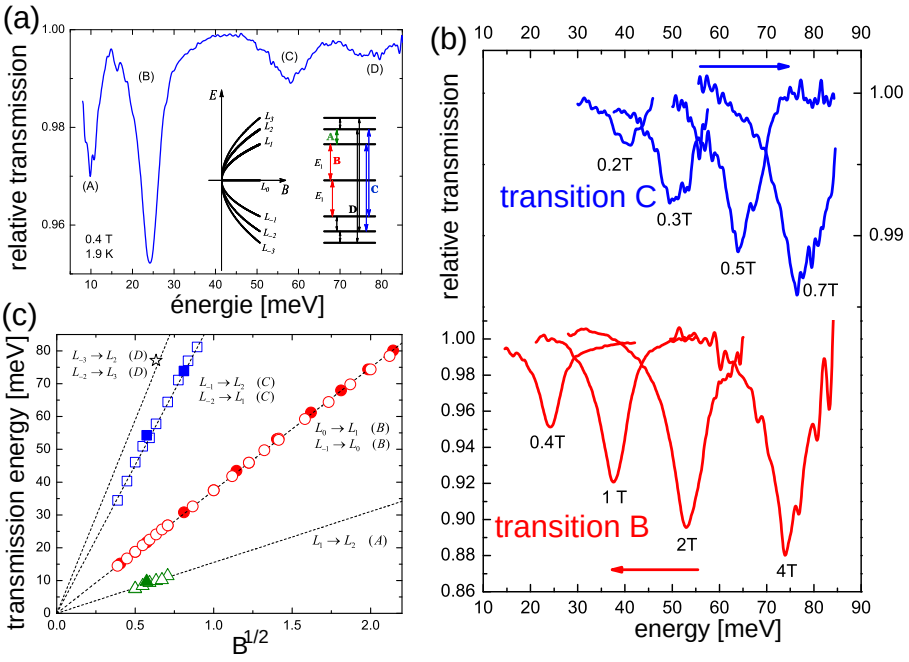

图 2.4: (from Sadowski *et al.*, 2006 石墨烯中的 LL 谱). *(a)* 对恒定磁场 0.4 T，传输谱中共振位置关于激发的光子能量的关系。共振与相对论性 Landau 能级的偶极跃迁相关。*(b)* 共振位置关于磁场的位置移动。*(c)* 共振关于磁感应强度 $\sqrt{B}$ 的平方根的关系，得到与理论温和的线性结果。

2.3.3 Level degeneracy
能级简并

前面的小节里面，我们了解了 2D 相对论/非相对论性带电粒子的 n-Landau 能级 (对于相对论性粒子还有一个额外能带指标 λ)。然而，我们会从下面的维度的角度看到，这个量子系统还是没有确定下来。原本的 Hamiltonian(2.7) 和 (2.8) 分别是两对共轭算符 x 与 p_x，y 与 p_y 的函数，而当 Hamiltonian 用规范不变动量 $\mathbf{\Pi}$ 或者阶梯算符 a 与 $a^\dagger$ 表示出来后 (2.15) 和 (2.20)，它们只与一对共轭算符相关。从原来的模型来看，我们会觉得得有两个相关的量子数来描述才对 (对应每一个空间维度)。对于零场模型 (2.4) 来说确实是这样的，量子态有两个量子数 p_x 和 p_y，即 2D 动量的分量，来描述。对于量子态的完备描述也从而必须要用另外的共轭算符来描述，而且其必须与 Hamiltonian 对易，使得 LL 形成除了如自旋[12]或石墨烯的两个谷自由度等内禀自由度之外的能级简并。

类比规范不变动量 $\mathbf{\Pi} = \mathbf{p} + e\mathbf{A}(\mathbf{r})$，我们考虑其相反的符号的组合形式

$$\tilde{\mathbf{\Pi}} = \mathbf{p} - e\mathbf{A}(\mathbf{r}), \tag{2.26}$$

我们管这个算符叫赝动量。我们可以把动量算符 $\mathbf{p}$ 和矢势算符 $\mathbf{A}(\mathbf{r})$ 用 $\mathbf{\Pi}$ 和 $\tilde{\mathbf{\Pi}}$ 表示出来

$$\mathbf{p} = \frac{1}{2}(\mathbf{\Pi} + \tilde{\mathbf{\Pi}}) \qquad \text{以及} \qquad \mathbf{A}(\mathbf{r}) = \frac{1}{2e}(\mathbf{\Pi} - \tilde{\mathbf{\Pi}}). \tag{2.27}$$

注意到，不像规范不变动量那样，赝动量是依赖规范的，而且因此不是一个物理量[13]。然而，赝动量两个分量的对易关系则是规范不变的，

$$\left[\tilde{\Pi}_x, \tilde{\Pi}_y\right] = i\frac{\hbar^2}{l_B^2}\ . \tag{2.28}$$

[12] 只在忽略 Zeeman 效应下不同自旋态简并

[13] 尽管如此，我们还是会尝试在半经典的角度给它一个图像

这个计算和 Π_x 与 Π_y 的对易计算 (2.11) 一样；当然也可以计算规范不变动量和赝动量的对易，

$$\begin{aligned}\left[\Pi_x, \tilde{\Pi}_x\right] &= 2ie\hbar\frac{\partial A_x}{\partial x}\,,\\ \left[\Pi_y, \tilde{\Pi}_y\right] &= 2ie\hbar\frac{\partial A_y}{\partial y}\,,\\ \left[\Pi_x, \tilde{\Pi}_y\right] &= ie\hbar\left(\frac{\partial A_x}{\partial y}+\frac{\partial A_y}{\partial x}\right) = -\left[\tilde{\Pi}_x, \Pi_y\right].\end{aligned} \tag{2.29}$$

赝动量与 Hamiltonian 不对易 $[\tilde{\Pi}_{x/y}, H] \neq 0$，从而这些交错的对易量会带来不物理的动力学效应——这不是我们希望的。然而，通过选取一组合适的规范，比如对称规范，

$$\mathbf{A}_S(\mathbf{r}) = \frac{B}{2}(-y, x, 0), \tag{2.30}$$

所有的交错的对易量 (2.29) 都为零，从而赝动量与 Hamiltonian 也对易。

注意，矢势的规范还通常选取*Landau*规范，我们上面已经提过

$$\mathbf{A}_L(\mathbf{r}) = B(-y, 0, 0), \tag{2.31}$$

而使得最后一个交错对易量 (2.29) 并不为零。would not vanish. This gauge choice may even occur simpler: because the vector potential only depends on the y-component of the position, the system remains then translation invariant in the x-direction. Therefore, the associated momentum p_x is a good quantum number, which may be used to label the quantum states in addition to the LL quantum number n. For the Landau gauge, which is useful in the description of geometries with translation invariance in the y-direction, the wave functions are calculated in Sec. (2.4.2). However, the symmetric gauge, the wave functions of which are presented in Sec. (2.4.1), plays an important role in two different aspects; first, it allows for a semi-classical interpretation more easily than the Landau gauge, and second, the wave functions obtained from the symmetric gauge happen to be the basic ingredient in the construction of trial wave functions *à la Laughlin* for the description of the FQHE, as we will see in Chap. 4.

The pseudo-momentum, with its mutually conjugate components $\tilde{\Pi}_x$ and $\tilde{\Pi}_y$, allows us to introduce, in the same manner as for the gauge-invariant momentum $\mathbf{\Pi}$, ladder operators,

$$b = \frac{l_B}{\sqrt{2}\hbar}\left(\tilde{\Pi}_x + i\tilde{\Pi}\right) \qquad \text{以及} \qquad b^\dagger = \frac{l_B}{\sqrt{2}\hbar}\left(\tilde{\Pi}_x - i\tilde{\Pi}\right), \tag{2.32}$$

which again satisfy the usual commutation relations $[b, b^\dagger] = 1$ and which, in the symmetric gauge, commute with the ladder operators a and $a^\dagger$, $[b, a^{(\dagger)}] = 0$, and thus with the Hamiltonian, $[b^{(\dagger)}, H_B] = 0$. One may then introduce a number operator $b^\dagger b$ associated with these ladder operators, the eigenstates of which satisfy the eigenvalue equation

$$b^\dagger b|m\rangle = m|m\rangle.$$

One thus obtains a second quantum number, an integer $m \geq 0$, which is necessary to describe, as expected from the above dimensional argument, the full quantum states in addition to the LL quantum number n. The quantum states therefore become tensor products of the two Hilbert vectors

$$|n, m\rangle = |n\rangle \otimes |m\rangle \tag{2.33}$$

for non-relativistic particles. In the relativistic case, one has

$$\psi_{\lambda n,m} = \psi_{\lambda n,m} \otimes |m\rangle = \frac{1}{\sqrt{2}}\begin{pmatrix} |n-1, m\rangle \\ \lambda|n, m\rangle \end{pmatrix} \tag{2.34}$$

for $n \neq 0$ and

$$\psi_{n=0,m} = \psi_{n=0} \otimes |m\rangle = \begin{pmatrix} 0 \\ |n=0, m\rangle \end{pmatrix} \tag{2.35}$$

for the zero-energy LL.

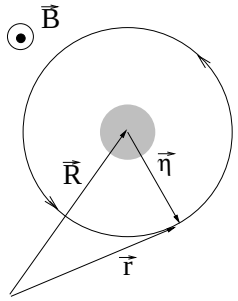

图 2.5: Cyclotron motion of an electron in a magnetic field around the guiding centre **R**. The grey region indicates the quantum-mechanical uncertainty of the guiding-centre position due to the non-commutativity (2.39) of its components.

2.3.4 Semi-classical interpretation of the level degeneracy
能级简并的半经典解释

How can we illustrate this somewhat mysterious pseudo-momentum introduced formally above? Remember that, because the pseudo-momentum is a gauge-dependent quantity, any physical interpretation needs to be handled with care. However, within a semiclassical treatment, the symmetric gauge allows us to make a connection with a classical constant of motion that one obtains from solving the classical equations of motion for a massive electron in a magnetic field,

$$m_b\ddot{\mathbf{r}} = -e(\dot{\mathbf{r}}\times\mathbf{B}) \qquad \Leftrightarrow \qquad \left\{\begin{array}{rcl} \ddot{x} &=& -\omega_C\dot{y} \\ \ddot{y} &=& \omega_C\dot{x} \end{array}\right. \tag{2.36}$$

which is nothing other than the electron's acceleration due to the Lorentz force. These equations may be integrated, and one then finds

$$\left.\begin{array}{rcl} \dot{x} = \frac{\Pi_x}{m_b} &=& -\omega_C(y-Y) \\ \dot{y} = \frac{\Pi_y}{m_b} &=& \omega_C(x-X) \end{array}\right\} \quad \Leftrightarrow \quad \left\{\begin{array}{rcl} y &=& Y - \frac{\Pi_x}{eB} \\ x &=& X + \frac{\Pi_y}{eB} \end{array}\right. \tag{2.37}$$

where $\mathbf{R} = (X, Y)$ is an integration constant, which physically describes a constant of motion. This quantity may easily be interpreted: it represents the centre of the electronic cyclotron motion (see 图. 2.5). Indeed, further integration of the equations (2.37) yields the classical cyclotron motion

$$x(t) = X - r\sin(\omega_C t + \phi) \qquad 以及 \qquad y(t) = Y + r\cos(\omega_C t + \phi),$$

where the phase ϕ is another constant of motion. The cyclotron motion itself is described by the velocities (or else the gauge-invariant momenta) Π_x/m and Π_y/m. Whereas the energy depends on these velocities that determine the radius r of the cyclotron motion, it is completely independent of the position of its centre **R**, which we call *guiding centre* from now on, as one would expect from the translational invariance of the equations of motion (2.36).

In order to relate the guiding centre **R** to the pseudo-momentum $\tilde{\mathbf{\Pi}}$, we use Eq. (2.27) for the vector potential in the symmetric gauge,

$$e\mathbf{A}(\mathbf{r}) = \frac{eB}{2}\begin{pmatrix} -y \\ x \end{pmatrix} = \frac{1}{2}(\mathbf{\Pi} - \tilde{\mathbf{\Pi}}).$$

The postions x and y may then be expressed in terms of the momenta $\mathbf{\Pi}$ and $\tilde{\mathbf{\Pi}}$,

$$\begin{array}{rcl} y &=& \frac{\tilde{\Pi}_x}{eB} - \frac{\Pi_x}{eB} \\ x &=& -\frac{\tilde{\Pi}_y}{eB} + \frac{\Pi_y}{eB}\ . \end{array}$$

A comparison of these expresssions with Eq. (2.37) allows us to identify

$$X = -\frac{\tilde{\Pi}_y}{eB} \qquad 以及 \qquad Y = \frac{\tilde{\Pi}_x}{eB} \; . \tag{2.38}$$

This means that, in the symmetric gauge, the components of the pseudo-momentum are nothing other, apart from a factor to translate a momentum into a position, than the the components of the guiding centre, which are naturally constants of motion. In a quantum-mechanical treatment, these operators therefore necessarily commute with the Hamiltonian, as we have already seen above. Furthermore, the commutation relation (2.28) between the components of the pseudo-momentum, $[\tilde{\Pi}_x, \tilde{\Pi}_y] = i\hbar^2/l_B^2$ induces the commutation relation

$$[X, Y] = il_B^2 \tag{2.39}$$

between the components of the guiding-centre operator. This means that there is a Heisenberg uncertainty associated with the guiding-centre position of a quantum-mechanical state – one cannot know its x- and y-components simultaneously, and the guiding centre is, therefore, smeared out over a surface

$$\Delta X \Delta Y = 2\pi l_B^2 \tag{2.40}$$

(see grey region in 图. 2.5).[14] This minimal surface plays the same role as the surface (action) h in phase space and therefore allows us to count the number of possible quantum states of a given (macroscopic) surface $\mathcal{A}$,

$$N_B = \frac{\mathcal{A}}{\Delta X \Delta Y} = \frac{\mathcal{A}}{2\pi l_B^2} = n_B \times \mathcal{A},$$

where we have introduced the flux density

$$n_B = \frac{1}{2\pi l_B^2} = \frac{B}{h/e}, \tag{2.41}$$

which is nothing other than the magnetic field measured in units of the flux quantum h/e. Therefore, *the number of quantum states in a LL equals the number of flux quanta threading the sample surface $\mathcal{A}$, and each LL is macroscopically degenerate*. We will show in a more quantitative manner than in the above argument based on the Heisenberg inequality that the number of states per LL is indeed given by N_B when discussing, in the next section, the electronic wave functions in the symmetric and the Landau gauges.

Similarly to the guiding-centre operator, we may introduce the *cyclotron variable* $\boldsymbol{\eta} = (\eta_x, \eta_y)$, which determines the cyclotron motion and which fully describes the dynamic properties. The cyclotron variable is perpendicular to the electron's velocity and may be expressed in terms of the gauge-invariant momentum $\boldsymbol{\Pi}$,

$$\eta_x = \frac{\Pi_y}{eB} \qquad 以及 \qquad \eta_y = -\frac{\Pi_x}{eB} \; , \tag{2.42}$$

as one sees from Eq. (2.37). The position of the electron is thus decomposed into its guiding centre and its cyclotron variable, $\mathbf{r} = \mathbf{R} + \boldsymbol{\eta}$. Also the components of the cyclotron variable do not commute, and one finds with the help of Eq. (2.11)

$$[\eta_x, \eta_y] = \frac{[\Pi_x, \Pi_y]}{(eB)^2} = -il_B^2 = -[X, Y]. \tag{2.43}$$

Until now, we have only discussed a single particle and its possible quantum states. Consider now N independent quantum-mechanical electrons at zero-temperature. In the absence of a magnetic field, electrons in a metal, due to their fermionic nature and the Pauli principle which prohibits double occupancy of a single quantum state, fill all quantum states up to the Fermi energy, which depends thus on the number of electrons itself. The situation is similar in the presence of a magnetic field: the electrons preferentially occupy the lowest LLs, i.e. those of lowest energy. But once a LL is filled, the remaining electrons are forced to populate

[14] Mathematicians speak of a *non-commutative geometry* in this context, and the charged 2D particle may be viewed as a pardigm of this concept.

higher LLs. In order to describe the LL filling it is therefore useful to introduce the dimensionless ratio between the number of electrons $N_{el} = n_{el} \times \mathcal{A}$ and that of the flux quanta,

$$\nu = \frac{N_{el}}{N_B} = \frac{n_{el}}{n_B} = \frac{h n_{el}}{eB}, \tag{2.44}$$

which is called *filling factor*. Indeed the integer part, $[\nu]$, of the filling factor counts the number of completely filled LLs. Notice that one may vary the filling factor either by changing the particle number or by changing the magnetic field. At fixed particle number, lowering the magnetic field corresponds to an increase of the filling factor.

2.4 Eigenstates
本征态

2.4.1 Wave functions in the symmetric gauge
对称规范下的波函数

The algebraic tools established above may be used calculate the electronic wave functions, which are the space representations of the quantum states $|n, m\rangle$, $\phi_{n,m}(x, y) = \langle x, y|n, m\rangle$.[15] Notice first that one may obtain all quantum state $|n, m\rangle$ from a single state $|n = 0, m = 0\rangle$, with the help of

$$|n, m\rangle = \frac{\left(a^\dagger\right)^n}{\sqrt{n!}} \frac{\left(b^\dagger\right)^m}{\sqrt{m!}} |n = 0, m = 0\rangle, \tag{2.45}$$

which is a generalisation of Eq. (2.18). Naturally, this equation translates into a differential equation for the wave functions $\phi_{n,m}(x, y)$.

A state in the lowest LL ($n = 0$) is characterised by the condition (2.17)

$$a|n = 0, m\rangle = 0, \tag{2.46}$$

which needs to be translated into a differential equation. Remember from Eq. (2.12) that $a = (l_B/\sqrt{2}\hbar)(\Pi_x - i\Pi_y)$ and, by definition, $\mathbf{\Pi} = -i\hbar\nabla + e\mathbf{A}(\mathbf{r})$ where we have already represented the momentum as a differential operator in position representation, $\mathbf{p} = -i\hbar\nabla$. One then finds

$$a = -i\sqrt{2}\left[\frac{l_B}{2}\left(\partial_x - i\partial_y\right) + \frac{x - iy}{4l_B}\right],$$

where ∂_x and ∂_y are the components of the gradient $\nabla = (\partial_x, \partial_y)$, and one sees from this expression that it is convenient to introduce *complex coordinates* to describe the 2D plane. We define $z = x - iy$, $z^* = x + iy$, $\partial = (\partial_x + i\partial_y)/2$ and $\bar{\partial} = (\partial_x - i\partial_y)/2$. The lowest LL condition (2.46) then becomes a differential equation,

$$\left(\frac{z}{4l_B} + l_B\bar{\partial}\right)\phi_{n=0}(z, z^*) = 0, \tag{2.47}$$

which may easily be solved by the complex function

$$\phi_{n=0}(z, z^*) = f(z)e^{-|z|^2/4l_B^2}, \tag{2.48}$$

where $f(z)$ is an *analytic* function, i.e. $\bar{\partial}f(z) = 0$, and $|z|^2 = zz^*$. This means that there is an additional degree of freedom because $f(z)$ may be *any* analytic function. It is not unexpected that this degree of freedom is associated with the second quantum number m, as we will now discuss.

[15] We limit the discussion to the non-relativistic case. The spinor wave functions for relativistic electrons are then easily obtained with the help of Eqs. (2.34) and (2.35).

The ladder operators b and $b^\dagger$ may be expressed in position representation in a similar manner as a, and one obtains the space representation of the different ladder operators,

$$a = -i\sqrt{2}\left(\frac{z}{4l_B} + l_B\bar{\partial}\right), \qquad a^\dagger = i\sqrt{2}\left(\frac{z^*}{4l_B} - l_B\partial\right)$$
$$b = -i\sqrt{2}\left(\frac{z^*}{4l_B} + l_B\partial\right), \qquad b^\dagger = i\sqrt{2}\left(\frac{z}{4l_B} - l_B\bar{\partial}\right). \tag{2.49}$$

In the same manner as for a state in the lowest LL, the condition for the reference state with $m = 0$ is $b|n, m = 0\rangle = 0$, which yields the differential equation

$$\left(z^* + 4l_B^2\partial\right)\phi'_{m=0}(z, z^*) = 0$$

with the solution

$$\phi'_{m=0}(z, z^*) = g(z^*)e^{-|z|^2/4l_B^2},$$

in terms of an *anti-analytic* function $g(z^*)$ with $\partial g(z^*) = 0$. The wave function $\phi_{n=0,m=0}(z, z^*)$ must therefore be the Gaussian with a prefactor that is both analytic and anti-analytic, i.e. a constant that is fixed by the normalisation. One finds

$$\phi_{n=0,m=0}(z, z^*) = \langle z, z^*|n = 0, m = 0\rangle = \frac{1}{\sqrt{2\pi l_B^2}}e^{-|z|^2/4l_B^2}, \tag{2.50}$$

and a lowest-LL state with arbitrary m may then be obtained with the help of Eq. (2.45),

$$\begin{aligned}\phi_{n=0,m}(z, z^*) &= \frac{i^m\sqrt{2^m}}{\sqrt{2\pi l_B^2 m!}}\left(\frac{z}{4l_B} - l_B\bar{\partial}\right)^m e^{-|z|^2/4l_B^2} \\ &= \frac{i^m}{\sqrt{2\pi l_B^2 m!}}\left(\frac{z}{\sqrt{2}l_B}\right)^m e^{-|z|^2/4l_B^2}.\end{aligned} \tag{2.51}$$

The states within the lowest LL are therefore, apart from the Gaussian, given by the usual polynomial basis states z^m of analytic functions. In an arbitrary LL, the states may be obtained in a similar manner, but they happen to be more complicated because the differential operators (2.49) no longer act on the Gaussian only but also on the polynomial functions. They may be expressed in terms on Laguerre polynomials.

To conclude the discussion about the wave functions in the symmetric gauge, we calculate the average value of the guiding-centre operator in the state $|n = 0, m\rangle$. With the help of Eqs. (2.32) and (2.38), one may express the components of the guiding-centre operator in terms of the ladder operators b and $b^\dagger$,

$$X = \frac{l_B}{i\sqrt{2}}(b^\dagger - b) \qquad 以及 \qquad Y = \frac{l_B}{\sqrt{2}}(b^\dagger + b), \tag{2.52}$$

and the ladder operators act, in analogy with Eq. (2.16), on the states $|n, m\rangle$ as

$$b^\dagger|n, m\rangle = \sqrt{m+1}|n, m+1\rangle \qquad 以及 \qquad b|n, m\rangle = \sqrt{m}|n, m-1\rangle.$$

The average value of the guiding-centre operator is therefore zero in the states $|n, m\rangle$,

$$\langle\mathbf{R}\rangle \equiv \langle n = 0, m|\mathbf{R}|n = 0, m\rangle = 0,$$

but we have

$$\langle|\mathbf{R}|\rangle = \left\langle\sqrt{X^2 + Y^2}\right\rangle = l_B\left\langle\sqrt{2b^\dagger b + 1}\right\rangle = l_B\sqrt{2m+1}. \tag{2.53}$$

This means that the guiding centre is situated, in a quantum state $|n, m\rangle$, somewhere on a circle of radius $l_B\sqrt{2m+1}$ whereas its angle (or phase) is completely undetermined.

The symmetric gauge is the natural gauge to describe a sample in the form of a disc. Consider the disc to have a radius R_{max} (and a surface $\mathcal{A} = \pi R_{max}^2$). How many quantum states may be accomodated within the circle? The quantum state with maximal m quantum number, which we call M, has a radius $l_B\sqrt{2M+1}$, which must naturally coincide with the radius R_{max} of the disc. One therefore obtains $\mathcal{A} = \pi l_B^2(2M+1)$, and the number of states within the disc is then, in the thermodynamic limit $M \gg 1$,

$$M = \frac{\mathcal{A}}{2\pi l_B^2} = n_B \times \mathcal{A} = N_B, \tag{2.54}$$

in agreement with the result (2.41) obtained from the argument based on the Heisenberg uncertainty relation.

2.4.2 Wave functions in the Landau gauge
Landau 规范下的波函数

If the sample geometry is rectangular, the Landau gauge (2.31), $\mathbf{A}_L(\mathbf{r}) = B(-y, 0, 0)$, is more appropriate than the symmetric gauge to describe the physical system. As already mentioned above, the momentum $p_x = \hbar k$ is a good quantum number due to translational invariance in the x-direction. One may therefore use a plane-wave ansatz

$$\psi_{n,k}(x, y) = \frac{e^{ikx}}{\sqrt{L}} \chi_{n,k}(y),$$

for the wave functions. In this case, the Hamiltonian (2.7) becomes

$$H_S^B = \frac{(p_x - eBy)^2}{2m} + \frac{p_y^2}{2m} = \frac{p_y^2}{2m} + \frac{1}{2} m\omega_C (y - y_0)^2, \tag{2.55}$$

where we have defined

$$y_0 = k l_B^2. \tag{2.56}$$

The Hamiltonian (2.55) is nothing other than the Hamiltonian of a one-dimensional oscillator centred around the position y_0, and the eigenstates are

$$\chi_{n,k}(y) = H_n\left(\frac{y - y_0}{l_B}\right) e^{-(y-y_0)^2/4l_B^2},$$

in terms of Hermite polynomials $H_n(x)$ [28]. The coordinate y_0 plays the role of the guiding centre component Y, the component X being smeared over the whole sample length L, as it is dictated by the Heisenberg uncertainty relation resulting from the commutation relation (2.39) $[X, Y] = il_B^2$.

Using periodic boundary conditions $k = m \times 2\pi/L$ for the wave vector in the x-direction, one may count the number of states in a rectangular surface of length L and width W (in the y-direction), similarly to the above arguments in the symmetric gauge. Consider the sample to range from $y_{min} = 0$ to $y_{max} = W$, the first corresponding via the above-mentioned condition (2.56) to the wave vector $k = 0$ and the latter to a wave vector $k_{max} = M \times 2\pi/L$. Two neighbouring quantum states are separated by the distance $\Delta y = \Delta k l_B^2 = \Delta m (2\pi/L) l_B^2 = 2\pi l_B^2/L$, and each state therefore occupies a surface $\sigma = \Delta y \times L = 2\pi l_B^2$, which agrees with the result (2.40) obtained above with the help of the consideration based on the Heisenberg uncertainty relation. The total number of states is, as in the symmetric gauge and the general argument leading to Eq. (2.41),

$$M = N_B = n_B \times LW = n_B \times \mathcal{A},$$

i.e. the number of flux quanta threading the (rectangular) surface $\mathcal{A} = LW$.

Chapter 3

Integer Quantum Hall Effect
整数量子 Hall 效应

The quantum-mechanical treatment of the 2D electron in a perpendicular magnetic field is the backbone for the understanding of the basic properties of the quantum Hall effect. However, we need to relate the kinetic-energy quantisation to the resistance quantisation, which is the essential feature of the IQHE. In the present chapter, we discuss the transport properties of electrons in the IQHE, namely the somewhat mysterious role that disorder plays in this type of transport. Remember from the introduction that the Hall resistance is quantised with an astonishingly high precision (10^{-9}), such that it is now used as the standard of resistance [see Eq. (1.13)]. The resistance quantisation in the IQHE therefore does reflect neither a particular disorder distribution nor a particular sample geometry. Nevertheless, disorder turns out to play an essential role in the occurence of the IQHE, as we will see in this chapter.

We will first consider, in Sec. 3.1, the motion of a 2D electron in a perpendicular magnetic field when also an external electrostatic potential is present, such as the one generated by disorder or the confinement potential that defines the sample boundaries. In Sec. 3.2, we then calculate the conductance of a single LL within a mesoscopic picture and discuss the difference between a two-terminal and a six-terminal transport measurement in Sec. 3.3. Furthermore, we discuss, in Sec. 3.4, the IQHE within a percolation picture and present some scaling properties that characterise the plateau transitions. We terminate this chapter with a short discussion of the pecularities of the relativistic quantum Hall effect in graphene the understanding of which requires essentially the same ingredients as the IQHE in non-relativistic quantum Hall systems.

3.1 Electronic Motion in an External Electrostatic Potential
外静电势下电子的运动

We consider a system the length L of which is much larger than the width W (see 图. 3.1). This may be modeled by a confinement potential $V_{\text{conf}}(y)$ that only depends on the y-direction, i.e. the system remains translation-invariant in the x-direction with respect to this potential.[1] In addition to the confinement, we consider a smoothly varying electrostatic potential $V_{\text{imp}}(x, y)$ that is caused by the impurities in the sample. This impurity potential breaks the translation invariance in the x-direction as well as that in the y-direction, which is already broken by the confinement potential. The Hamiltonian of a 2D particle in a perpendicular magnetic field then needs to be completed by a potential term

$$V(\mathbf{r}) = V_{\text{conf}}(y) + V_{\text{imp}}(x, y), \tag{3.1}$$

which creates a potential landscape that is schematically depicted in 图. 3.1.

[1] Naturally, the system is also confined in the x-direction, but since we consider a sample with $L \gg W$, the system appears as translation-invariant in the x-direction when one considers intermediate length scales. The latter may be taken into account with the help of periodic boundary conditions that discretise the wave vector in the x-direction, as we have seen in the preceding chapter within the quantum-mechanical treatment of the 2D electron in the Landau gauge (see Sec. 2.4.2).

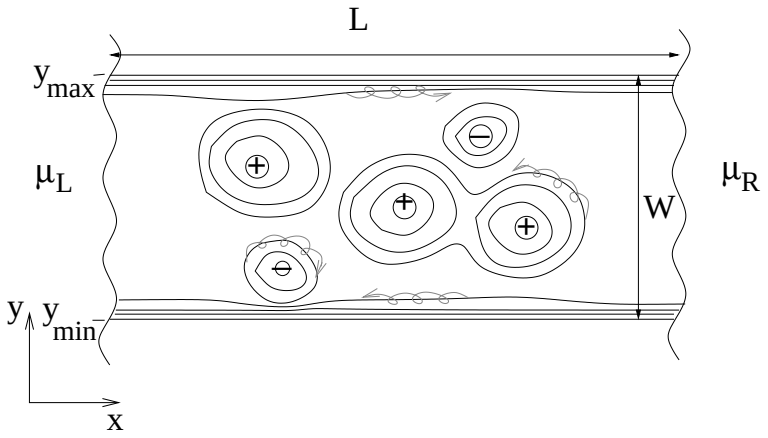

图 3.1: Potential landscape of an electrostatic potential in a sample. The metallic contacts are described by the chemical potentials μ_L and μ_R for the left and right contacts, respectively. We consider $L \gg W \gg \xi \gg l_B$, where ξ is the typical length scale for the variation of the electrostatic potential. The sample is confined in the y-direction between y_{max} and y_{min}. The thin lines indicate the equipotential lines. When approaching one of the sample edges, they become parallel to the edge. The grey lines indicate the electronic motion with the guiding centre moving along the equipotential lines. The electron turns clockwise around a summit of the potential landscape, which is caused e.g. by a negatively charged impurity (−), and counter-clockwise around a valley (+). At the sample edges, the equipotential lines due to the confinement potential connect the two contacts on the left and on the right hand side.

3.1.1 Semi-classical treatment
半经典处理

In a first step, we consider a potential $V(\mathbf{r})$ that varies smoothly on the scale set by the magnetic length, i.e. $\xi \gg l_B$, where ξ describes the characteristic length scale for the variation of $V(\mathbf{r})$. Notice first that the external electrostatic potential *lifts the LL degeneracy* because the Hamiltonian $H = H_B + V(\mathbf{r} = \mathbf{R} + \boldsymbol{\eta})$ no longer commutes with the guiding-centre operator $\mathbf{R}$, in contrast to the "free" Hamiltonian H_B, $[H, \mathbf{R}] = [V, \mathbf{R}] \neq 0$. Physically, this is not unexpected: the guiding centre is a constant of motion due to translation invariance, i.e. it does not matter whether the electron performs its cyclotron motion around a point $\mathbf{R}_1$ or $\mathbf{R}_2$ in the 2D plane as long as the cyclotron radius is the same. However, the electrostatic potential $V(\mathbf{r})$ breaks this translation invariance and thus lifts the degeneracy associated with the guiding centre.

In the case where the electrostatic potential varies smoothly on a length scale set by the magnetic length and does not generate LL mixing, i.e. when $|\nabla V| \ll \hbar\omega_C/l_B$, we may approximate the argument $\mathbf{r}$ in the potential (3.1) by the guiding-centre variable $\mathbf{R}$,[2]

$$V(\mathbf{r}) \simeq V(\mathbf{R}). \tag{3.2}$$

Notice that this approximation may seem unappropriate when we consider the confinement potential in the y-direction which may vary abruptly when approaching the sample edges. The confinement potential with translation invariance in the x-direction will be discussed separately in the following subsection.

As a consequence of the non-commutativity of the potential term $V(\mathbf{R})$ with the guiding-centre operator, the latter quantity acquires dynamics, as may be seen from the Heisenberg equations of motion

$$\begin{aligned} i\hbar\dot{X} &= [X, H] = [X, V(\mathbf{R})] = \frac{\partial V}{\partial Y}[X, Y] = il_B^2 \frac{\partial V}{\partial Y} \\ i\hbar\dot{Y} &= [Y, V(\mathbf{R})] = -il_B^2 \frac{\partial V}{\partial X}, \end{aligned} \tag{3.3}$$

[2]This approximation may be viewed as the first term of an expansion of the electrostatic potential in the coherent (or vortex) state basis, where the states are maximally localised around the guiding-centre position $\mathbf{R}$ [33].

i.e. $\dot{\mathbf{R}} \perp \nabla V$. Here, we have used the commutation relation (2.39) for the guiding-centre components and Eq. (2.10). The Heisenberg equations of motion are particularly useful in the discussion of the semi-classical limit because the averaged equations satisfy the classical equations of motion,

$$\langle \dot{\mathbf{R}} \rangle \perp \nabla V, \tag{3.4}$$

which means that, within the semi-classical picture, *the guiding centres move along the equipotential lines of the smoothly varying external electrostatic potential*. This feature, which is also called the *Hall drift*,

$$\mathbf{v}_D = \frac{\mathbf{E} \times \mathbf{B}}{B^2} = \langle \dot{\mathbf{R}} \rangle = \frac{-\nabla V \times \mathbf{B}}{eB^2}, \tag{3.5}$$

in terms of the (local) electric field $\mathbf{E} = -\nabla V/e$, is depicted in 图. 3.1 by the grey lines.

In the bulk, the potential landscape is created by the charged impurities in the sample, and the electrons turn clockwise on an equipotential line around a summit that is caused by a negatively charged impurity and counter-clockwise around a valley created by a positively charged impurity. If the equipotential lines are closed, as it is the case for most of the equipotential lines in a potential landscape,[3] an electron cannot move from one point to another one over a macroscopic distance, e.g. from one contact to the other one. An electron moving on a closed equipotential line can therefore not contribute to the electronic transport, and the electron is thus *localised*. Notice that this type of localisation it different from other popular types. Anderson localisation in 2D, e.g., is due to quantum interferences of the electronic wave functions [34]. Here, however, the localisation is a purely *classical* effect. The high-field localisation is also different from the interaction-driven Mott insulator, where the electrons freeze out in order to minimise the mutual Coulomb repulsion between the electrons.

At the edge, the equipotential lines reflect the confinement potential, which is zero in the bulk but rapidly increases when approaching the sample edge at y_{min} and y_{max} (see 图. 3.1). In this case, the equipotential lines are open and therefore connect the two different electronic contacts. The electrons occupying quantum states at these equipotential lines then contribute to the electronic transport, in contrast to those on closed equipotential lines in the bulk. These quantum states are called *extended states*,[4] as opposed to the *localised states* discussed above. The difference between localised and extended states turns out to be essential in the understanding of the IQHE, as we will see below (Sec. 3.4).

3.1.2 Electrostatic potential with translation invariance in the x-direction
x-平移对称性的静电势

Although the above semi-classical considerations yield the correct physical picture of localised and extended states, it is based on the assumption that the electrostatic potential varies smoothly on the scale set by the magnetic length, such that we may replace the electron's position by that of its guiding centre [Eq. (3.2)]. This assumption is, however, problematic in view of the confinement potential which varies strongly at the sample edges, i.e. in the vicinity of y_{min} and y_{max}. We will therefore treat the y-dependent confinement potential in a quantum treatment. Naturally, the appropriate gauge for the quantum-mechanical treatment is the Landau gauge (2.31), which respects the translation invariance in the x-direction, and the Hamiltonian (2.55) becomes

$$H = \frac{p_y^2}{2m} + \frac{1}{2} m\omega_C (y - y_0)^2 + V_{\text{conf}}(y). \tag{3.6}$$

Remember that for a fixed wave vector k in the x-direction, the position around which the one-dimensional harmonic oscillator is centred is fixed by Eq. (2.56), $y_0 = kl_B^2$. We may therefore expand the confinement

[3] In order to illustrate this point, consider a hiking tour in the mountains, e.g. around Les Houches in the French Alps. To go from one point to another one at the same height, one usual needs go downhill as well as uphill. It is very rare to be able to stay on the same height unless one wants to turn in circles that are just the closed countour lines which correspond to closed equipotential lines in our potential landscape. For those who participated at the Les Houches session which was outsourced to Singapore, where there are no mountains and where the whether is anyway too hot for hiking, just look at a hiking map of some mountainous region. Then search for countour lines that connect one border of the map to the opposite border. It turns out to be very hard to find such lines as compared to a large number of closed countour lines.

[4] In the semi-classical picture the extended states are also called *skipping orbits*.

potential, even in the case of a strong variation, around this position,

$$V(y) \simeq V(y_0 = kl_B^2) - eE(y_0)(y - y_0) + \mathcal{O}\left(\frac{\partial^2 V}{\partial y^2}\right),$$

where the local electric field is given in terms of the first derivative of the potential at y_0,

$$eE(y_0) = -\left.\frac{\partial V_{\text{conf}}}{\partial y}\right|_{y_0}.$$

This expansion yields the Hamiltonian

$$H = \frac{p_y^2}{2m} + \frac{1}{2}m\omega_C(y - y_0')^2 + V_{\text{conf}}(y_0) - \frac{1}{2}mv_D^2(y_0),$$

where the local drift velocity reads $v_D = E(y_0)/B$ and the position of the harmonic oscillator is shifted, $y_0 \to y_0' = y_0 + eE(y_0)/m\omega_C^2$. Notice that the last term is quadratic in the electric field $E(y_0)$ and therefore a second-order term in the expansion of the confinement potential. We neglect this term in the following calculations. The final Hamiltonian then reads

$$H = \frac{p_y^2}{2m} + \frac{1}{2}m\omega_C(y - y_0')^2 + V_{\text{conf}}(y_0'), \tag{3.7}$$

where we have replaced the argument y_0 by the shifted harmonic-oscillator position y_0', which is valid at first order in the expansion of the confinement potential. One therefore obtains the energy spectrum

$$\epsilon_{n,y_0} = \hbar\omega_C\left(n + \frac{1}{2}\right) + V(y_0), \tag{3.8}$$

where we have omitted the prime at the shifted harmonic-oscillator position to simplify the notation. One therefore obtains the same LL spectrum as in the absence of a confinement potential, apart from an energy shift that is determined by the value of the confinement potential at the harmonic-oscillator position, which may indeed vary strongly. This position y_0 plays the role of the guiding-centre position, as we have already mentioned in the last chapter, where we have calculated the electronic wave functions in the Landau gauge (2.4.2). One thus obtains a result that is consistent with the semi-classical treatment presented above.

3.2 Conductance of a Single Landau Level
单一 Landau 能级的电导

We now calculate the conductance of a completely filled LL for the geometry depicted in 图. 3.1, i.e. when all quantum states (described within the Landau gauge) of the n-th LL are occupied. In a first step, we calculate the current of the n-th LL, which flows from the left to the right contact, with the help of the formula [35]

$$I_n^x = -\frac{e}{L}\sum_k \langle n, k|v_x|n, k\rangle, \tag{3.9}$$

i.e. as the sum over all N_B quantum channels labelled by the wave vector $k = 2\pi m/L$, with the velocity

$$\langle n, k|v_x|n, k\rangle = \frac{1}{\hbar}\frac{\partial \epsilon_{n,k}}{\partial k} = \frac{L}{2\pi\hbar}\frac{\Delta\epsilon_{n,m}}{\Delta m},$$

in terms of the dispersion relation (3.8).[5] Notice that the velocity in the y-direction is zero because the energy does not disperse as a function of the y-component of the wave vector. The above expression is

[5] This relation may be obtained from the Heisenberg equations of motion, $i\hbar\dot{x} = [x, H] = (\partial H/\partial p_x)[x, p_x] = i\partial H/\partial k$, where we have used Eq. (2.10) and $p_x = \hbar k$. One therefore obtains the operator equation

$$\dot{x} = \frac{1}{\hbar}\frac{\partial H}{\partial k},$$

which we evaluate in the state $|n, k\rangle$. In the last step we have used the periodic boundary conditions.

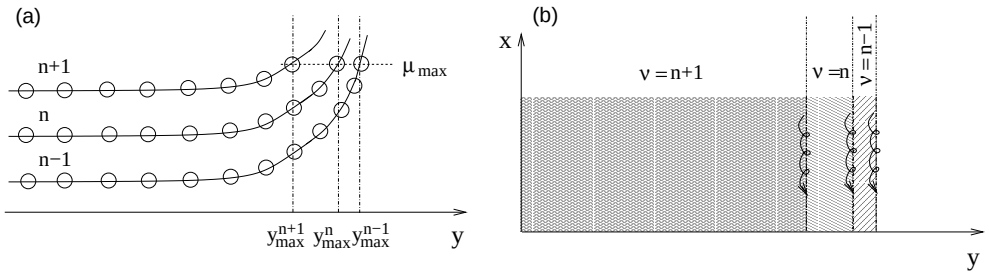

图 3.2: Edge states. *(a)* The LLs are bent upwards when approaching the sample edge, which may be modeled by an increasing confinement potential. One may associate with each LL n a maximal value y^n_{max} of the y-component where the LL crosses the chemical potential μ_{max}. *(b)* At each position y^n_{max}, the filling factor decreases by a jump of 1. The n-th edge state is associated with the jump at y^n_{max} and the gradient of the confinement potential imposes a direction to the Hall drift of this state *(chirality)*. This chirality is the same for all edge states at the same edge.

readily evaluated with $\Delta m = 1$, and one obtains

$$\langle n,k|v_x|n,k\rangle = \frac{L}{h}\left(\epsilon_{n,m+1} - \epsilon_{n,m}\right).$$

With the help of this expression, the current (3.9) of the n-th LL becomes

$$I_n = -\frac{e}{L}\sum_m \frac{L}{h}\left(\epsilon_{n,m+1} - \epsilon_{n,m}\right),$$

and one notices that all terms in the sum cancel apart from the boundary terms $\epsilon_{n,m_{min}}$ and $\epsilon_{n,m_{min}}$, which correspond to the chemical potentials μ_{min} and μ_{max}, respectively. The difference between these two chemical potentials may be described in terms of the (Hall) voltage V between the upper and the lower edge, $\mu_{max} - \mu_{min} = -eV$. One thus obtains the final result

$$I_n = -\frac{e}{h}\left(\mu_{max} - \mu_{min}\right) = \frac{e^2}{h}V. \tag{3.10}$$

This means that each LL contributes one *quantum of conductance* $G_n = e^2/h$ to the electronic transport and n completely filled LLs contribute a conductance[6]

$$G = \sum_{n'=0}^{n-1} G_{n'} = n\frac{e^2}{h}. \tag{3.11}$$

Notice furthermore that this is a particular example of the Landauer-Büttiker formula of quantum transport

$$G_n = \frac{e^2}{h}T_n$$

through a conduction channel n, where T_n is the transmission coefficient of the channel [36, 35, 37]. Because $T_n + R_n = 1$, in terms of the reflexion coefficient, the above result (3.10) indicates that each filled LL may be viewed as a conduction channel with perfect transmission $T_n = 1$, i.e. where an injected electron is not reflected or backscattered.

3.2.1 Edge states
边界态

The astonishing feature of perfect transmission, which is independent of the length L (or more precisely of the aspect ratio L/W, see the discussion in Sec. 1.1.2 of the introduction) or the particular geometry of

[6]Notice that, because the lowest LL is labelled by $n' = 0$, the last one has the index $n-1$ in the case of n completely filled levels.

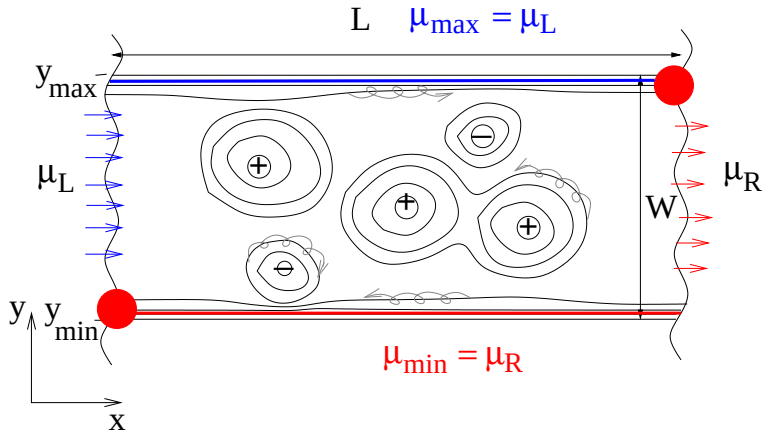

图 3.3: Two-terminal measurement. The current is driven through the sample via the left and the right contacts, where one also measures the voltage drop and thus a resistance. The upper edge is in thermodynamic equilibrium with the left contact (blue), whereas the lower one is in equilibrium with the right contact (red). The chemical potential drops abruptly when the upper edge reaches the right contact, and when the lower edge reaches the left contact. Dissipation occurs in these hot spots (red dots). The measured resistance between the two contacts thus equals the Hall resistance.

the sample, may be understood from the edge-state picture which we have introduced above (see 图. 3.2). Consider the upper edge, without loss of generality. The current-transporting edge state of the n-th LL is the one situated at y^n_{max}, where the n-th LL crosses the Fermi energy and where the filling factor jumps from $\nu = n+1$ to n.[7] Due to the upward bent of the confinement potential a particular direction is imposed on the electronic motion, which is nothing other than the Hall drift (see 图. 3.1). This uni-directional motion is also called *chirality* of the edge state. Notice that this is the same chirality which one expects from the semi-classical expression (3.5) for the drift velocity. The chirality is the same for all edge states n at the same sample edge where the gradient of the confinement potential does not change its direction. Therefore, even if an electron is scattered from one channel n to another one n' at the same edge it does not change its direction of motion, and the electron cannot be backscattered unless it is scattered to the opposite edge with inverse chirality. However, in a usual quantum Hall system, the opposite edges are separated by a macroscopic distance $\sim W$, and backscattering processes are therefore strongly (exponentially) suppressed in the ratio l_B/W between the magnetic length, which determines the spatial extension of quantum-mechanical state, and the macroscopic sample width W. Notice that the quantum Hall system at integer filling factors $\nu = n$ is therefore a very unusual electron liquid: it is indeed a bulk insulator with perfectly conducting (non-dissipative) edges.

3.3 Two-terminal versus Six-Terminal Measurement
两端 vs 六端法测量

3.3.1 Two-terminal measurement
两端法测量

In the preceding section Sec. (3.2), we have calculated the conductance of a single LL (and n filled LLs) within a so-called two-terminal measurement, where we inject a current in the left contact with chemical potential μ_L and collect the outcoming current at the right contact with μ_R. As a consequence of Eq. (3.10), this current builds up a voltage V between the upper and the lower sample edge. This voltage drop is therefore

[7] Strictly speaking the filling factor does not jump not abruptly when one takes interactions between the electrons into account. In this case, two incompressible strips, of $\nu = n+1$ and $\nu = n$ are separated by a *compressible* strip of finite width. The picture of chiral electron transport remains, however, essentially the same when considering such compressible regions.

associated with a Hall resistance, which is the inverse of the conductance $G = ne^2/h$,

$$R_H = G^{-1} = \frac{h}{e^2}\frac{1}{n} , \tag{3.12}$$

and which coincides with the contact (or interface) resistance of a mesoscopic system [37]. However, the voltage drop V_L between the left and the right contact is given by the difference of the chemical potentials in the contacts, $\mu_R - \mu_L = -eV_L$, and the associated longitudinal resistance V_L/I is non-zero, in contrast to what we have seen in the introduction. This is due to the fact that the difference between the longitudinal and the Hall resistance is not clearly defined in such a two-terminal measurement.

This feature may be understood from 图. 3.3. Indeed, due to the above-mentioned absence of backscattering, the chemical potential is constant along a sample edge, but there is a potential difference between the two edges. This means that the chemical potential must change somewhere along the edge. Consider the upper edge that is fed with electrons by the left contact, i.e. the upper edge is in thermodynamic equilibrium with the left contact and the chemical potentials therefore coincide, $\mu_L = \mu_{max}$ (see Fig.3.3). Now, when the upper edge touches the right contact which is at a different chemical potential μ_R, the chemical potential of the upper edge must rapidly relax to be in equilibrium with the right contact. In the same manner, the lower edge is in equilibrium with the right contact, $\mu_{\min} = \mu_R$, and abruptly changes when touching the left contact. The rapid change in the chemical potential is associated with a dissipation of energy (at so-called *hot spots*) that has been observed experimentally [38]. In this experiment, the sample was put in liquid helium and the heating at the hot spots caused a local vaporisation of the helium observable in form of a fountain of gas bubbles.

Due to the equivalence of the chemical potentials $\mu_L = \mu_{max}$ and $\mu_{\min} = \mu_R$, the voltage drops V, between the upper and the lower edge, and V_L between the current contacts are equal, $V = V_L$. An unexpected consequence of this equation is that in a resistance measurement between the two contacts, in the two-terminal configuration, the two-terminal resistance equals the Hall resistance,

$$R_{R-L} = R_H = \frac{h}{e^2}\frac{1}{n} , \tag{3.13}$$

and *not* the (vanishing) longitudinal resistance, when the bulk is insulating (at $\nu = n$).

3.3.2 Six-terminal measurement
六端法测量

A more sophisticated geometry that allows for the simulaneous measurement of a well-defined longitudinal and Hall resistance is the six-terminal geometry, with two additional contacts at the upper and two at the lower edge [see 图. 3.4(a)]. These additional contacts (2 and 3 at the upper and 5 and 6 at the lower edge, the left and the right contacts being labelled by 1 and 4, respectively) are used to measure a voltage, i.e. they have ideally an infinitely high internal resistance to prevent electrons to leak out of or into the sample. The chemical potential therefore remains constant at the upper edge $\mu_L = \mu_2 = \mu_3$, as well as that at the lower edge $\mu_R = \mu_5 = \mu_6$, and one measures a zero-resistance, $R_L = (\mu_2 - \mu_3)/eI = (\mu_5 - \mu_6)/eI = 0$, as one expects from the calculation of the conductance through n LLs (see Sec. 3.11), which is entirely transverse. The conductance matrix is thus off-diagonal, as well as the resistance matrix,

$$G = \begin{pmatrix} 0 & n\frac{e^2}{h} \\ -n\frac{e^2}{h} & 0 \end{pmatrix} \qquad 以及 \qquad R = \begin{pmatrix} 0 & -\frac{h}{e^2}\frac{1}{n} \\ \frac{h}{e^2}\frac{1}{n} & 0 \end{pmatrix}, \tag{3.14}$$

and one precisely measures the diagonal elements of the resistance matrix, the longitudinal resistance, between the contacs 3 and 2 (or 6 and 5). The off-diagonal elements, i.e. the Hall resistance, may e.g. be measured between the contacts 5 and 3 [as shown in 图. 3.4(a)], and one measures then the result $R_H = G_n^{-1} = h/e^2 n$ obtained from the calculation presented in Sec. 3.11 because of the voltage drop $V = (\mu_L - \mu_R)/e = (\mu_3 - \mu_3)/e$ between the upper and the lower edge.

Finally we mention that there exists an intermediate geometry that consists of four terminals (van-der-Pauw geometry), where the resistance measurements are equally well defined [图. 3.4(b)]. If one labels the contacts from 1 to 4 in a clockwise manner, one may measure a Hall resistance between the contacts 2 and

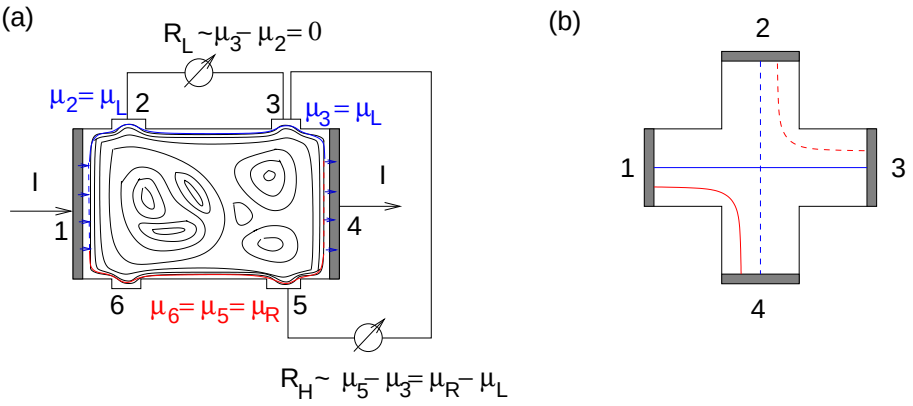

図 3.4: *(a)* Six-terminal measurement. The current I is driven through the sample via the contacts 1 and 4. Between these two contacts the chemical potential on the upper edge μ_L (blue) does not vary because the electrons do not leak out or in at the contacts 2 and 3, where one measures the longitudinal resistance. In the same manner, the chemical potential μ_R (red) remains constant between the contacts 5 and 6 on the lower edge. The longitudinal resistance measured between 2 and 3 as well as between 5 and 6 is therefore $R_L = (\mu_2 - \mu_3)/eI = (\mu_5 - \mu_6)/eI = 0$. The Hall resistance is determined by the potential difference between the two edges and thus measured, e.g. between the contacts 5 and 3, where $\mu_5 - \mu_3 = \mu_R - \mu_L$, and thus $R_H = (\mu_3 - \mu_5)/eI$. *(b)* Four-terminal measurement in the van-der-Pauw geometry. In a Hall-resistance measurement, one drives a current through the sample via the contacts 1 and 3 (connected by the continuous blue line) and measures the Hall resistance via the contacts 2 and 4 (dashed blue line). In a measurement of the longitudinal resistance, the current is driven through the sample via the contacts 1 and 4 (continuous red line) and one measures a resistance between the contacts 2 and 3 (connected by the dashed red line).

3 while driving a current through the sample by the contacts 1 and 3 [blue lines in 図. 3.4(b)]. In this case, one may use the clear topological definition mentioned at the beginning of the introduction. If one connects the contacts 2 and 3 by an imaginary line through the sample (dashed blue line) it necessarily crosses the imaginary line (continuous blue) which connects the current contacts 1 and 3 through the sample. This is precisely the topological definition of a Hall-resistance measurement.

Similarly, one may measure the longitudinal resistance between the contacts 2 and 3 if one drives a current through the sample via the contacts 1 and 4. In this case, the imaginary line (dashed red) which connects the contacts 2 and 3 where one measures a resistance does not need to cross the line (continuous red) between the contacts 1 and 4 at which one injects and collects the current, respectively. As we have already mentioned at the beginning of the introduction, this defines topologically a measurement of the longitudinal resistance.

These considerations show that a resistance measurement, although it does not depend on the microscopic details of the sample, depends nevertheless on the geometry in which the contacts are placed at the sample [39, 35]. This aspect is often not sufficiently appreciated in the literature, namely the fact that one measures, in a two-terminal geometry, a Hall resistance between the contacts that are used to inject and collect the current and not a longitudinal resistance, as one may have expected naively, when the system is in the IQHE condition.

3.4 The Integer Quantum Hall Effect and Percolation

Until now we have shown that the Hall resistance is quantised [Eq. (3.12)] when n LLs are completely filled, i.e. when the filling factor is exactly $\nu = n$. However, we have not yet explained the occurence of plateaus in the Hall resistance, i.e. a Hall resistance that remains constant even if one varies the filling factor, e.g. by sweeping the magnetic field, around $\nu = n$.[8] In order to explain the constance of the Hall resistance

[8]Strictly speaking, we have not gained anything because the quantum treatment allows us only to determine the Hall resistance at certain points of the Hall curve, those at the magnetic fields corresponding to $\nu = hn_{el}/eB = n$. If we substitute

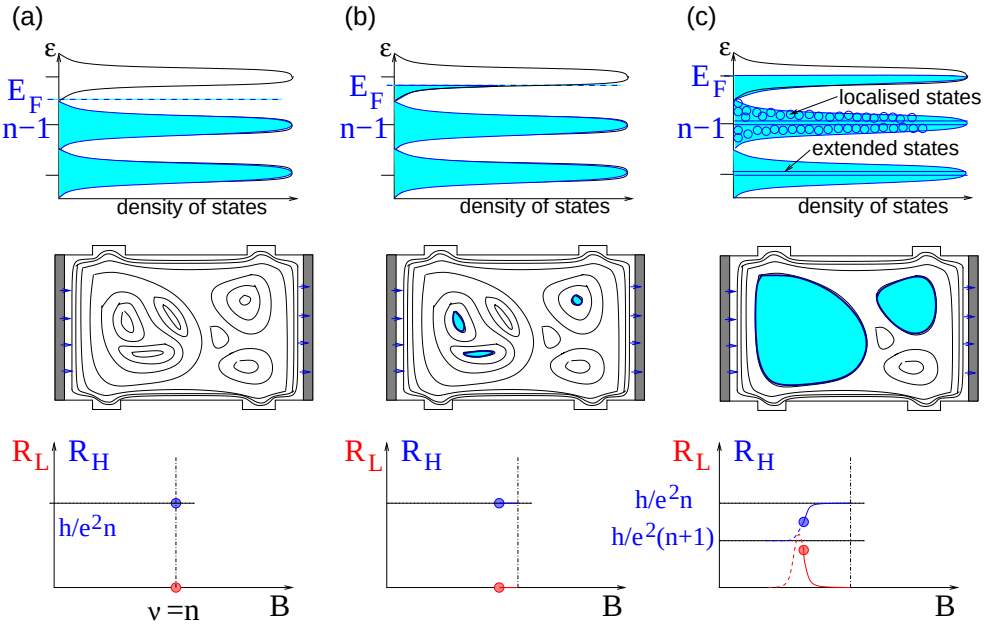

图 3.5: Quantum Hall effect. The (impurity-broadened) density of states is shown in the first line for increasing fillings (a) - (c) described by the Fermi energy E_F. The second line represents the impurity-potential landscape the valleys of which become successively filled with electrons when increasing the filling factor, i.e. when lowering the magnetic field at fixed particle number. The third line shows the corresponding Hall (blue) and the longitudinal (red) resistance measured in a six-terminal geometry, as a function of the magnetic field. The first figure in column (c) indicates that the bulk extended states are in the centre of the DOS peaks, whereas the localised states are in the tails.

over a rather large interval of magnetic field around $\nu = n$, we need to take into account the semi-classical localisation of additional electrons (or holes) described in Sec. 3.1. This is shown in 图. 3.5, where we represent the filling of the LLs (first line), the potential landscape of the last partially-filled level (second line) and the resistances as a function of the magnetic field, measured in a six-terminal geometry (third line). We start with the situation of n completely filled LLs [column (a) of 图. 3.5], which we have extensively discussed above: the LL n (and its potential landscape) is unoccupied.[9] In a six-terminal measurement, one therfore measures the Hall resistance $R_H = h/e^2 n$ and a zero longitudinal resistance, as we have seen in Eq. (3.14).

In column (b) of 图. 3.5, we represent the situation where the LL n gets moderately filled by electrons when the magnetic field B is decreased. These electrons in n populate preferentially the valleys of the potential landscape, or more precisely the closed equipotential lines that enclose these valleys. The electrons in the LL n are thus (classically) localised somewhere in the bulk and do not affect the global transport characteristics, measured by the resistances, because they are not probed by the sample contacts. Therefore, the Hall resistance remains unaltered and the longitudinal resistance remains zero despite the change of the magnetic field. This is the origin of the plateau in the Hall resistance.

If one continues to lower the magnetic field, the regions of the potential landscape in the LL n occupied by electrons become larger, and they are eventually enclosed by equipotential lines that pass through the bulk and that connect the opposite edges. In this case, an electron injected at the left contact and travelling a certain distance at the upper edge may jump into the state associated with this equipotential line and thus reach the lower edge. Due to its chirality, the electron is then backscattered to the left contact, which causes

the filling factor in Eq. (3.12), we see immediately that $R_H = h/e^2\nu = B/en_{el}$, i.e. one retrieves the *classical* result for the Hall resistance.

[9] Remember that due to the label 0 for the lowest LL, all LLs with $n' = 0, ..., n-1$ are the completely filled and the LL n is then the lowest *unoccupied* level.

an increase in the longitudinal resistance. Indeed, if one measures the resistance between the two contacts at the lower edge, a potential drop is caused by the electron that leaks in from this equipotential connecting the upper and the lower edge. It is this potential drop that causes a non-zero longitudinal resistance. At the same moment the Hall resistance is no longer quantised and jumps to the next (lower) plateau, a situation that is called *plateau transition*. This situation of electron-filled equipotential lines connecting opposite edges, which are thus *extended states* [see first line of 図. 3.5(c)] as opposed to the bulk *localised states*, arises when the LL n is approximately half-filled. Notice that these extended states, which are found in the centre of the DOS peaks [see upper part of 図. 3.5(c)], are bulk states in contrast to the above-mentioned edge states, which are naturally also extended

The clean jump in the Hall resistance at the plateau transition accompanied by a peak in the longitudinal one is only visible in the six- (or four-)terminal measurement. As we have argued in Sec. 3.3.2, there is no clear cut between the longitudinal and the Hall resistivity in the two-terminal configuration, where the resistance measured between the current contacts is indeed quantised in the IQHE. At the plateau transition, however, the chemical potential at the edges is no longer constant because of backscattered electrons and the resistance is no longer quantised. One observes indeed the resistance peak associated with the *longitudinal* resistance in the six- or four-terminal configuration. As a consequence, one measures, at the plateau transition, the superposition of the Hall and the longitudinal resistances.

If one increases even more the filling of the LL n, the same arguments apply but now in terms of *hole states*. The Hall resistance is quantised as $R_H = h/e^2(n+1)$, and the holes (i.e. the lacking electrons with respect to $n+1$ completely filled LLs) get localised in states at closed equipotential lines around the potential summits. As a consequence, the longitudinal resistance drops to zero again.

3.4.1 Extended and localised bulk states in an optical measurement

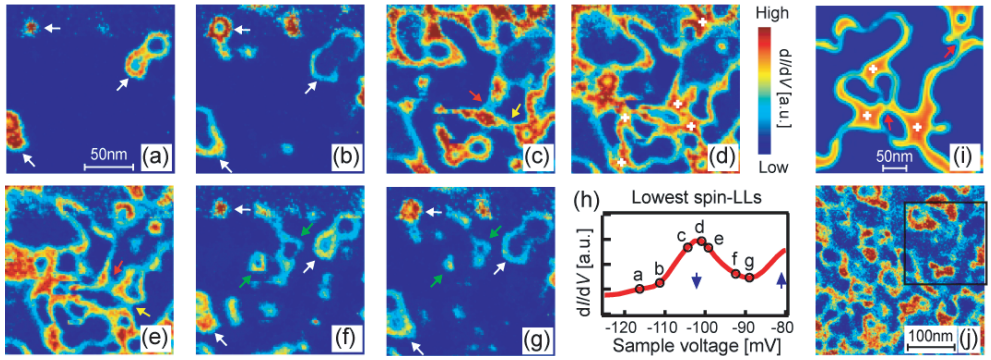

図 3.6: STS measurements by Hashimoto *et al.*, 2008, on a 2D electron system on a n-InSb surface. The figures (a) - (g) show the local DOS at various sample voltages, around the peak obtained from a dI/dV measurement (h). Figure (i) shows a calculated characteristic LDOS, and figure (j) an STS result on a larger scale.

The physical picture presented above, in terms of localised and extended bulk states, has recently been confirmed in scanning-tunneling spectroscopy (STS) of a 2D electron system that was prepared on an n-InSb surface instead of the more common GaAs/AlGaAs heterostructure [40]. Its advantage consists of its accessibility by an "optical" (surface) measurement that cannot be performed if the 2D electron gas is buried deep in a semiconductor heterostructure. In an STS measurement one scans the sample and thus measures the *local* density of states at a certain energy that can be tuned via the voltage between the tip of the electron microscope and the sample. When measuring the differential conductance dI/dV, which is proportional to the DOS, one observes a peak that corresponds to the centre of a LL [図. 3.6(h)] where the extended states are capable of transporting a current between the different electric contacts, as mentioned above. Whereas the quantum states at energies corresponding to closed equipotential lines of the impurity landscape are clearly visible as closed orbits in 図. 3.6(a),(b) and (f),(g), the states in the vicinity of the peak are more and

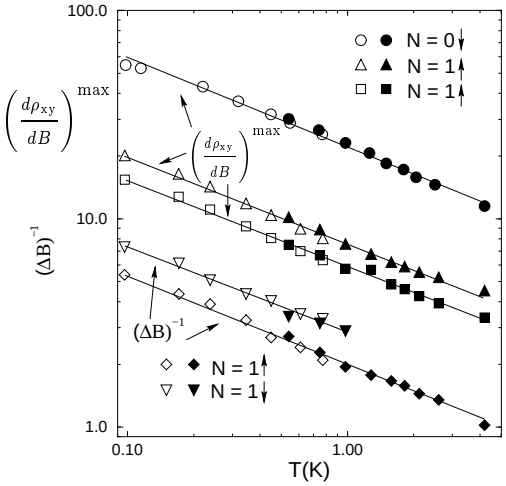

图 3.7: Experiment by Wei *et al.*, 1988. The width of the transition ΔB and of the derivative of the Hall resisitivity $\partial\rho_{xy}/\partial B$, measured as a function of temperature, reveals a scaling law with an exponent $1/z\nu = 0.42 \pm 0.04$, for the transition between the filling factors $1 \to 2$ ($N = 0\downarrow$), $2 \to 3$ ($N = 1\uparrow$) and $3 \to 4$ ($N = 1\downarrow$).

more extended, as shown by the spaghetti-like lines in Figs. 3.6(c),(d) and (e), as one would expect from the arguments presented above.

3.4.2 Plateau transitions and scaling laws
平台期的转移与标度变换律

The physical picture presented above suggests that the plateau transition in the Hall resistance is related to a *percolation* transition, where initially separated electron-filled valleys start to percolate between the opposite sample edges beyond a certain threshold of the filling. Because of the second-order character of a percolation transition, this scenario suggests that the plateau transition is a *second-order quantum phase transition* described by universal scaling laws, where the control parameter is just the magnetic field B [41, 42]. We finish this chapter on the IQHE with a brief overview over these scaling laws, and refer the interested reader to the literature [41, 42] and the class given by G. Batrouni at the same Singapore session of Les Houches Summer School 2009.[10]

The phase transition occurs at the critical magnetic field B_c and is characterised by an algebraically diverging correlation length

$$\xi \sim |B - B_c|^{-\nu}\,, \tag{3.15}$$

where ν is called the *critical exponent*.[11] In the same manner, the temporal fluctuations are described by a correlation "length" ξ_τ that is related to the spatial correlation length ξ,

$$\xi_\tau \sim \xi^z \sim |B - B_c|^{-z\nu}\,, \tag{3.16}$$

where z is called *dynamical critical exponent*. It is roughly a measure of the anisotropy between the spatial and temporal fluctuations, which is often encountered in non-relativistic condensed-matter systems.[12]

[10] The lecture notes for this class are availabel on the School's program webpage: http://www.ntu.edu.sg/ias/upcomingevents/LHSOPS09/Pages/programme.aspx

[11] Although we use the same Greek letter ν for the critical exponent, it must not be confunded with the filling factor, which plays no role in this subsection.

[12] Notice that in relativity, time is considered as the "fourth" dimension, and Lorentz invariance would require that spatial and temporal fluctuations be equivalent, i.e. $z = 1$.

At the phase transition B_c, the longitudinal and transverse resistivities $\rho_{L/H}$ are described in terms of *universal* functions that are functions of the ratio τ/ξ_τ between the (imaginary) time τ, which is proportional to the inverse temperature, $\hbar/\tau = k_B T$ [41, 42] and the temporal correlation length ξ_τ,

$$\rho_{L/H} = f_{L/H}\left(\frac{\tau}{\xi_\tau}\right) = f_{L/H}\left(\frac{\Delta B^{z\nu}}{T}\right), \tag{3.17}$$

where we have defined $\Delta B \equiv |B - B_c|$. In the case of an AC (alternating current) measurement at frequency ω, another dimensionless quantity, namely the ratio between the frequency and the temperature, $\hbar\omega/k_B T$, needs to be taken into account such that the universal function reads

$$\rho^{AC}_{L/H} = f_{L/H}\left(\frac{\tau}{\xi_\tau}, \frac{\hbar\omega}{k_B T}\right).$$

However, we do not consider an alternating current here. Equation (3.17) then yields the scaling of the width of the peak in the longitudinal resistance (or else the plateau transition)

$$\Delta B \sim T^{1/z\nu}. \tag{3.18}$$

A measurement of this width by Wei *et al.* [43] has confirmed such critical behaviour with an exponent $1/z\nu = 0.42 \pm 0.04$ (see 图. 3.7).

Furthermore, one may distinguish between the two exponents ν and z within a measurement of the plateau-transition width as a function of the electric field E via current fluctuations. One may identify the energy fluctuation $eE\xi$ at the correlation length ξ with the energy scale $\hbar/\xi_\tau \sim \hbar/\xi^z$ set by the temporal fluctuation ξ_τ, which yields $E \sim \xi^{-(1+z)} \sim \Delta B^{\nu(1+z)}$, and thus

$$\Delta B \sim E^{1/\nu(1+z)}. \tag{3.19}$$

Other measurements by Wei *et al.* [44] have shown that these types of fluctuations yield $z \simeq 1$, i.e. $\nu \simeq 2.3$. The precision of the measured critical exponent has since been improved – more recent experiments [45, 46] have revealed $\nu = 2.38 \pm 0.06$.

Theoretically one knows that the critical exponent for classical 2D percolation is $\nu_{\text{class}} = 4/3$ and thus much smaller than the measured one. This discrepancy is due to the quantum nature of the percolation in quantum Hall systems. Indeed, quantum-mechanical tunneling and the typical extension $\sim l_B$ of the wave functions associated with the equipotential lines enhance percolation, i.e. the electron puddles in the potential valleys may percolate *before* they touch each other in the classical sense. A model that takes into account this effect has been proposed by Chalker and Coddington [47], though with simplifying assumptions for the puddle geometry,[13] and one obtains a critical exponent $\nu = 2.5 \pm 0.5$ from numerical studies of this model [47, 48], in quite a good agreement with the experimental data [43, 44].

In spite of the good agreement with experimental findings, these theoretical results need to be handled with care – indeed, analytical calculations have shown that the dynamical exponent should be exactly $z = 2$ for non-interacting electrons, whereas the measured value $z \simeq 1$ is obtained when interactions are taken into account on the level of the Hartree-Fock approximation [49]. Furtherrmore, very recent numerical calculations within the Chalker-Coddington model have shown that the accurate value of the critical exponent is slightly larger ($\nu \simeq 2.59$) than the measured one when interactions are not taken into account [50].

3.5 Relativistic Quantum Hall Effect in Graphene 石墨烯中的相对论性 Hall 效应

We finish this chapter on the IQHE with a short presentation of the relativistic quantum Hall effect (RQHE) in graphene, which is understandable in the same framework of LL quantisation and (semi-classical) one-particle localisation as the IQHE in a non-relativistic 2D electron system. Indeed, the above arguments also apply to relativistic electrons in graphene, but we need to take into account the two different carrier types, electrons

[13] Notice, however, that due to the universality of the scaling laws and the fluctuations at all length scales, the results are expected to be independent on these *microscopic* assumptions.

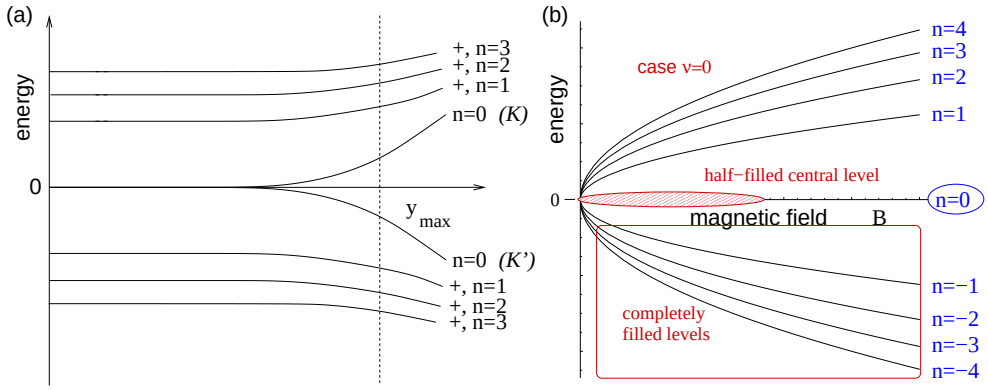

図 3.8: *(a)* Mass confinement for relativistic Landau levels. Whereas the electron-like LLs ($\lambda = +$) are bent upwards when approaching the sample edge (y_{max}), the hole-like LLs ($\lambda = -$) are bent downwards. The fate of the $n = 0$ LL depends on the valley (parity anomaly) – in one valley (K), the level energy decreases, whereas it increases in the other valley (K'). *(b)* Filling of the bulk Landau levels at $\nu = 0$. All electron-like LLs ($\lambda = +$) are unoccupied whereas all hole-like LLs ($\lambda = -$) are completely filled. The $n = 0$ LL is altogether half-filled.

and holes, which carry a different charge. This is not so much a problem in the case of the impurity potential with its valleys and summits: in a particle-hole transformation, a valley becomes a summit and *vice versa*.[14] Furthermore, the direction of the Hall drift changes in this transformation. Because of the universality of the quantum Hall effect, both types of impurity distributions related by particle-hole symmetry yield the *same* quantisation of the Hall resistance. The picture of semi-classical localisation therefore applies also in the case of relativistic electrons in graphene.

The situation is different for the confinement potential. An ansatz of the form $V(y)\mathbb{1}$ – remember that the Hamiltonian of electrons in relativistic graphene is a 2×2 matrix that reflects the two different sublattices A and B – has the problem that an increase $V(y - y_{max/min}) \to \infty$ at the sample edge confines electrons but not the holes of the valence band for which we would need $V(y - y_{max/min}) \to -\infty$ for an efficient confinement. A possible confinement potential may be formed with the Pauli matrix σ^z,

$$V_{\text{conf}}(y) = V(y)\,\sigma^z = \begin{pmatrix} V(y) & 0 \\ 0 & -V(y) \end{pmatrix}, \tag{3.20}$$

which, together with the Hamiltonian (2.8), yields the Hamiltonian which corresponds to the non-relativistic model (3.6). For a constant term $M = V(y)$ the contribution (3.20) plays the role of a mass of a relativistic particle (see also Appendix B). Therefore, the confinement (3.20) is sometimes also called *mass confinement*. The corresponding energy spectrum, which one obtains within the same approximation as in Sec. 3.1 via the replacement $y \to y_0 = kl_B^2$ in the Landau gauge, reads [c.f. Eq. (B.8) in Appendix B]

$$\epsilon_{\lambda n, y_0} = \lambda \sqrt{M^2(y_0) + 2\frac{\hbar^2 v^2}{l_B^2} n}, \tag{3.21}$$

and is schematically represented in 図. 3.8(a). Notice that Eq. (3.21) is only valid for $n \neq 0$ – indeed, the $n = 0$ acquires a non-zero energy $M(y_0)$, which is negative for our particular choice (see Appendix B). This feature is sometimes called *parity anomaly* in high-energy physics. Remember that in the case of graphene, one has two inequivalent low-energy points in the first BZ which give rise to a relativistic energy spectrum. The Dirac Hamiltonians (2.4) and (2.8) for the zero-B and magnetic-field case, respectively, applies principally only to one of the two valleys (say K), whereas that for the other valley is given by $-H_D$ (or $-H_D^B$) if one interchanges the A and B components [c.f. Eq. (A.16) in Appendix A]. The confinement term

[14] The particle-hole transformed landscape corresponds to an impurity distribution in which one interchanges negatively and positively charged impurities.

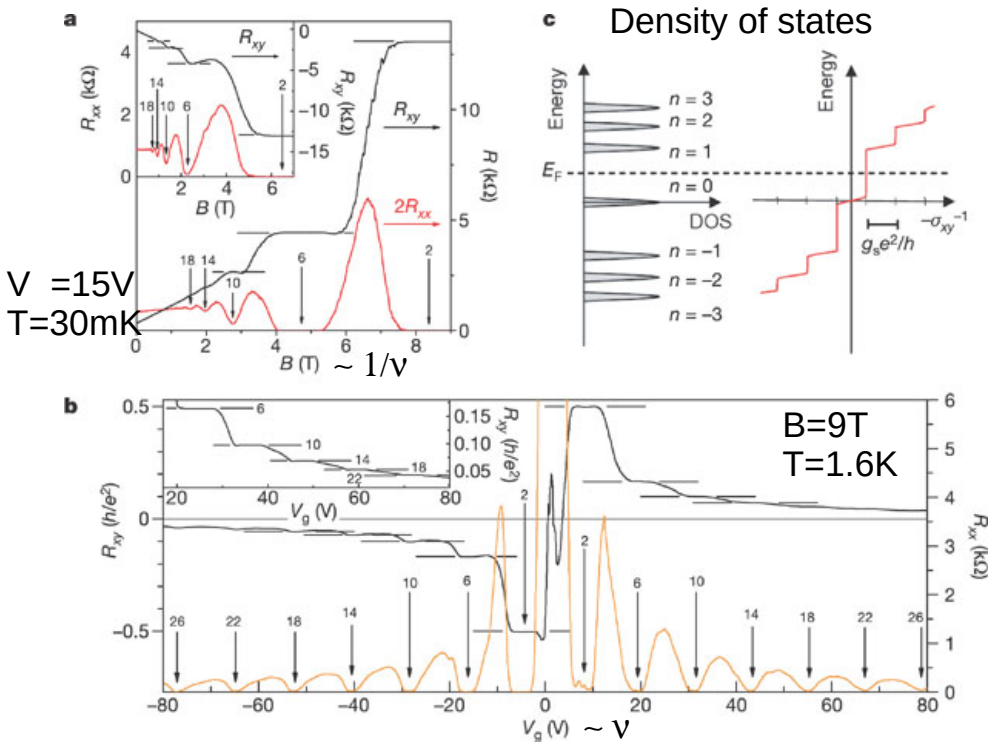

図 3.9: Measurement of the relativistic quantum Hall effect (Zhang *et al.*, 2005). *(a)* RQHE at fixed carrier density ($V_G = 15$ V) at $T = 30$ mK. The filling factor is varied by sweeping the magnetic field. *(b)* Sketch of the DOS with the Fermi energy between the LLs $n = 0$ and $+, n = 1$. *(c)* RQHE at fixed magnetic field ($B = 9$ T) at higher temperatures, $T = 1.6$ K. The filling factor is now varied by changing the gate voltage.

(3.20) therefore reads $-V_{\text{conf}}(y)$ in the other valley, i.e. with a negative mass. The $n = 0$ LL thus shifts to positive energies in the second valley, and the two-fold valley degeneracy is lifted in this level. A more detailed discussion of the mass confinement (3.20) in graphene may be found in the Appendix B.

This type of confinement may seem to be somewhat artificial, whereas the confinement in the non-relativistic case is easier to accept. Notice, however, that the whole model of massless Dirac fermions [second Hamiltonian in Eq. (2.4)] only describes the physical properties at length scales that are large compared to the lattice spacing (in graphene). In the true lattice model, the electrons are naturally confined because one does not allow for hopping from a lattice site at the edge into free space. The expression (3.20) is therefore only an *effective* model to describe confinement. We notice that, although the effective model yields a qualitatively correct picture, the fine structure of the dispersion at the edge depends on the edge geometry [51]. For further reading, we refer the interested reader to the literature [21].

With the help of these preliminary considerations, we are now prepared to understand the RQHE in graphene – the semi-classical localisation is the same as in the non-relativistic case, and the confinement, which needed to be adopted to account for the simultaneous presence of electron- and hole-like LLs, yields the edge states which are responsible for the quantum transport and, thus, the resistance quantisation. The RQHE was indeed discovered in 2005 by two different groups [6, 7], and the results are shown in 図. 3.9 [7]. The phenomenology of the RQHE is the same as that of the IQHE in non-relativistic LLs: one observes plateaus in the Hall resistance while the longitudinal resistance vanishes. Notice that one may vary the filling factor either by changing the B-field at fixed carrier density [図. 3.9(a)] or one keeps the B-field fixed while changing the carrier density with the help of a gate voltage [図. 3.9(c)]. The latter measurement is much easier to perform in graphene than in non-relativistic 2D electron gases in semiconductor heterostructures.

In spite of the similarity with the non-relativistic IQHE, one notices, in 図. 3.9, an essential difference:

the quantum Hall effect is observed at the filling factors

$$\nu = \pm 2(2n + 1), \tag{3.22}$$

in terms of the LL quantum number n, whereas the IQHE is observed at $\nu = n$ (or $\nu = 2n$ if the LLs are spin-degenerate). The step in units of 4 is easy to understand: each relativistic LL in graphene is four-fold degenerate (in addition to the guiding-centre degeneracy), due to the two-fold spin and the additional two-fold valley degeneracy. However, there is an "offset" of 2. This is due to the fact that the filling factor $\nu = 0$ corresponds to no carriers in the system, i.e. to a situation where the Fermi energy is exactly at the Dirac point (undoped graphene). In this case, one has a perfect electron-hole symmetry, and the $n = 0$ LL must therefore be *half-filled* [see 图. 3.8(b)], or else: there are as many electrons as holes in $n = 0$. According to the considerations presented in Sec. 3.4, this does not correspond to a situation where one observes a quantum Hall effect due to percolating extended states. Indeed, the system turns out to be *metallic* at $\nu = 0$ with a finite non-zero longitudinal resistance [6, 7]. A situation, where one would expect a quantum Hall effect, arises when the central LL $n = 0$ is completely filled (or completely empty). As a consequence of the four-fold level degeneracy, one obtains the quantum Hall effect at $\nu = 2$ (or $\nu = -2$) observed in the experiments (see 图. 3.9). This is the origin of the particular filling-factor sequence (3.22) of the RQHE in graphene.

Chapter 4

Strong Correlations and the Fractional Quantum Hall Effect
强关联与分数量子 Hall 效应

In the preceding chapter, we have seen that one may understand the essential featues of the IQHE within a one-particle picture, i.e. in terms of Landau quantisation; at integer filling factors $\nu = n$, which correspond to n completely filled LLs,[1] an additional electron is forced, as a result of the Pauli principle, to populate the next higher (unoccupied) LL [see 图. 4.1(a)]. It therefore, needs to "pay" a finite amount of energy $\hbar\omega_C$ [or $\sqrt{2}(\hbar v/l_B)(\sqrt{n}-\sqrt{n-1})$ in the case of the RQHE in graphene] and is localised by the impurities in the sample, due to the classical Hall drift which forces the electron to move on closed equipotential lines. The system is said to be *incompressible* because one may not vary the filling factor and pay only an infinitesimal amount of energy – indeed in the case of a fixed particle number, consider an infinitesimal decrease of the magnetic field which amounts to an infinitesimal change of the surface $2\pi l_B^2$ occupied by each quantum state. Since the total surface of the system remains constant, the infinitesimal increase of $2\pi l_B^2$ may not be accomodated by an infinitesimal change in energy, due to the gap between the LL $n-1$ and n where at least one electron must be promoted to. This gives rise to a zero compressibility.

In view of this picture of the quantum Hall effect, it was therefore a big surprise to observe a FQHE at a filling factor $\nu = 1/3$, with the corresponding Hall quantisation $R_H = h/e^2\nu = 3h/e^2$ [13], and, later, at a large set of other fractional filling factors. Indeed, if only the kinetic energy is taken into account, the ground state at $\nu = 1/3$ is highly degenerate and there is no evident gap present in the system: the Pauli principle no longer prevents an additional electron to populate the next higher LL, but it finds enough place in the lowest LL which is only one-third filled.

Notice that we have neglected so far the mutual Coulomb repulsion between the electrons, which happens to be responsible for the occurence of the FHQE. The relevance of electronic interactions is discussed in the next section (Sec. 4.1). In Sec. 4.2, we present the basic results of Laughlin's theory of the FQHE, such as the ground-state wave functions, fractionally charged quasi-particles and the interpretation of Laughlin's wave function in terms of a 2D one-component plasma. The related issue of fractional statistics is introduced in a section apart (Sec. 4.3), and we close this chapter with a short discussion of different generalisations of Laughlin's wave function, such as CF theory or the Moore-Read wave function in half-filled LLs.

4.1 The Role of Coulomb Interactions
库伦相互作用的表现

As already mentioned above, the situation of a partially filled LL is somewhat opposite to that of n completely occupied levels, where one observes the IQHE. This difference is summarised in 图. 4.1 and it is also the

[1] As before, we neglect the electron spin to render the discussion as simple as possible. The role of spin will be discussed briefly in the last chapter on multi-component systems.

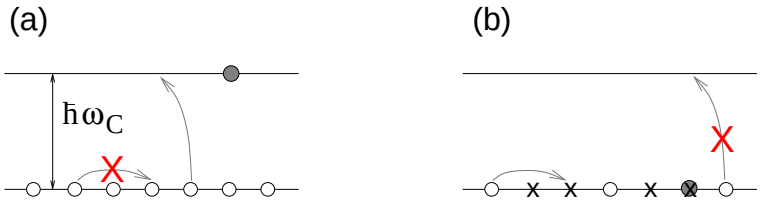

图 4.1: *(a)* Sketch of a completely occupied LL. An additional electron (grey circle) is forced to populate the next higher LL because of the Pauli principle. *(b)* Sketch of a partially filled LL. Because of the presence of unoccupied states in the LL (crosses), the Pauli principle does not prevent an additional electron (grey circle) to populate the next higher LL. The low-energy dynamical properties of the electrons are described by excitations within the same LL (no cost in kinetic energy), and inter-LL excitations are now part of the high-energy degrees of freedom.

origin of the different role played by the Coulomb repulsion between the electrons. In the case of n completely filled LLs, one has a non-degenerate (Fermi-liquid-like) ground state, where the interactions may be treated within a perturbative approach. Indeed, any type of excitation involves a transition between two adjacent LLs that are separated by an energy gap of $\hbar\omega_C$ [see 图. 4.1(a)],[2] and we need to compare the Coulomb energy at the characteristic length scale $R_C = l_B\sqrt{2n+1}$ to this gap,

$$\frac{V_C}{\hbar\omega_C} \sim \frac{me^{3/2}}{\epsilon\hbar^{3/2}}(Bn)^{-1/2},$$

which turns out to be nothing other than the usual dimensionless coupling constant

$$r_s = \frac{me^2}{\epsilon\hbar^2}n_{el}^{-1}$$

for the 2D Coulomb gas in Fermi liquid theory [52, 53]. The last expression is obtained by identifying the Fermi energy $E_F = \hbar^2 k_F^2/2m$, in terms of the Fermi wave vector k_F, with the energy of the last occupied LL $\hbar\omega_C n$. The perturbative approach allows one, e.g., to describe collective electronic excitations in the IQHE, such as magneto-plasmon modes (the 2D plasmon in the presence of a magnetic field) or magneto-excitons (inter-LL excitations that acquire a dispersion due to the Coulomb interaction) [54], or else the corresponding modes of the RQHE in graphene [55, 56].

In the case of a partially filled LL n the situation is inverted: for an electronic excitation, there are enough unoccupied states in the LL n for an electron of the same level to hop to. From the point of view of the kinetic energy, there is no energy cost associated with such an excitation (*low-energy* degrees of freedom) whereas an excitation to the next higher (unoccupied) LL costs an energy $\hbar\omega_C$. Inter-LL excitations may then be neglected as belonging to *high-energy* degrees of freedom [图. 4.1(b)]. Notice that all possible distributions of N electrons within the same partially filled LL n therefore have the same kinetic energy, which effectively drops out of the problem. The macroscopic degeneracy may be lifted by phenomena due to other energy scales, such as those associated with the impurities in the sample or else the electron-electron interactions. The first hypothesis (impurities) may be immediately discarded as the driving mechanism of the FQHE because, in contrast to the IQHE, the FQHE only occurs in high-quality samples with low impurity concentrations. Indeed, the hierarchy of energy scales in the FQHE may be characterised by the succession

$$\hbar\omega_C \gtrsim V_C \gg V_{imp}, \tag{4.1}$$

and we therefore need to consider seriously the Coulomb repulsion, which govern the low-energy electronic properties in a partially filled LL.[3] Notice that we thus obtain a system of *strongly-correlated* electrons for

[2] In order to simplify the discussion, we consider only the IQHE in non-relativistic quantum Hall systems, but the arguments apply also to the RQHE in graphene.

[3] As for the IQHE, impurities play nevertheless an important role in the localisation of quasi-particles, which we need to invoke later in this chapter in order to explain the transport properties of the FQHE.

the description of which all perturbative approaches starting from the Fermi liquid are doomed to fail. The only hope one may have to describe the FQHE is then a well-educated guess of the ground state.

The most natural guess would be that the electrons in a partially filled LL behave as classical charged particles that form a crystalline state in order to minimise their mutual Coulomb repulsion. Such a state is also called Wigner crystal (WC) because it was first proposed by Wigner in 1934 [57]. A WC has indeed been thought – before the discovery of the FQHE – to be the ground state of electrons in a partially filled LL [58]. Even if the WC is the ground state at very low filling factors, as it has been shown experimentally [59], this state may not allow for an explanation of the FQHE. Indeed, the WC is a state that breaks a continuous spatial symmetry (translation invariance) and any such state has gapless long-wave-length excitations (*Goldstone modes*). The Goldstone mode of the WC (as of any other crystal) is the acoustic phonon the energy of which tends to zero at zero wave vector. One may thus compress the WC by changing the occupied surface in an infinitesimal manner or else by adding an electron without changing the macroscopic surface and pay only an infinitesimal amount of energy. The ground state is therefore compressible, i.e. it is not separated by an energy gap from its single-particle excitations, a situation that is at odds with the FQHE.

4.2 Laughlin's Theory
Laughlin 理论

As a consequence of the above-mentioned considerations on the WC, one thus needs to search for a candidate for the ground state that does not break any continuous spatial symmetry and that has an energy gap. Such a state is the *incompressible quantum liquid* which was proposed by Laughlin in 1983 [14] the basic features of which we present in the present section. We consider, here, only the FQHE in the lowest LL (LLL), for simplicity. There are different prescriptions to generalise the associated wave functions to higher LLs, e.g. with the help of Eq. (2.18) (see MacDonald, 1984). Experimentally, several FQHE states have been observed in the next higher LL $n = 1$ although the majority of FQHE states is found in the LLL.[4]

4.2.1 Laughlin's guess from two-particle wave functions
二粒子波函数与 Laughlin 规范

In order to illustrate – one cannot speak of a derivation – Laughlin's wave function, we first need to remember the one-particle wave function of the LLL and then consider the corresponding two-particle wave function. We have already seen in Sec. 2.4.1 that a one-particle wave function in the LLL is described in terms of an analytic function times a Gaussian,[5]

$$\psi \sim z^{m'} e^{-|z|^2/4},$$

in terms of the integer $m' = 0, ..., N_B - 1$, where we have absorbed now (and in the remainder of these lecture notes) the magnetic length in the definition of the complex position, $z = (x - iy)/l_B$.

Consider, in a second step, an arbitrary two-particle wave function. This wave function must also be an analytic function of both postions z_1 and z_2 of the first and second particle, respectively, and may be a superposition of polynomials, such as e.g. of the basis states

$$\psi^{(2)}(z, Z) \sim Z^M z^m e^{-(|z_1|^2+|z_2|^2)/4}, \tag{4.2}$$

where we have defined the centre of mass coordinate $Z = (z_1 + z_2)/2$ and the relative coordinate $z = (z_1 - z_2)$. The quantum number m plays the role of the *relative* angular momentum between the two particles, and M is associated with the *total* angular momentum of the pair. Because of the analyticity of the LLL wave functions, m must be an integer, and the exchange of the positions z_1 and z_2 imposes on m to be *odd* because of the electrons' fermionic nature.

Laughlin's wave function [14] is a straight-forward N-particle generalisation of the two-particle wave function (4.2),

$$\psi_m^L\left(\{z_j, z_j^*\}\right) = \prod_{k<l} (z_k - z_l)^m \, e^{-\sum_j |z_j|^2/4}, \tag{4.3}$$

[4] There is even some slight indication for a 1/5 FQHE state in the next excited LL $n = 2$ [60].

[5] We neglect the numerical prefactors here that account for the normalisation of the wave functions.

where we have omitted the normalisation constants in order to simplify the notation and where all indices run from 1 to the total number of particles N. Notice that there is no dependence on the centre of mass, but only on the relative coordinates between the particle pairs. Had there been such a dependence, described by a non-zero value of the total angular momentum quantum number $M \neq 0$, one would have broken a continuous spatial symmetry, in which case the state would describe a compressible rather than an incompressible state required for the FQHE, as we have mentioned above. We emphasize once again that Laughlin's wave function is not based on a mathematical derivation, although we will see below that there exist some mathematical models for which it describes the *exact ground state*, but it is more appropriately characterised as a *variational* wave function.

Variational parameter
变分法的参数

The variational parameter in Laughlin's wave function (4.3) is nothing other than the exponent m, with respect to which we would, in principle, need to optimised the wave function in order to approximate the true ground state of the system. Notice, however, that due to the LLL analyticity condition and fermionic statistics, the exponent is restricted to odd integers, $m = 2s + 1$, in terms of the integer s. Furthermore, this variational parameter turns out to be fully determined by the filling factor ν, as we will show with the following argument.[6]

Consider Laughlin's wave function as a function of the position z_k of some arbitrary but fixed electron k. There are $N - 1$ factors of the type $(z_k - z_l)^m$, one for each of the remaining $N - 1$ electrons, l, occuring in the ansatz (4.3), such that the highest power of z_k is $m(N - 1)$,

$$\prod_{k<l} (z_k - z_l)^m \sim z_k^{m(N-1)}.$$

Now, remember from Sec. 2.4.1 [see Eq. (2.54)] that the highest power of the complex particle position is fixed by the number of states N_B in each LL. This yields the relation

$$mN - \delta = N_B \tag{4.4}$$

between the number of particles N and the number of flux quanta N_B threading the system. Here, δ is some *shift* that is on the order of unity and that plays no role in the thermodynamic limit $N, N_B \to \infty$.[7] Because the ratio between the number of particles and that of flux quanta is nothing other than the LL filling factor (2.44), $\nu = N/N_B$, one notices that, in the thermodynamic limit, the "variational parameter" is entirely fixed by the filling factor, i.e.

$$m = 2s + 1 = \frac{1}{\nu} \qquad \Leftrightarrow \qquad \nu = \frac{1}{m} = \frac{1}{2s+1}, \tag{4.5}$$

and Laughlin's wave function is therefore a candidate wave function for the ground state at the filling factors

$$\nu = 1, 1/3, 1/5, ...$$

Remember that the odd value $m = 2s + 1$ is required by the fermionic nature of the electrons. Formally, one may though lift this restriction and generalise Laughlin's wave function to *bosonic* particles by choosing an even exponent $2s$. Such bosonic Laughlin wave functions have been studied theoretically in the context of rotating cold Bose gases in an optical trap [61].

Laughlin's wave function at $\nu = 1$
在 $\nu = 1$ 的 Laughlin 波函数

It may seem, at first sight, astonishing that also the case of a completely filled LL for $\nu = 1$ is described in terms of a Laughlin wave function with $m = 1$ (or $s = 0$). Indeed, the state

$$\psi(\{z_j\}) = f_N(\{z_j\})\, e^{-\sum_j |z_j|^2/4}$$

[6] We are therefore confronted with the somewhat bizarre situation where we dispose of a variational wave function with no possible variation.

[7] Notice, however, that this shift plays an important role in numerical calculations, such as exact diagonalisation, when performed on special geometries, such as on a sphere.

would be non-degenerate and could thus be described in terms of a Slater determinant,

$$f_N(\{z_j\}) = \det \begin{pmatrix} z_1^0 & z_1^1 & \dots & z_1^{N-1} \\ z_2^0 & z_2^1 & \dots & z_2^{N-1} \\ \vdots & \vdots & & \vdots \\ z_N^0 & z_N^1 & \dots & z_N^{N-1} \end{pmatrix}, \tag{4.6}$$

where we have omitted the ubiquitous Gaussian factor $\exp(-\sum_j |z_j|^2/4)$. Notice that the j-th line in this determinant corresponds to all LLL states of the j-th particle described in terms of the polynomials z_j^m. The determinant takes into account all permutations of the N particles over the N particle positions, $z_1, ..., z_N$, and may be rewritten in a compact manner with the help of the co-called Vandermonde determinant,

$$f_N(\{z_j\}) = \prod_{i<j} (z_i - z_j)\,, \tag{4.7}$$

which is indeed nothing other than the polynimial prefactor in Laughlin's wave function (4.3) with $m = 1$.

Until now we have obtained an N-particle wave function from some very general symmetry considerations (LLL analyticity condition, fermionic statistics, no broken continuous spatial symmetries), but we have not at all shown that it describes indeed the ground state responsible of the FQHE. In the following parts, we will therefore discuss the basic physical properties of this, for the moment rather abstract, mathematical entity. In a first step, we will discuss some energy properties of the ground state and show that Laughlin's wave function is the exact ground state of a certain class of models that are qualitatively compared to the physical one (Coulomb interaction). We will then discuss the fractionally charged quasi-particle excitations of this wave function.

4.2.2 Haldane's pseudopotentials
Haldane 贗势

In order to describe the energetic properties of Laughlin's wave function (4.3), we consider again the two-particle wave function (4.2). Notice that this wave function is an *exact* eigenstate for any central interaction potential that depends only on the relative coordinate z between particle pairs, such as it is the case for the Coulomb interaction, $V = V(|z|)$. One may therefore decompose the interaction potential in the relative angular momentum quantum numbers m,

$$v_m \equiv \frac{\langle m, M|V|m, M\rangle}{\langle m, M|m, M\rangle}, \tag{4.8}$$

where the denominator takes into account the fact that we have not properly normalised the two-particle wave functions (4.2), $\psi^{(2)}(z, Z) = \langle z, Z|m, M\rangle$.[8] The fact that there is no dependence on M is a direct consequence of the assumption that we deal with a central interaction potential, i.e. $\langle z, Z|V|z', Z'\rangle = V(|z|)\delta_{z,z'}\delta_{Z,Z'}$. Furthermore, there are no off-diagonal terms of the form $\langle m, M|V|m', M\rangle$, with $m' \neq m$, as one may show explicitly in the polar representation $z = \rho\exp(i\phi)$,

$$\langle m, M|V|m', M\rangle \propto \int_0^{2\pi} d\phi \int_0^{\infty} d\rho\, \rho^{m+m'+1} V(\rho) e^{-i(m-m')\phi} \propto \delta_{m,m'},$$

due to the integration over the polar angle. The potentials v_m obtained from the decomposition into relative angular momentum states are also called *Haldane's pseudopotentials* [62]. They fully characterise the two-particle energy spectrum because the kinetic energy is the same for all two-particle states $|m, M\rangle$, as described above. Notice that this is a very special case: normally any repulsive interaction potential yields unbound states with a continuous energy spectrum, such as the plane-wave states in scattering theory. Here, the energy spectrum is discrete even if the interaction is repulsive, due to the presence of a quantising magnetic field. Notice further that Haldane's pseudopotentials are an image of the real-space form of the interaction

[8] In order to simplify the notations, we have omitted the LL quantum number $n = 0$, which is the same for both particles in this wave function.

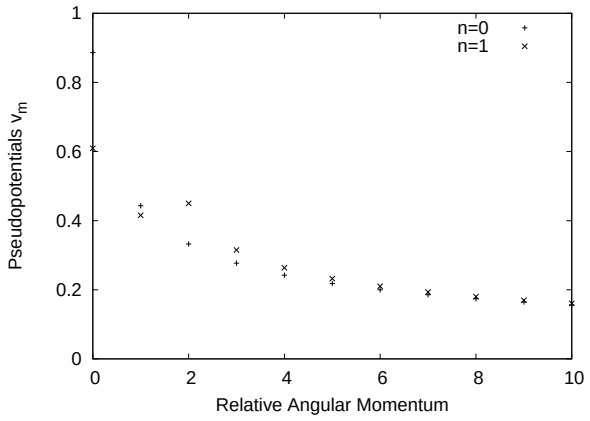

图 4.2: Haldane's pseudopotentials for the Coulomb interaction in the LLs $n = 0$ and $n = 1$. Notice that we have plotted the pseudopotentials for both odd and even values of the relative angular momentum m even though only odd values matter in the case of fermions.

potential. Indeed, if a pair of electrons is in a quantum state with relative angular momentum m, the average distance between the electrons is $|z| \sim l_B\sqrt{2m}$.[9] Haldane's pseudopotential v_m is therefore roughly the value of the original interaction potential at the relative distance $l_B\sqrt{2m}$,

$$v_m \simeq V\left(|z| = l_B\sqrt{2m}\right), \tag{4.9}$$

and the small-m components of Haldane's pseudopotentials correspond to the short-range components of the underlying interaction potential. Figure 4.2 shows the pseudopotential expansion for the Coulomb interaction in the lowest ($n = 0$) and the first excited ($n = 1$) LL.

Haldane's pseudopotentials are extremely useful in the description of the N-particle state as well. Indeed, the N-particle interaction Hamiltonian V may be rewritten in terms of pseudopotentials as

$$V = \sum_{i<j} V(|z_i - z_j|) = \sum_{i<j} \sum_{m'=0}^{\infty} v_{m'} \mathcal{P}_{m'}(ij), \tag{4.10}$$

where the operator $\mathcal{P}_{m'}(ij)$ projects the electron pair ij onto the relative angular momentum state m'. Notice that due to the factor $\prod_{k<l}(z_k - z_l)^m$ in Laughlin's wave function (4.3), no particle pair is in a relative angular momentum state $m' < m$. If one then chooses, though somewhat artificially, all pseudopotentials with a $m < m'$ to be positive (say 1) and all others zero,

$$v'_m = \begin{cases} 1 & \text{for } m' < m \\ 0 & \text{for } m' \geq m \end{cases} \tag{4.11}$$

one obtains $V\psi^L_m = 0$, i.e. Laughlin's wave function is the zero-energy eigenstate of the model (4.11). Since the model describes an entirely repulsive interaction, all possible states must have an energy $E \geq 0$. Therefore, Laughlin's wave function is even the *exact* ground state of the model (4.11). Furthermore, it is the only zero-energy state because if one keeps the total number of particles and flux fixed, any other state different from that described by Laughlin's wave function involves a particle pair in a state with an angular momentum quantum number different from m. If it is smaller than m, this particle pair is affected by the associated non-zero pseudopotential m' and thus costs an energy on the order of $v_{m'} > 0$. If the particle pair is in a momentum state with $m' > m$, there is at least another pair with $m'' < m$ in order to keep the filling factor fixed, and this pair raises the energy. These general arguments show that any excited state involves a

[9] This is similar to the average value of the radius at which the electron's guiding centre is placed in the symmetric gauge (see Sec. 2.4.1). Remember (e.g. from classical mechanics) that the decomposition of a two-particle wave function in relative and centre-of-mass coordinates maps the two-body problem to an effective one-body problem.

finite (positive) energy given by a pseudopotential $v_{m'}$, with $m' < m$, which plays the role of an *energy gap*. In this sense, the liquid state described by Laughlin's wave function is indeed an *incompressible* state that already hints at the possibility of a quantum Hall effect if we can identify the correct quasi-particle of this N-particle state that becomes localised by the sample impurities.

Notice that the above considerations are based on an extremely artificial model interaction (4.11) that has, at first sight, very little to do with the physical Coulomb repulsion. However, the model is often used to generate numerically (in exact-diagonali-sation calculations) the Laughlin state, which may then be compared to the Coulomb potential decomposed in Haldane's pseudopotentials. This procedure has shown that theL aughlin state generated in this manner has an overlap of more than 99% with the state obtained from the Coulomb potential [63, 64], which is amazingly high for a wave function obtained from a well-educated guess. This high accuracy of Laughlin's wave function may be understood in the following manner: when one decomposes the Coulomb interaction potential in Haldane's pseudopotentials, one obtains a monotonically decreasing function when plotted as a function of m (see 图. 4.2). Furthermore, the component v_1 is much larger than v_3 and all other pseudopotentials v_m with higher values of m.[10] These higher terms may be treated in a perturbative manner and do not change the ground state which is protected by the above-mentioned gap on the order of $v_1 > v_m$, with $m > 1$.

Furthermore, we mention that, apart from its successful verification by exact-diagonalisation calculations [63, 64], Laughlin, in his original paper [14], showed within a variational calculation that the quantum liquid described by his wave function (4.3) has indeed a lower energy than the previously proposed WC. Again the reason for this unexpected feature is the capacity of Laughlin's wave function, which varies as r^{2m} when two particles i and j approach each other with $r = |z_i - z_j|$, to screen the short-range components of the interaction potential. Notice that for a WC of fermions, the corresponding N-particle wave function decreases as r^2, as dictated by the Pauli principle.

4.2.3 Quasi-particles and quasi-holes with fractional charge
分数电荷的准粒子与准空穴

Until now, we have discussed some ground-state properties of Laughlin's wave function. We have seen that the Laughlin state at $\nu = 1/m$ is insensitive to the short-range components of the interaction potential described by Haldane's pseudopotentials $v_{m'}$ with $m' < m$, whereas excited states must be separated from the ground state by a gap characterised by these short-range pseudopotentials. However, we have not characterised so far the nature of the excitations.

There are two different sorts of excitations: (i) elementary excitations (quasi-particles or quasi-holes) that one obtains by adding or removing charge from the system, and (ii) collective excitations at fixed charge. The latter are simply a charge-density-wave excitation which consist of a superposition of particle-hole excitations at a fixed wave vector $\mathbf{q}$ (the momentum of the pair) and which may be shown to be gapped at all values of $\mathbf{q}$. Its dispersion reveals a minimum (called *magneto-roton minimum*) at a non-zero value of the wave vector that indicates a certain tendency to form a ground state with modulated charge density, such as a WC. The characteristic dispersion relation of these collective excitations is shown in 图. 4.3(a). However, we do not discuss collective excitations here and refer the interested reader to the literature for a more detailed discussion [65, 1, 4], and concentrate here on a presentation of the elementary excitations.

Quasi-holes
准空穴

Elementary excitations are obtained when sweeping the filling factor slightly away from $\nu = 1/m$. Remember that there are two possibilities for varying the filling factor: adding charge to the system by changing the electronic density or adding (or removing) flux by varying the magnetic field. Remember further [see Eq. (4.4)] that the number of flux is intimitely related to the number of zeros in Laughlin's wave function. We

[10] One has $v_1/v_3 \simeq 1.6$ in the LLL. Notice that pseudopotentials with even angular momentum quantum number m do not play any physical role because of the fermionic nature of the electrons.

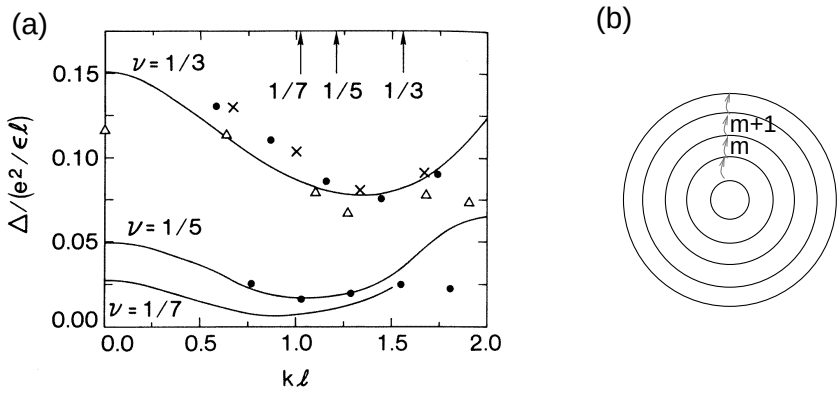

図 4.3: *(a)* Dispersion relation for collective charge-density-wave excitations (Girvin, MacDonald and Platzman, 1986; Girvin, 1999). The continuous lines have been obtained in the so-called single-mode approximation (Girvin, MacDonald and Platzman, 1986) for the Laughlin states at $\nu = 1/3$, $1/5$ and $1/7$, whereas the points are exact-diagonalisation results (Haldane and Rezayi, 1985; Fano, Ortolani and Colombo, 1986). The arrows indicated the characteristic wave vector of the WC state at the corresponding densities. *(b)* Quasi-hole excitation. Each electron jumps from the state m to the next-higher angular momentum state $m + 1$.

therefore consider the ansatz

$$\psi_{qh}\left(z_0, \{z_j, z_j^*\}\right) = \prod_{j=1}^{N} (z_j - z_0)\, \psi_m^L\left(\{z_j, z_j^*\}\right) \tag{4.12}$$

for an excited state. Each electron at the positions z_j thus "sees" an additional zero at z_0. In order to verify that this wave function adds indeed another flux quantum to the system, we may expand Laughlin's wave function (4.3) formally in a polynomial,

$$\psi_m^L(\{z_j, z_j^*\}) = \sum_{\{m_i\}} \alpha_{m_1,\ldots,m_N} z_1^{m_1} \ldots z_N^{m_N} e^{-\sum_j |z_j|^2/4},$$

where the $\alpha_{m_1,\ldots,m_N}$ describe the expansion coefficients. We now choose the position z_0 at the centre of the disc, in which case the wave function of the excited state (4.12) simply reads

$$\psi_{qh}(\{z_j, z_j^*\}) = \sum_{\{m_i\}} \alpha_{m_1,\ldots,m_N} z_1^{m_1+1} \ldots z_N^{m_N+1} e^{-\sum_j |z_j|^2/4},$$

i.e. each exponent is increased by one, $m_i \to m_i + 1$. This may be illustrated in the following manner: each electronjumps from the angular momentum state m to a state in which the angular momentum is increased by one (see 図. 4.3), leaving behind an empty state at $m = 0$. The excitation is therefore called a *quasi-hole* as we have already suggested by the subscript in Eq. (4.12). This also affects the quantum state with highest angular momentum M, i.e. we have increased the sample size by the surface occupied by one flux quantum, while keeping the number of electrons fixed.[11] Furthermore, this quasi-hole is associated with a *vorticity* if one considers the phase of the additional factor in Eq. (4.12),

$$\psi_{qh}(z_0 = 0, \{z_j, z_j^*\}) \propto \prod_j^N e^{-i\theta_j} \times \psi_m^L\left(\{z_j, z_j^*\}\right),$$

[11] Naturally, the total surface of the quantum Hall system remains constant, but physically we have slightly *increased* the B-field. Each quantum state occupies then an infinitesimally smaller surface $2\pi l_B^2$, such that the system may accomodate for one more quantum state, $M = N_B \to N_B + 1$.

i.e. each particle that circles around the origin $z_0 = 0$ experiences an additional phase shift of 2π as compared to the original situation described in terms of Laughlin's wave function (4.3). This is reminiscent of the vortex excitation in a type-II superconductor [66].

We have seen above that one can create a quasi-hole excitation at the postion z_0 by introducing one additional flux quantum, $N_B \to N_B + 1$, which lowers the filling factor by a tiny amount. However, we have not yet determined the charge associated with this elementary excitation. This charge may be calculated by considering the filling factor fixed, i.e. we need to add some (negative) charge to compensate the extra flux quantum in the system. From Eq. (4.4), we notice that the relation between the extra flux ΔN_B and the compensating extra charge ΔN is simply given by

$$m\Delta N = \Delta N_B \qquad \Leftrightarrow \qquad \Delta N = \frac{\Delta N_B}{m}\,. \tag{4.13}$$

This very important result is somewhat unexpected: in order to compensate one additional flux quantum ($\Delta N_B = 1$), one would need to add the *m-th fraction of an electron*. The charge deficit caused by the quasi-hole excitation is therefore

$$e^* = \frac{e}{m}\,, \tag{4.14}$$

i.e. the quasi-hole carries *fractional charge*.

Quasi-particles
准粒子

In the preceding paragraph, we have considered a quasi-hole excitation that is obtained by introducing an additional flux quantum in the system [or, mathematically, an additional zero in the Laughlin wave function, see Eq. (4.12)]. Naturally, one may also *lower* the number of flux quanta by one in which case one obtains a *quasi-particle* excitation with opposite vorticity as compared to that of the quasi-hole excitation. This opposite vorticity suggests that we use a prefactor $\prod_{j=1}^{N}(z_j^* - z_0^*)$, instead of $\prod_{j=1}^{N}(z_j - z_0)$ as in the expression (4.12), in order to create a quasi-particle excitation at the position z_0. Remember, however, that the resulting wave function would have unwanted components in higher LLs because the analyticity condition of the LLL is no longer satisfied. In order to heal the quasi-particle expression, one formally projects it into the LLL,

$$\psi_{qp}\left(z_0, \{z_j, z_j^*\}\right) = \mathcal{P}_{LLL} \prod_{j=1}^{N}(z_j^* - z_0^*)\, \psi_m^L\left(\{z_j, z_j^*\}\right). \tag{4.15}$$

There are several manners of taking into account this projection $\mathcal{P}_{LLL}$. A common one consists of replacing each occurence of the non-analytic variables z_j^* (and powers of them) in the polynomial part of the wave function by a derivative with respect to z_j in the same polynomial [67]. By partial integration, this amount to deriving the Gaussian factor by $(\partial_{z_j})^m$ which, up to a numerical prefactor, yields exactly the non-analytic polynomial factor z_j^{*m}. We will encounter this projection scheme again in the discussion of the CF generalisation of Laughlin's wave function (Sec. 4.4.1).

4.2.4 Experimental observation of fractionally charged quasi-particles
分数电荷准粒子的实验观察

That the fractional charge of Laughlin quasi-particles[12] is not only a mathematical concept but a physical reality has been proven in a spectacular manner in so-called *shot-noise* experiments on the $\nu = 1/3$ FQHE state [68, 69].[13] In these experiments, one constrains the quantum Hall system with the help of side gates (see 图. 4.4) that are used to deplete the region in their vicinity via the application of a gate voltage V_{sg}. As a consequence of this depletion the quantum Hall system has a bottleneck where the corresponding edge states are brought into spatial vicinity [图. 4.4(a)] or where the incompressible quantum liquid may even be cut into two parts separated by a completely depleted barrier [图. 4.4(b)]. In the first case, an injected charge

[12] From now on, we use the term "(Laughlin) quasi-particles" generically in order to denote quasi-particles *and* quasi-holes.
[13] Later this kind of experiment has been repeated for other FQHE states.

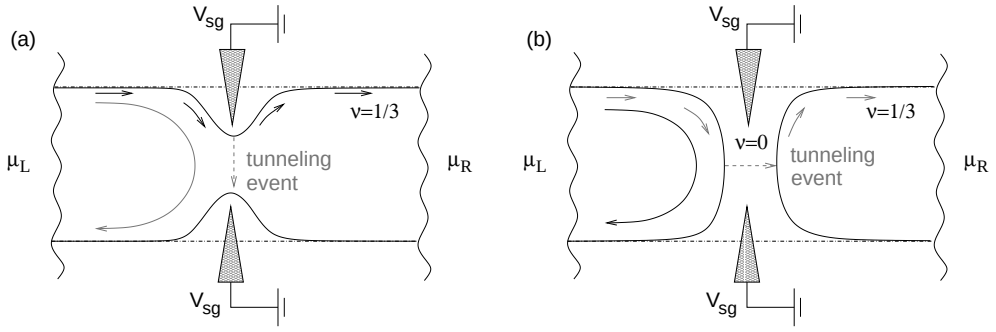

图 4.4: Experimental setup for the observation of fractionally charged quasi-particles. In addition to the usual geometry, one adds, at the upper and the lower edges, side gates that are used to deplete the region around the gates by the application of a voltage V_{sg}. The filling factor is chosen to be $\nu = 1/3$. As a result, the edge states at the opposite edges are brought into close vicinity. *(a)* Weak-backscattering limit. The incompressible liquid has a *bottleneck* at the side gates, i.e. the edges are so close to each other that a tunneling event between them has a finite probability. A particle injected at the left contact may thus be backscattered (grey arrow) in a region filled by the incompressible Laughlin liquid, although the majority of the particles reaches the right contact (black arrows). *(b)* Strong-backscattering limit. If one increases the side-gate voltage V_{sg}, the incompressible $\nu = 1/3$ liquid is eventually cut into two parts separated by a fully depleted region ($\nu = 0$). In this case, backscattering is the majority process (black arrow), and a tunneling may occur over the depleted region such that a particle injected at the left contact may still reach the right one (grey arrows).

may be backscattered in a tunneling event at the bottleneck over a region filled by the $\nu = 1/3$ liquid (weak-backscattering limit). If one increases the side-gate voltage, the incompressible liquid becomes eventually cut into two parts separated by a completely depleted barrier, and one obtains the strong-backscattering limit.

In a shot-noise measurement, one does not only measure the average current $\bar{I}$ (over a certain time interval) but simultaneously the (square of the) current fluctuation $(\Delta\bar{I})^2$ which is proportional to the carrier charge. If the elementary charged excitations are $e^* = e/3$ quasi-particles and not electrons, one may expect to measure this particular charge. The experiments [68, 69] have indeed shown that the charge measured in the shot noise is $e^* = e/3$ if the tunneling process takes place at a bottleneck filled with the incompressible quantum liquid [图. 4.4(a)], whereas it is the usual elementary charge e in the case of a tunneling process over a depleted region [图. 4.4(b)].

4.2.5 Laughlin's plasma analogy
Laughlin 的等离子体类比

A compelling physical picture of Laughlin's wave function (4.3) and the properties of its elementary excitations (4.12) and (4.15) with fractional charge has been provided by Laughlin himself [14], in terms of an analogy with a *classical 2D one-component plasma*. In the present subsection, we present the basic ideas and results of this plasma analogy, for completeness and pedagogical reasons. However, no new results will come out of this analogy here, as compared to those derived above.

Remember from basic *quantum mechanics* that the modulus square of a quantum-mechanical wave function may be interpreted as a statistical probability distribution. For Laughlin's wave function (4.3), one obtains the probability distribution

$$\left|\psi_m^L\left(\{z_j\}\right)\right|^2 = \prod_{i<j} |z_i - z_j|^{2m} \, e^{-\sum_j |z_j|^2/2}.$$

Now, remember from *classical statistical mechanics* that a probability distribution in the canonical ensemble is the Boltzmann weight, $\exp(-\beta\mathcal{H})$, of some Hamiltonian $\mathcal{H}$ and that the classical partition function, which encodes all relevant statistical information, is obtained from a sum over the Boltzmann weights of all possible

configurations $\mathcal{C}$, $\mathcal{Z} = \sum_{\mathcal{C}} \exp[-\beta \mathcal{H}(\mathcal{C})]$. Laughlin's plasma analogy consists precisely of the identification of the modulus square of his wave function with the Boltzmann weight of some *mock* Hamiltonian U_{cl}.[14] The mock Hamiltonian may be obtained exactly from this identification,

$$-\beta U_{cl} = \ln \left| \psi_m^L \left(\{z_j\} \right) \right|^2 , \tag{4.16}$$

and one obtains, by choosing somewhat artificially $\beta = 2/q$,[15]

$$U_{cl} = -q^2 \sum_{i<j} \ln |z_i - z_j| + q \sum_j \frac{|z_j|^2}{4}. \tag{4.17}$$

This is nothing other than the classical Hamiltonian of a 2D one-component plasma, in terms of the charge

$$q = m = 2s + 1 \tag{4.18}$$

of the plasma particles. The first term of Eq. (4.17) reflects the interactions between the charged plasma particles, whereas the second term describes their interaction with a neutralising background of positive charge, as in the case of the jellium model of the Coulomb gas [52, 53]. This may be seen best with the help of Poisson's equation, $-\Delta\phi = 2\pi q n_q(\mathbf{r})$, for an electrostatic 2D potential due to the charge density qn_q. The first term describes then indeed particles with charge q interacting via the 2D Coulomb interaction potential $\phi(\mathbf{r}) = -\ln(|\mathbf{r}|/l_B)$, and the second term is the interactions with the neutralising background because $\Delta|\mathbf{r}|^2/4l_B^2 = 1/l_B^2 = 2\pi n_B$, where the flux density n_B may thus be viewed as the charge density of the positively charged background.

In order to minimise the energy of the mock Hamiltonian U_{cl}, which corresponds to a distribution of highest weight, the 2D plasma thus needs to be charge-neutral, i.e. the charge density of the plasma particles qn_{el} must be compensated by that of the background n_B,

$$n_B - q n_{el} = 0, \tag{4.19}$$

which, together with Eq. (4.18), yields nothing other than the relation between the filling factor ν and the exponent in Laughlin's wave function (4.5), $\nu = n_{el}/n_B = 1/m$.

The plasma analogy does not only apply to the ground-state wave function (4.3) but also to the quasi-hole excitation (4.12). The additional factor $\prod_{j=1}^N (z_j - z_0)$ in the quasi-hole wave function (4.12) yields, within the plasma analogy (4.16), an additional term

$$V = -q \sum_{j=1}^N \ln |z_j - z_0| \tag{4.20}$$

to the mock Hamiltonian (4.17), $U_{cl} \to U_{cl} + V$. This additional term may be interpreted as the interaction of the plasma particles with an "impurity" of unit charge at the position z_0. In order to maintain charge neutrality, the impurity needs to be screened by the plasma particles. Since the charge of each plasma particle is $q = m = 2s+1$ and thus greater than unity, one needs $1/q$ plasma particles to screen the impurity of charge one. Remember that each plasma particle represents one electron of unit charge in the original Laughlin liquid. One therefore obtains the same charge fractionalisation of the Laughlin quasi-particle (4.14), $e^* = e/m$, as in the original quantum model.

4.3 Fractional Statistics
分数统计

4.3.1 Bosons, fermions and anyons – an introduction
波色子，费米子，任意子——简介

One of the most exotic consequences of charge fractionalisation in 2D quantum mechanics, exemplified by Laughlin quasi-particles, is *fractional statistics*. Remember that, in three space dimensions, the quantum-mechanical treatment of two and more particles yields a *superselection rule* according to which quantum

[14] mock: *singlish* for fake; mainly used the description of Singaporean catering food.

[15] Notice that Laughlin's wave function describes a system at $T = 0$, such that temperature does not intervene in the expressions. The choice is purely formal.

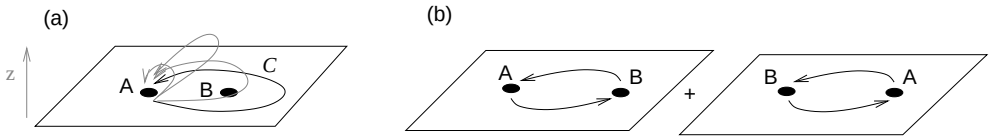

図 4.5: *(a)* Process in which a particle A moves on a path $\mathcal{C}$ around another particle B. In three space dimensions, one may profit from the third direction (z-direction) to lift the path over particle B and thus to shrink the path into a single point. *(b)* Process equivalent to moving A on a closed path around B which consists, apart from a topologically irrelevant translation, of two successive exchanges of A and B.

particles are, from a statistical point of view, either *bosons* or *fermions*. This superselection rule is no longer valid in 2D (two space dimensions), and one may find intermediate statistics between bosons and fermions. The corresponding particles are called *anyons*, because the statistics may be *any*. The present section is meant to illustrate these amazing aspects of 2D quantum mechanics, and we try to avoid a too formal or mathematical treatment. We refer, again, the interested reader to the more detailed literature [70].

In order to illustrate the different statistical (i.e. exchange) properties of two quantum particles in three and two space dimensions, consider a particle A that moves adiabatically on a closed path $\mathcal{C}$ in the xy-plane around another one B of the same species (see 図. 4.5). We choose the path to be sufficiently far away from particle B and the two particles to be sufficiently localised such that we can neglect corrections due to the overlap between the two corresponding wave functions. Notice first that such a process $\mathcal{T}$ is equivalent, apart from a topologically unimportant translation, to two successive exchange processes $\mathcal{E}$, in which one exchanges the positions of A and B. Algebraically, this may be expressed in terms of the corresponding operators as

$$\mathcal{E}^2 = \mathcal{T} \qquad \text{or} \qquad \mathcal{E} = \pm\sqrt{\mathcal{T}}, \tag{4.21}$$

modulo a translation.

Let us discuss first the three-dimensional case. Because of the presence of the third direction (z-direction), one may elevate the closed path in this direction while keeping the position of particle A fixed in the xy plane. We call the elevated path $\mathcal{C}'$. Furthermore, one may now shrink the closed loop $\mathcal{C}'$ into a single point at the position A without passing by the position of particle B which remains in the xy-plane. This final (point-like) path is called $\mathcal{C}''$. Although this procedure may seem somewhat formal, a quantum-mechanical exchange process does principally not specify the exchange path in order to define whether a particle is a boson or a fermion, but only its *topological* properties. From a topological point of view, all paths that may be continuously deformed into each other define a *homotopy class* [71]. Equation (4.21) must therefore be viewed as an equation for homotopy classes in which a simple translation and an allowed deformation are irrelavant. As a consequence of these considerations, the simple point-like path $\mathcal{C}''$ at the position of particle A, which may be formally described by $\mathcal{C}'' = 1$, is in the same homotopy class as the original path $\mathcal{C}$. Therefore, the associated processes are the same, and one has

$$\mathcal{T} = \mathcal{T}(\mathcal{C}) = \mathcal{T}(\mathcal{C}'') = \mathbb{1} \qquad \text{and thus} \qquad \mathcal{E} = \sqrt{\mathbb{1}}, \tag{4.22}$$

where the last equation is symbolic in terms of the one operator. It indicates that the quantum-mechanical operator $\mathcal{E}$, corresponding to particle exchange, has two eigenvalues that are the two square roots of unity, $e_B = \exp(2i\pi) = 1$ and $e_F = \exp(i\pi) = -1$. This is precisely the above-mentioned superselection rule, according to which all quantum particles in three space dimensions are either *bosons* ($e_B = 1$) or *fermions* ($e_F = -1$).

In two space dimensions, this topological argument yields a completely different result. It is not possible to shrink a path $\mathcal{C}$ enclosing the second particle B into a single point at the position of A, without passing by B itself. This means that the position of B must be an element of the path at a certain moment of the shrinking process, which cannot profit from a third dimension in order to elevate the loop on which it moves above the xy-plane. The single point still represents a homotopy class of paths, but these paths do not enclose another particle, and $\mathcal{C}$ is therefore an element of another homotopy class, i.e. the one of all paths starting from A and enclosing only the particle B. If there are more than two particles present, the homotopy classes are described by the integer number of particles enclosed by the paths in this class. From an algebraic

point of view, the exchange processes are no longer described by the two roots of unity, 1 and −1, but by the so-called *braiding group*, and the classification in bosons and fermions is no longer valid. In the simplest case of Abelian statistics,[16] one needs to generalise the commutation relation

$$\psi(\mathbf{r}_1)\psi(\mathbf{r}_2) = \pm\psi(\mathbf{r}_2)\psi(\mathbf{r}_1), \tag{4.23}$$

for bosons and fermions, respectively, to

$$\psi(\mathbf{r}_1)\psi(\mathbf{r}_2) = e^{i\alpha\pi}\psi(\mathbf{r}_2)\psi(\mathbf{r}_1), \tag{4.24}$$

where α is also called the *statistical angle*. One has $\alpha = 0$ for bosons and $\alpha = 1$ for fermions, and all other values of α in the interval between 0 and 2 for *anyons*. Sometimes anyonic statistics is also called *fractional statistics* – indeed all physical quasi-particles, such as those relevant for the FQHE, have an angle that is a fractional (or rational) number, but there is no fundamental objection that irrational values of the statistical angle should be excluded.

Before discussing the anyonic nature of Laughlin quasi-particles, we need to mention an important issue in these statistical considerations. We know that fermions are forced to satisfy Pauli's principle which excludes double occupancy of a single quantum state, whereas the number of bosons per quantum state is unrestricted. What about anyons then? In the context of quantum fields the Pauli principle yields, via Eq. (4.23) for $\mathbf{r} = \mathbf{r}_1 = \mathbf{r}_2$,

$$\psi(\mathbf{r})\psi(\mathbf{r}) = 0.$$

For an arbitrary statistical angle, one obtains in the same manner, from Eq. (4.24),

$$\left(1 - e^{i\alpha\pi}\right)\psi(\mathbf{r})\psi(\mathbf{r}) = 0, \tag{4.25}$$

which may be viewed as a *generalised Pauli principle for 2D anyons* [72]. Only if $\alpha = 0$ modulo 2, we may have $\psi(\mathbf{r})\psi(\mathbf{r}) \neq 0$ in order to satisfy Eq. (4.25). Otherwise, when $\alpha \neq 0$ modulo 2, we necessarily have $\psi(\mathbf{r})\psi(\mathbf{r}) = 0$. Anyons are, thus, from an exclusion-principle point of view more similar to fermions than to bosons.

4.3.2 Statistical properties of Laughlin quasi-particles
Laughlin 准粒子的统计性质

We may now apply the above general statistical considerations to the case of Laughlin quasi-particles. The basic idea is to describe the statistical angle as an Aharonov-Bohm phase due to some gauge field that is generated by the flux bound to the charges included in a closed loop $\partial\Sigma$. This closed loop, around which a quasi-particle moves adiabatically, encloses a surface Σ. The gauge field is not to be confunded with the one which generates the true magnetic field B – it is rather a *mock* (or fake) field $\mathbf{A}_M$ (with $\mathbf{B}_M = \nabla \times \mathbf{A}_M$) that generates the flux bound, e.g., by the electrons in the Laughlin liquid via the relation (4.4). We consider the case where the area Σ is filled with $N_{el}(\Sigma)$ electrons condensed in an incompressible quantum liquid described by Laughlin's wave function (4.3) and $N_{qh}(\Sigma)$ quasi-hole excitations (4.12), such that there are two contributions to $B_M = |\mathbf{B}_M|$,

$$B_M\Sigma = N_{\text{flux}}\frac{h}{e} = \left[mN_{el}(\Sigma) + N_{qh}(\Sigma)\right]\frac{h}{e}\ . \tag{4.26}$$

The corresponding Aharonov-Bohm phase, which the quasi-particle picks up when turning around the area Σ on the boundary path $\partial\Sigma$, is given by

$$\Gamma_{A-B} = 2\pi\frac{e^*}{h}\oint_{\partial\Sigma} d\mathbf{r}\cdot\mathbf{A}_M(\mathbf{r}) = 2\pi\frac{e^*}{h}\int_\Sigma d^2r\, B_M(\mathbf{r}),$$

where $e^* = e/m$ is the charge of the quasi-particle and where we have used Stoke's theorem to convert the line integral of $\mathbf{A}_M$ on $\partial\Sigma$ into a surface integral of B_M over the area Σ. The Aharonov-Bohm phase has

[16] There are more complicated cases of non-Abelian statistics, in which the exchange processes of more than two different particles no longer commute, but we do not discuss this case here and refer the reader to the review by Nayak *et al.* [70].

therefore two contributions, one Γ_{el} that stems from the electrons condensed in the Laughlin liquid and the other one Γ_{qh} that is due to the enclosed quasi-holes. One obtains from Eq. (4.26)

$$\Gamma_{el} = 2\pi \frac{e^*}{e} m N_{el} = 2\pi N_{el}, \tag{4.27}$$

for the enclosed electrons, i.e. an integer times 2π. Notice that this contribution to the Aharonov-Bohm phase may not be interpreted in terms of a statistical angle because it does not describe a true exchange process: the involved particles are not of the same type – we have chosen a quasi-particle to move on a path enclosing condensed electrons. However, had we chosen an *electron* rather than a *quasi-hole* to move along the path $\partial\Sigma$, the Aharonov-Bohm phase,

$$\Gamma_{el-el} = 2\pi \frac{e}{e} m N_{el}(\Sigma),$$

would give rise to a statistical angle $\alpha = m N_{el}(\Sigma)$.[17] If we have only one electron enclosed by the path, $N_{el}(\Sigma) = 1$, the statistical angle is simply the odd integer m, which is equal to 1 (modulo 2), as it should be for fermions.

A more interesting situation arises when the path encloses Laughlin quasi-holes, in which case the Aharonov-Bohm phase reads

$$\Gamma_{el} = 2\pi \frac{e^*}{e} N_{qh} = 2\pi \frac{N_{qh}}{m}. \tag{4.28}$$

Consider a single quasi-hole in the area Σ, $N_{qh} = 1$: one encounters the rather unusual situation in which the Aharonov-Bohm phase is a *fraction* of 2π, and the associated statistical angle is $\alpha = 1/m$. This illustrates that Laughlin quasi-holes are indeed anyons with fractional statistics, as we have argued above.

4.4 Generalisations of Laughlin's Wave Function
Laughlin 波函数的推广

Although Laughlin's wave function (4.3) has been extremely successful in the description of the FQHE at $\nu = 1/3$ and $1/5$, it is not capable of describing all observed FQHE states. Indeed, there are e.g. FQHE states at $\nu = 2/5, 3/7, 4/9, \ldots$ corresponding to the series $p/(2p+1)$, or more generally to $p/(2sp+1)$, in terms of the integers s and p, which may be accounted for within composite-fermion (CF) theory, which we present below. Furthermore, even-denominator FQHE states have been observed at $\nu = 5/2$ and $7/2$ [17], in the first excited LL ($n = 1$), and, in wide quantum wells or bilayer quantum Hall systems, at $\nu = 1/2$ and $\nu = 1/4$ [73, 74]. Whereas the latter may be understood within a multi-component picture, which we will briefly introduce in Chap. 5, the states at $\nu = 5/2$ and $7/2$ may find their explanation in terms of a so-called *Pfaffian* wave function. Both the CF and the Pfaffian wave functions are sophisticated generalisations of Laughlin's original idea.

4.4.1 Composite Fermions
复合费米子

Soon after the discovery of the most prominent FQHE state at $\nu = 1/3$, a lot of other states have been observed at the filling factors $\nu = p/(2sp+1)$. In a first theoretical approach, these states were interpreted in the framework of a hierarchy scheme [62, 75] according to which the quasi-particles of the Laughlin (parent) state, such as $\nu = 1/3$, condense themselves into a Laughlin-type (daughter) state, due to their residual Coulomb repulsion – remember that the Laughlin quasi-particles are charged with charge $e^* = e/m$. In this picture, the 2/5 state would be the daughter state formed of Laughlin quasi-particle excitations of the 1/3 state.

An alternative picture, though related to the above-mentioned hierarchy scheme, was proposed by Jain in 1989 [15, 16]. The basic idea consists of a reinterpretation of Laughlin's wave function (4.3): consider only

[17] Remember that the statistical angle is defined with respect to an exchange process $\mathcal{E}$ which is the square root of the process $\mathcal{T}$ considered here [Eq. (4.21)]. The relation between the statistical angle and the Aharononv-Bohm phase is therefore $\Gamma = 2\pi\alpha$ and not $\pi\alpha$.

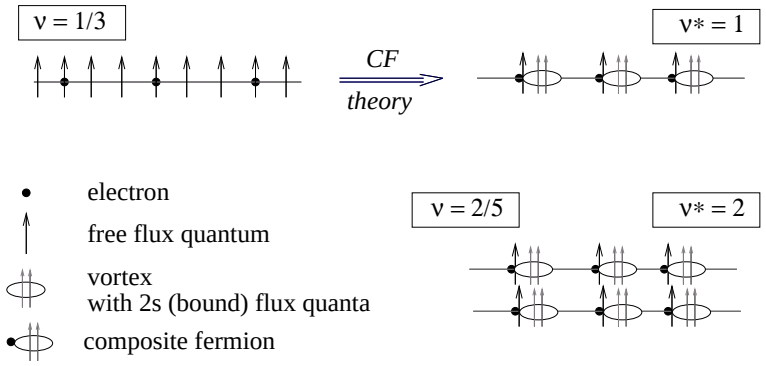

図 4.6: Schematic view of composite fermions. The electronic state at $\nu = 1/3$ may be interpreted as a CF state at an integer CF filling factor $\nu^* = 1$, where each vortex bound to an electron carries $2s$ (here $s = 1$) flux quanta. In the same manner a CF filling factor $\nu^* = 2$ gives rise to an (electronic) FQHE state at $\nu = 2/5$.

the polynomial part, the Gaussian $\exp(-\sum_j^N |z_j|^2/4)$ being an ubiquitous factor which finally needs to be multiplied with the polynomial wave function,

$$\psi_m^L(\{z_j\}) = \prod_{k<l}(z_k - z_l)^{2s+1} = \prod_{k<l}(z_k - z_l)^{2s} \prod_{k<l}(z_k - z_l). \tag{4.29}$$

In the last step of this equation, we have split the product into two parts, one with the exponent $2s$, which we call the *vortex* part, and another one with the exponent 1.

Before introducing Jain's generalisation, let us interpret the above wave function in terms of the statistical properties introduced in the last section. Quite generally, one may express any LLL N-particle wave function ψ_{LLL} as a product of such a vortex factor and another (residual) wave function ψ_{res},

$$\psi_{LLL}(\{z_j\}) = \prod_{k<l}(z_k - z_l)^{m'} \psi_{res}(\{z_j\}).$$

If the original wave function is fermionic, i.e. anti-symmetric with respect to an exchange process of an arbitrary particle pair, the symmetry properties of ψ_{res} depend on the parity of m'. If it is odd, ψ_{res} must be a symmetric (bosonic) wave function, and if it even, both the original and the residual wave functions are anti-symmetric (fermionic). In terms of the above-mentioned gauge field $\mathbf{A}_M(\mathbf{r})$, the statistical angle associated with the vortex factor is just given by the parity of m', which may be viewed as the number of *flux quanta attached to each particle* at the positions z_j. Flux attachment may thus be used, in 2D quantum mechanics, to transform fermions into bosons and *vice versa*.

In the case of the above decomposition (4.29) of Laughlin's wave function, the vortex part attaches s pairs of flux quanta to each particle position and therefore does not affect the statistical properties of the wave function. The second factor

$$\chi_{\nu^*=1}(\{z_j\}) = \prod_{k<l}(z_k - z_l)$$

is indeed fermionic and corresponds, as we have mentioned in Sec. 4.2.1, to a completely filled LL at a virtual (CF) filling factor of $\nu^* = 1$, the true filling factor being still $\nu = 1/(2s+1)$. This is schematically represented in 図. 4.6.

Jain's generalisation consists of replacing the term $\prod_{k<l}(z_k - z_l)$ by any other Slater determinant $\chi_{\nu^*=p}(\{z_j, z_j^*\})$ of p completely filled LLs, with a CF filling factor $\nu^* = p$,

$$\psi^J(\{z_j, z_j^*\}) = \mathcal{P}_{LLL} \prod_{k<l}(z_k - z_l)^{2s} \chi_{\nu^*=p}(\{z_j, z_j^*\}), \tag{4.30}$$

where we need to take into account the same projection $\mathcal{P}_{LLL}$ to the LLL as in the case of quasi-particle excitations (4.15) because, contrary to the $\nu^* = 1$ case, the wave function $\chi_{\nu^*=p}(\{z_j, z_j^*\})$ has by construction non-analytic components, i.e. components in higher (CF) LLs.

Jain's wave function (4.30) may be illustrated in the following manner. Via the first factor $\prod_{k<l}(z_k - z_l)^{2s}$, we have effectively bound $2s$ flux quanta to each of the electrons, as we have already mentioned above. This novel type of particle is what we call the *composite fermion* (CF). The residual (free) flux quanta effectively determine the effective number of states per (CF) LL,

$$N_B \to N_B^* = N_B - 2sN_{el},$$

which correspond to a renormalised magnetic field

$$B \to B^* = B - 2s\left(\frac{h}{e}\right) n_{el}. \tag{4.31}$$

Similarly the CF filling factor is defined with respect to the renormalised number of flux quanta,

$$\nu^* = \frac{N_{el}}{N_B^*} \qquad \to \qquad \nu^{*-1} = \nu^{-1} - 2s, \tag{4.32}$$

which leads to the relation

$$\nu = \frac{\nu^*}{2s\nu^* + 1} \tag{4.33}$$

between the CF filling factor and the usual one ν [Eq. (2.44)]. For completely filled LLs, $\nu^* = p$, this yields the above-mentioned series

$$\nu = \frac{p}{2sp + 1} \tag{4.34}$$

for the FQHE states which may thus be interpreted as IQHE states of CFs. To be explicit, the physical picture of CF theory is the following: the ground state is described by the wave function (4.30), which describes an incompressible quantum liquid in the same manner as Laughlin's wave function does. The elementary excitation in the CF theory consists of a CF promoted to the next higher CF LL, which is separated from the ground state by an energy gap, in analogy with the electron as compared to n completely filled (electronic) LLs in the IQHE.[18] Again, these elementary CF excitations become localised by the sample impurities, and one therefore obtains a plateau in the Hall resistance which is thus quantised.

Numerically, Jain's CF wave function (4.30) has been successful in the description of the series (4.34) of FQHE states: even if the overlap with the exact ground states decreases when the quantum number p, which describes the number of completely filled CF LLs, increases, the overlap is still reasonably high (above 95%) for the number of particles accessible in state-of-the-art exact diagonalisation calculations. Notice, however, that the physical interpretation is more involved as compared to Laughlin's wave function, because of the LLL projection $\mathcal{P}_{LLL}$, which is rather complicated to implement in analytical as well as numerical calculations. For a further review of CF theory, we refer the interested reader to the literature. The above-mentioned wave-function approaches are thoroughly reviewed in Jain's recent book [76]. Furthermore, there have been field-theoretical approaches beyond the numerical wave-function description presented above, such as in terms of Chern-Simons theories [77, 78] or in terms of a Hamiltonian theory [5]. For a review of these complementary theories we refer the reader to the book edited by Heinonen [79] or the excellent pedagogical review by Murthy and Shankar [5].

4.4.2 Half-filled LLs and Pfaffian states
半满 Landau 能级和 Pfaffian 态

Within the CF picture, we have seen that the effective magnetic field becomes renormalised due to flux attachment [Eq. (4.31)]. An interesting situation arises when the filling factor is $\nu = 1/2$, which corresponds to the limit $p \to \infty$ in Eq. (4.34). In this limit the effective magnetic field (4.31) vanishes, $B^* = 0$, and one may then expect the corresponding phase to be described in terms of a metallic state, such as a Fermi liquid that one would obtain for electrons when the magnetic field vanishes. A natural ansatz for the N-particle wave function of such a Fermi-liquid state is given by the Slater determinant

$$\psi_{FL} = \det\left(e^{i\mathbf{k}_i\cdot\mathbf{r}_j}\right),$$

[18] Remember, however, that the energy scale of this gap is not given in terms of a kinetic energy $\hbar eB/m$, but in terms of the Coulomb interaction $e^2/\epsilon l_B$.

where the N electrons occupy the states described by the wave vectors $\mathbf{k}$, $i = 1, ..., N$, the modulus of which is delimited by the Fermi wave vector $|\mathbf{k}_i| \leq k_F$, and $\mathbf{r}_j$ is the position of the j-th particle. Notice that this state is nevertheless unappropriate in the description of a state in the LLL. Indeed, if the scalar product in the exponent is rewritten in terms of complex variables, $\mathbf{k}_i \cdot \mathbf{r}_j = (k_i z_j^* + k_i^* z_j)/2$, one realises that the Fermi-liquid state violates the LLL condition of analyticity. Formally, one may again avoid this problem by projecting the Fermi-liquid state into the LLL, and one obtains indeed a state,

$$\psi_{FL}^{\nu=1/2} = \mathcal{P}_{LLL} \prod_{k<l} (z_k - z_l)^2 \det\left(e^{i\mathbf{k}_i \cdot \mathbf{r}_j}\right), \tag{4.35}$$

that was proposed by Rezayi and Read for the description of a compressible metallic state at $\nu = 1/2$ [80]. The first term is the same factor as in CF theory, which attaches 2 flux quanta to each particle and which cancels thus the external magnetic field, $B^* = B - 2(h/e)n_{el} = 0$.

Because the wave function (4.35) describes a compressible state, one should not observe a quantised Hall resistance, in agreement with most experimental data. A FQHE at $\nu = 1/2$ (and 1/4) has only been observed in very wide quantum wells [73, 74], which are likely to be described by two-component wave functions [81] that we will briefly introduce in Chap. 5.

In contrast to the LLL, the half-filled LL $n = 1$ reveals, in both spin branches, a FQHE (5/2 and 7/2 states). The difference between the half-filled LL $n = 0$ and $n = 1$ is due to a different *effective* interaction potential that takes into account the wave function overlap between two (interacting) particles, which we do not discuss in detail here. Indeed, the Fermi-liquid-like state (4.35) turns out to be quite unstable with respect to particle pairing. This is reminiscent of the BCS (Bardeen-Cooper-Schrieffer) instability of a conventional Fermi liquid that gives rise to superconductivity [52, 66], although the glue between the particles is no longer a phonon-mediated attractive interaction, but only the *repulsive* Coulomb interaction in a strong magnetic field. As we have already mentioned in Sec. 4.2.2, such an interaction may yield a discrete two-particle spectrum, in contrast to a repulsive interaction in the absence of a magnetic field. As a consequence, pairing may occur at certain relative angular momenta for particular pseudopotential sequences and for sufficiently high filling factors.[19] In the present case, one may exclude s-wave pairing, i.e. in the relative angular momentum state with $m = 0$ due to the Pauli principle, and the most natural candidate would therefore be p-wave pairing in the relative angular momentum state $m = 1$ [19].

A wave function that accounts for p-wave pairing was proposed by Moore and Read in 1991 [18],

$$\psi_{MR}(\{z_j\}) = \mathrm{Pf}\left(\frac{1}{z_i - z_j}\right) \prod_{k<l} (z_k - z_l)^2, \tag{4.36}$$

where we have again omitted the ubiquitous Gaussian factor. As for the CF wave functions (4.30) and the Rezayi-Read wave function (4.35), the factor $\prod_{k<l}(z_k - z_l)^2$ attaches two flux quanta to each electron and therefore does not change the statistical properties of the wave function. If the wave function consisted only of this factor (times the Gaussian), one would have a *bosonic* Laughlin wave function that describes an incompressible quantum liquid at the desired filling factor $\nu = 1/2$. However, it does not have the correct statistical properties. This problem is healed by the first factor $\mathrm{Pf}[1/(z_i - z_j)]$ which represents the *Pfaffian* of the $N \times N$ matrix $\mathcal{M}_{ij} = 1/(z_i - z_j)$. The Pfaffian may be viewed as the square root of the more familiar determinant, $\mathrm{Pf}(\mathcal{M}) = \sqrt{\det(\mathcal{M})}$, and has the same anti-symmetric properties as the determinant in an exchange of two particles i and j, such that it generates a fermionic wave function. Notice, furthermore, that this Pfaffian seems, at first sight, to take away some of the zeros such that one could expect the filling factor to increase. However, the function $\prod_{k<l}(z_k - z_l)^2$ is a product of $N(N-1) \sim N^2$ terms, whereas the Pfaffian is a sum of products of $N/2 \sim N$ terms. Therefore, the number of zeros, and thus the filling factor, is unchanged in the thermodynamic limit, $N \to \infty$.

A particularly interesting feature of the Pfaffian state are the quasi-particle excitations of charge $e/4$ which satisfy non-Abelian anyonic statistics [18], in contrast to the corresponding excitations of Laughlin's (4.3) or Jain's (4.30) wave functions. These non-Abelian quasi-particles are currently investigated in detail within the proposal of topologically-protected quantum computation [83]. A more detailed discussion of this issue is beyond the scope of these lecture notes, and we refer the reader to the review article by Nayak *et al.* [70].

[19] There have been attempts in the literature to formalise this point [63, 82].

Chapter 5

Brief Overview of Multicomponent Quantum-Hall Systems
多组分的量子 Hall 效应系统简介

5.1 The Different Multi-Component Systems
多组分系统的不同之处

5.1.1 The role of the electronic spin
电子自旋的效应

In the preceding chapters, we have completely neglected the physical consequences of possible internal degrees of freedom, apart from an occasional degeneracy factor that has been smuggled in to account for experimental data. This choice has been made simply for pedagogical reasons, but it is clear that one prominent internal degree of freedom – the electronic spin – may not be put under the carpet so easily. Naively, one may expect that each LL is split into two distinct spin-branches separated by the energy gap Δ_Z due to the Zeeman effect. If this gap is large, one may use the same one-particle arguments as in the case of the IQHE, but now for each spin branch separately: once the lowest spin branch of a paticular LL is completely filled, additional electrons must overcome an energy gap that is no longer given by the LL separation but by Δ_Z. This would indeed not change the presented explanation of the IQHE – instead of a localised electron in the next higher LL, one simply needs to invoke localisation in the upper spin branch.

Also in the case of the FQHE, the explanation would need to be modified only in the fine structure if the Zeeman gap is sufficiently large. If the electrons fill partially the lower spin branch of the lowest (or any) LL, one may omit all transitions to the upper spin branch and argue that they constitute the high-energy degrees of freedom, in the same manner as inter-LL excitations in the case of the "spinless" fermions which we have discussed in Sec. 4.1.

However, the situation is not so easy as the above picture might suggest. Indeed, already in 1983 Halperin pointed out [84] that the Zeeman gap in GaAs, with a g-factor of $g = -0.4$, is $\Delta_Z = g\mu_B B = g(\hbar e/2m_0)B \simeq 0.33B[\mathrm{T}]$ K and therefore much smaller than both the LL separation $\hbar\omega_C = (\hbar e/m)B \simeq 24B[\mathrm{T}]$ K, due to the rather small band mass ($m = 0.068m_0$, in terms of the bare electron mass m_0, in GaAs), and the Coulomb energy scale $V_C = e^2/\epsilon l_B \simeq 50\sqrt{B[\mathrm{T}]}$ K with a dielectric constant of $\epsilon \simeq 13$. For a characteristic field of 6 T, for which one typically reaches the LLL condition $\nu = 1$, one therefore has the energy scales

$$\Delta_Z \simeq 2\,\mathrm{K} \quad \ll \quad \frac{e^2}{\epsilon l_B} \simeq 120\,\mathrm{K} \quad \lesssim \quad \hbar\omega_C \simeq 140\,\mathrm{K}, \tag{5.1}$$

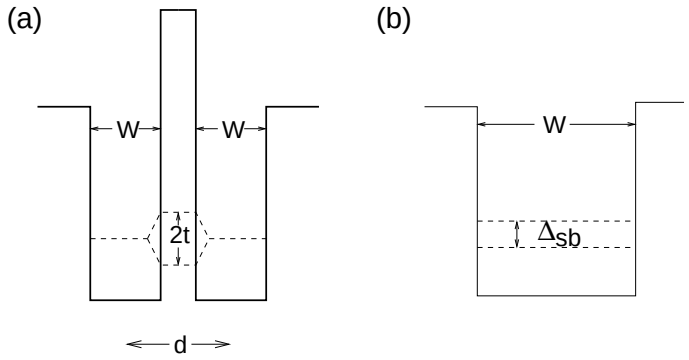

图 5.1: *(a)* Profile of a double quantum well. The two wells are separated by a distance d that is typically on the same order of magnitude as the well width W, $d \sim W \sim 10$ nm. In the presence of a tunneling term t between the two wells, the electronic subband is split into a symmetric and an anti-symmetric combination, separated by the energy scale $\Delta_{SAS} = 2t$. *(b)* Wide quantum well. In a wide quantum well the energy gap between the occupied lowest electronic subband and the unoccupied first excited subband, Δ_{sb}, is decreaased as compared to a narrow quantum well.

in GaAs. The situation is qualitatively the same in graphene, where one finds for a field[1] of 6 T

$$\Delta_Z \simeq 7\,\mathrm{K} \quad \ll \quad \frac{e^2}{\epsilon l_B} \simeq 620\,\mathrm{K} \quad \lesssim \quad \sqrt{2}\frac{\hbar v}{l_B} \simeq 1000\,\mathrm{K}, \tag{5.2}$$

for $g \simeq 2$ and $\epsilon \simeq 2.5$, which are the appropriate values for graphene on a SiO_2 substrate.[2]

The inevitable consequence of these considerations is that, even if one may neglect the kinetic energy scale in a low-energy description of a partially filled LL, one cannot do so with the Zeeman energy scale. One must therefore take into account the electron spin within a two-component picture in which each quantum state $|n, m\rangle$ is doubled, $|n, m; \sigma\rangle$ with $\sigma =\uparrow$ and $\downarrow$.

5.1.2 Graphene as a four-component quantum Hall system
石墨烯：四组分量子 Hall 系统

Another multi-component system that we have already discussed is precisely graphene, not only because of the tiny Zeeman gap which requires to take into account the electronic spin, but also because of its double valley degeneracy due to the two inequivalent Dirac points situated at the corners K and K' in the first BZ. Each quantum state $|n, m\rangle$ therefore occurs in *four* copies, $|n, m; \sigma\rangle$ with $\sigma = (K, \uparrow)$, $(K, \downarrow)$, $(K', \uparrow)$ and $(K', \downarrow)$. Formally this four-fold degeneracy may be described with the help of an SU(4) spin, whereas the two-fold spin degeneracy in GaAs, e.g., is represented by the usual SU(2) spin. Notice that it is very difficult in graphene to lift the valley degeneracy, and the associated energy scale is expected to be on the same order of magnitude as the Zeeman gap, i.e. it is tiny with respect to the one set by the Coulomb interactions.

5.1.3 Bilayer quantum Hall systems
双层量子 Hall 系统

A third multi-component system that we would like to mention consists of a double quantum well [see 图. 5.1(a)]. These bilayer systems, which are fabricated by molecular-beam epitaxy, consist of two quantum wells spatially separated by an insulating barrier that is on the same order of magnitude as the width of each of the wells. Formally, each of the wells (layers) may be described in terms of an SU(2) *pseudo-spin*,

[1] Remember that this field is somewhat arbitrary because the situation $\nu = 1$ may also be obtained easily for other fields by varying the gate voltage V_G.

[2] Naturally, the dielectric constant depends on the dielectric environment around the graphene sheet and thus also on the substrate.

$\sigma =\uparrow$ for an electron in the left well and $\sigma =\downarrow$ for one in the right well. In contrast to the true electron spin, the Coulomb interaction does not respect this SU(2) symmetry – indeed, the repulsion is stronger between particles within the same layer (i.e. with the same pseudo-spin orientation) than between particles in different layers (with opposite pseudo-spin orientation) because, in the second case, electrons may not be brought together closer than the distance d between the layers. In order to minimise the interaction energy, it is therefore favourable to charge both layers equally. Alternatively, this may be viewed as some capacitive energy, if one interprets the two-layer system in terms of a capacitor, that favours an equal charge distribution between the two layers as compared to a charging of only one layer. Notice, furthermore, that tunneling, with the tunneling energy t, between the two quantum wells lifts the pseudo-spin degeneracy: whereas the symmetric superposition $|+\rangle = (|\uparrow\rangle + |\downarrow\rangle)/\sqrt{2}$ of the layer pseudo-spin lowers the energy, the anti-symmetric superposition $|-\rangle = (|\uparrow\rangle - |\downarrow\rangle)/\sqrt{2}$ describes anti-binding. The energy separation between the associated subbands is given by $\Delta_{SAS} = 2t$ [see 图. 5.1(a)], but it may be strongly reduced experimentally with the help of a high potential barrier separating the two wells. The term Δ_{SAS}, which plays the role of a Zeeman gap (though in the x-quantisation axis), may become the lowest energy scale in the system, such that the SU(2) pseudo-spin symmetry breaking only stems from the difference in the Coulomb interaction between particles in the same and in different layers.

5.1.4 Wide quantum wells
宽量子阱

Another quantum Hall system that may be characterised as a multi-component system is a wide quantum well [图. 5.1(b)]. Indeed, the samples which reveal the highest mobilities are those fabricated in wide quantum wells, where the well width w is often much larger than the magnetic length l_B. As compared to a narrow quantum well, the energy difference between the lowest and the first excited electronic subbands, which are the energy levels of the confinement potential in the z-direction, is strongly decreased. Although the Fermi level still resides in the lowest electronic subband (pseudo-spin $\sigma =\uparrow$), the energy gap to the next unoccupied one (pseudo-spin $\sigma =\downarrow$) may then become smaller than the relevant Coulomb energy scale. In the same manner as for the electronic spin, one must therefore no longer discard higher electronic subbands. In a first approximation one may restrict the calculations to these two lowest subbands [85, 81] although the next higher subbands also shift to lower energies and need eventually be taken into account. Similarly to the quantum-Hall bilayer, which is sometimes also used in the description of the large quantum well, the Coulomb interaction decomposed in these electronic subband states is not pseudo-spin SU(2)-symmetric.

In the remainder of this chapter, we discuss some aspects of correlated states that one encounters in multi-component quantum Hall systems in general, starting (Sec. 5.2) with the completely spin-polarised state at $\nu = 1$ (quantum Hall ferromagnet) and its various manifestations in the different quantum Hall systems described above. We will not discuss, for reasons of space limitation, the amazing physical properties of the elementary excitations of the quantum Hall ferromagnet, which is a topological spin-texture state *(skyrmion)*, and refer the interested reader to the literature [86, 87, 4, 3]. In the line of the preceding chapter, we have chosen to discuss a generalisation of Laughlin's wave function, which we owe to Halperin [84], in order to account for the electronic spin (Sec. 5.3). These wave functions are further generalised to even more components than two, and we close this section with a discussion of their possible use in the description of multi-component FQHE states.

5.2 The State at $\nu = 1$
$\nu = 1$ 态

If one takes into account internal degrees of freedom, the state at $\nu = 1$ is no longer simply a Slater determinant of all occupied quantum states in the lowest LL, but one must take into account the macroscopic degeneracy due to the fact that each state $|n, m\rangle$ may now be occupied by 0, 1 or 2 particles. In this sense the situation at $\nu = 1$ is much more similar to the FQHE in a partially filled LL than to the IQHE which one obtains for completely filled LL [86], and the macroscopic degeneracy is again lifted by the mutual Coulomb interactions between the electrons.

5.2.1 Quantum Hall ferromagnetism
量子 Hall 反铁磁性

We first consider the generic case of electrons at $\nu = 1$ in the conventional monolayer quantum Hall system while taking into account their physical spin. In view of the above-mentioned energy arguments, we completely neglect the Zeeman effect, which would otherwise trivially lift the macroscopic degeneracy at $\nu = 1$ by polarising all electron spins. Because of the fact that two electrons, with opposite spin, may now occupy the same quantum state $|n, m\rangle$, the electron pair may in principle be in a relative angular momentum state with $m = 0$ – the Pauli principle, which only applies to fermions of the same species, does no longer prevent this quantum number to be odd. Indeed, such an electron pair is described by a two-particle wave function with the rather unspectacular polynomial factor $(z_{i,\uparrow} - z_{j,\downarrow})^0 = 1$, where $z_{i,\uparrow}$ is the position of an arbitrarily chosen spin-↑ electron and $z_{j,\downarrow}$ that of a spin-↓ electron. Such an electron pair therefore interacts via the Haldane pseudopotential v_0, which is the largest pseudopotential in the case of a repulsive Coulomb interaction because it characterises the interaction at the shortest possible length scale (see 图. 4.2).[3] Since $v_0 \simeq 2v_1$, the system thus tends to avoid double occupancy, and the ground state is described by the fully anti-symmetric (orbital) wave function (4.7) regardless of whether the electron at the position z_j is spin-↑ or spin-↓.

Notice that, although both spinless and spin-1/2 electrons are described by the same wave function, the physical origin of these ground states is different: in the case of spinless fermions, it is simply the non-degenerate wave function described by a Slater determinant, whereas in the case of electrons with spin, the state is formed in order to minimise the mutual Coulomb repulsion.

Because the orbital wave function (4.7) for electrons with spin at $\nu = 1$ is fully anti-symmetric, the spin wave function describing the internal degrees of freedom must be fully symmetric, e.g.

$$\chi_{FM} = |\uparrow_1, \uparrow_2, ..., \uparrow_N\rangle, \tag{5.3}$$

in order to form an overall wave function that is anti-symmetric. The subscript indicates the index of the particle that the spin is associated with. The global wave function, therefore, reads

$$\psi_{\nu=1,FM} = \prod_{k<l}(z_k - z_l) \otimes |\uparrow_1, \uparrow_2, ..., \uparrow_N\rangle. \tag{5.4}$$

This is nothing other than a (spin) wave function of a *quantum ferromagnet*, similar to ferromagnetism in a usual Fermi liquid. Indeed, the spontaneous spin polarisation in a Fermi liquid is also due to a minimisation of the Coulomb repulsion by the formation of an anti-symmetric orbital wave function. Notice, however, that the spin polarisation in a Fermi liquid comes along with an energy cost as a consequence of the mismatch between the Fermi energies of spin-↑ and spin-↓ electrons. The competition between the gain in interaction energy and the cost in kinetic energy determines the final polarisation of the system, which is never perfect. In the case of the quantum Hall ferromagnet, there is no cost in kinetic energy when the system is fully polarised because all quantum states have the same kinetic energy, and the system is therefore *fully* polarised.

Collective excitations
集体激发

Because the spontaneous spin polarisation in the quantum Hall ferromagnet chooses, in the absence of a Zeeman effect, an arbitrary direction in the three-dimensional spin space, one is confronted with a spontaneous SU(2) symmetry breaking. As a consequence of this broken continuous symmetry, there exists a gapless collective excitation (Goldstone mode) the energy of which tends to zero in the long wave-length limit. Indeed, even if we have chosen the ferromagnet in Eq. (5.3) to be oriented in the z-direction, any other orientation, such as the one described by the wave function

$$|\downarrow_1, \downarrow_2, ..., \downarrow_N\rangle \qquad \text{or} \qquad \bigotimes_{j=1}^{N} |+_j\rangle = |+_1, +_2, ..., +_N\rangle,$$

[3] This pseudopotential, as well as any other with an even value of m, does not play any physical role due to the Pauli principle if one considers only spinless electrons, as we have mentioned in Sec. 4.2.2.

where the $+_j$ sign indicates the symmetric superposition $|+_j\rangle = (|\uparrow_j\rangle + |\downarrow_j\rangle)/\sqrt{2}$ of both spin orientations of the j-th electron, would also describe a ground state. The Goldstone mode in the large wave-length limit may then be viewed as a global rotation of all spins into another ground-state configuration, which naturally does not imply an energy cost.

In the case of a ferromagnet, the Goldstone mode is nothing other than the spin-density wave[4] that disperses as $\omega \propto q^2$ in the small wave vector limit, $ql_B \ll 1$. At first sight, this mode seems in contradiction with the observation of a quantum Hall effect at $\nu = 1$, even in the absence of a Zeeman effect, which requires a gap as we have seen above. Notice, however, that this gap needs to be a transport gap in which a quasi-particle moves independently from a quasi-hole in order to transport a current. This is not the case in a spin wave with $ql_B \ll 1$, but one obtains freely moving quasi-particles and quasi-holes in the limit $ql_B \gg 1$. In this limit, the spin-wave dispersion tends to a finite value that is given by the exchange energy between particles of different spin orientation and that is proportional to the interaction energy scale $e^2/\epsilon l_B$, as in the case of the FQHE [87].

There are more exotic spin-texture excitations (skyrmions), which are described by a topological quantum number associated with the winding of the spin-texture. These are gapped excitation which carry an electric charge related to this topological quantum number. As mentioned above, a detailed discussion of these amazing excitations is beyond the scope of the present lecture notes.

5.2.2 Exciton condensate in bilayer systems
双层系统的激发态凝聚

The $\nu = 1$ in a bilayer system is remarkably different from the quantum Hall ferromagnet described in the preceding subsection. Although the electronic interactions still favour a fully anti-symmetric orbital wave function (4.7) and thus a symmetric, i.e. ferromagnetic, pseudo-spin wave function, the interaction potential is no longer SU(2) symmetric in the pseudo-spin degree of freedom.[5] As we have already mentioned above, a charge imbalance Q between the two quantum wells (layers) is penalised by a charging energy, $E_C = Q^2/2C$, in terms of the capacitance $C = \epsilon\mathcal{A}/d$, where $\mathcal{A}$ is the area of the 2D system. Because $Q = -e\nu n_{el}\mathcal{A} = -e\nu n_B\mathcal{A} = -e\nu\mathcal{A}/2\pi l_B^2$ when all electrons reside in a single layer and $Q = 0$ if they are equally distributed between the two layers, one obtains an energy cost

$$\frac{E_C}{N_{el}} \sim \nu \frac{e^2}{\epsilon l_B}\frac{d}{l_B},$$

per particle in the charge-imbalenced state, in agreement with a more sophisticated microscopic calculation [87]. In terms of the pseudo-spin magnetisation, this means that in the ground-state configuration, with a homogeneous charge distribution over both layers, all pseudo-spins are oriented in the xy-plane. Remember that a pseudo-spin $\uparrow$ corresponds to an electron in the upper layer and $\downarrow$ to one in the lower layer, and a configuration as the one described in Eq. (5.3) is therefore excluded, whereas the symmetric and anti-symmetric combinations

$$\chi_+ = \bigotimes_{j=1}^{N} |+_j\rangle \qquad \text{以及} \qquad \chi_- = \bigotimes_{j=1}^{N} |-_j\rangle,$$

with $|\pm_j\rangle = (|\uparrow_j\rangle \pm |\downarrow_j\rangle)/\sqrt{2}$ is not. These two states, which correspond to a ferromagnet in the x- and the y-direction, respectively, may be generalised by choosing any other direction described by the angle ϕ in the xy-plane,

$$\chi_\phi = \bigotimes_{j=1}^{N} |\phi_j\rangle, \tag{5.5}$$

where $|\phi_j\rangle \equiv [|\uparrow\rangle + \exp(i\phi)|\downarrow\rangle]/\sqrt{2}$. The states χ_+ and χ_- are obtained for $\phi = 0$ and $\phi = \pi$ (modulo 2π), respectively.

[4] Remember that for a crystaline ground state (WC), the Goldstone mode is the acoustic phonon, as we have briefly discussed in the previous chapter in Sec. 4.1.

[5] Naturally, such an anti-symmetric orbital wave function is only physical if the layer separation d is not too large (as compared to the magnetic length) – otherwise one would simply have completely decoupled layers.

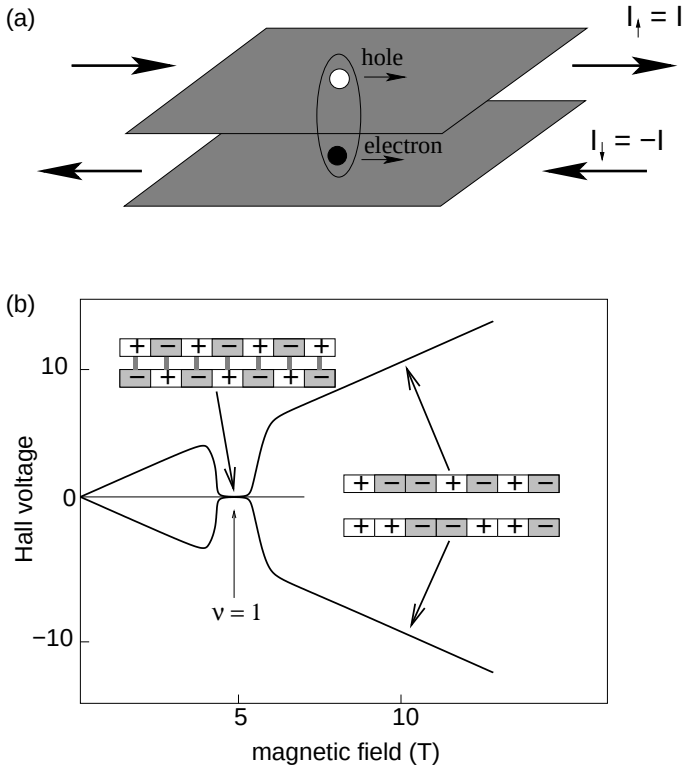

图 5.2: Hall resistance measurement used to detect excitonic condensation, adopted from (Eisenstein and MacDonald, 2004). *(a)* Counterflow configuration, in which one drives a current $I_\uparrow = I$ through the upper layer that is flowing in the opposite direction as that, $I_\downarrow = -I$ in the lower layer. The hole component of the excitonic quantum state in one layer thus moves in the same direction as the electron component in the other one. *(b)* The two curves schematically represent, when taking into account only excitonic superfluidity, the Hall resistance in both layers within the counterflow configuration. Because of the relative sign between the currents in the two layers, the measured Hall resistances are of opposite sign. Electrons with no interlayer correlations yield the usual linear B-field dependence of the Hall resistance in order to compensated the Lorentz force acting on them individually. In the case of exciton condensation (around $B = 5$ T), charge tranport is due to a uniform current of charge-neutral excitons, which are not affected by the Lorentz force, and the Hall resistance vanishes, as it has been observed in the experiments (Kellogg *et al.*, 2004; Tutuc *et al.*, 2004).

Contrary to the case of the spin ferromagnet with full SU(2) symmetry, where a general state would be described in terms of two angles θ and ϕ, the different possible *easy-plane* pseudo-spin ferromagnetic are characterised by the angle ϕ which may vary between 0 and 2π. The low-energy degrees of freedom are therefore described by a different *universality class* that turns out to be the same as the one that describes superfluidity or superconductivity. The relation between superfluidity and the easy-plane pseudo-spin ferromagnet in bilayer systems at $\nu = 1$ may indeed be understood in the following manner: on the average, the average filling factor per layer is $\nu_\uparrow = \nu_\downarrow = 1/2$ in order to minimise the charging energy due to the capacitive term, i.e. there are as many electrons as holes in the LLL of each layer. Naturally, because of the Coulomb interaction between the particles in the two different layers, an electron in one layer wants to be bound to a hole in the other one. Since the number of electrons in each layer equals, on the average, that of holes in the other one, all particles find their appropriate partner in the opposite layer. The electron-hole pair in the two layers may be viewed as a charge-neutral *interlayer exciton* that satisfies bosonic statistics [图. 5.2(a)]. Below a certain temperature, these bosons condense into a collective state that is nothing other than the *exciton superfluid* [88, 89, 90, 87]. The phase coherence between the different excitons is precisely described by the angle ϕ.

The first experimental indication of excitonic superfluidity in bilayer quantum Hall systems was a zero-bias anomaly in tunneling experiments [91]. Indeed, if one injects a charge in a tunneling experiment into one of the layers and collects it in a contact at the other layer, the tunneling conductance dI_z/dV is expected to be weak in the case of uncorrelated electrons because of the Coulomb repulsion between electrons in the opposite layers. However, below a critical value of d/l_B, where one expects the interlayer correlations to be sufficiently strong to form a phase-coherent excitonic condensate, the injected electron systematically finds a hole in the other layer, such that tunneling between the layers is strongly enhanced. This strong enhancement, which due to its reminiscence with the Josephson effect in superconductors [66] is also called *quasi-Josephson effect*,[6] has indeed been observed experimentally [91].

Another strong indication for excitons in bilayer quantum Hall systems stems from transport measurements in the counterflow configuration, where the current in the upper layer $I_\uparrow = I$ flows in the opposite direction as compared to that in the lower layer $I_\downarrow = -I$ [see 图. 5.2(a)]. From a technical point of view, it is indeed possible to contact the two layers separately such that one may measure the Hall resistance (and also the longitudinal resistance) in both layers independently. In the case of exciton condensation, the charges involved in transport are *zero* because the excitons are charge-neutral objects, which are not coupled to the magnetic field and thus not affected by the Lorentz force. In addition to a vanishing longitudinal resistance, one would therefore expect a vanishing Hall resistance because no density gradient between opposite edges is built up to compensate the Lorentz force [89, 90]. This is schematically shown in 图. 5.2(b). The simultaneous vanishing of the Hall and longitudinal resistances was indeed observed in 2004 by two different experimental groups [92, 93].

5.2.3 SU(4) ferromagnetism in graphene
石墨烯的 SU(4) 反铁磁性

The arguments in favour of a quantum Hall ferromagnetism may easily be generalised to the case of graphene, where the Coulomb interaction respects to great accuracy the four-fold spin-valley degeneracy, as we have described above. In order to avoid confusion about the filling factor, one first needs to remember that the filling factor ν_G in graphene is defined with respect to the charge-neutral point, which happens to be in the centre of the central $n = 0$ LL (see Sec. 3.5). Two of the four (degenerate) spin-valley branches are therefore completely filled at $\nu_G = 0$, which in non-relativistic quantum Hall systems would correspond rather to a filling factor $\nu = 2$. Similarly the filling factor $\nu = 1$ would correspond to a graphene filling factor $\nu_G = -1$, whereas $\nu_G = 1$ implies three completely filled spin-valley branches ($\nu = 3$).

Let us first consider the filling factor $\nu_G = -1$ and see how the above considerations apply to graphene with its SU(4) symmetry.[7] In the same manner as for the spin quantum Hall ferromagnet at $\nu = 1$, the short-range component v_0 of the Coulomb potential is screened in the completely anti-symmetric orbital

[6] Contrary to the Josephson effect, only the tunneling conductance dI_z/dV is strongly enhanced whereas the tunneling *current* remains zero in the quasi-Josephson effect in bilayer systems.

[7] The filling factor $\nu_G = 1$ is related to $\nu_G = -1$ by particle-hole symmetry and therefore does not require a separate discussion.

wave function (4.7), and the spin part of the wave function must therefore be completely symmetric. Notice, however, that one may now distribute the electron over the four internal states $|m;K,\uparrow\rangle$, $|m;K,\downarrow\rangle$, $|m;K',\uparrow\rangle$ and $|m;K',\downarrow\rangle$. The general spin wave function is therefore a superposition of all these states

$$\chi_{\mathrm{SU}(4)} = \bigotimes_{m=1}^{N} \left(u_{m,1}|m;K,\uparrow\rangle + u_{m,2}|m;K,\downarrow\rangle + u_{m,3}|m;K',\uparrow\rangle + u_{m,4}|m;K',\downarrow\rangle \right), \tag{5.6}$$

where the complex coefficients $u_{m,i}$ satisfy the normalisation condition $\sum_{i=1}^{4} |u_{m,i}|^2 = 1$. In the case of global coherence, all coefficients are independent of the guiding-centre quantum number m, $u_{m,i} = u_i$, and one thus obtains the spin wave function of an *SU(4) ferromagnetism* [94, 95, 96, 97]. These arguments may also be generalised to the case of $\nu_G = 0$, where two branches are completely filled [97], but the ground state does not reveal the same degeneracy as the SU(4) ferromagnet at $\nu_G = \pm 1$. Indeed, a general argument on K-component quantum Hall system shows that one has generalised ferromagnetic states at all integer values of the filling factor $\nu = 1, ..., K-1$ [98].

As a consequence of the SU(4) quantum Hall ferromagnet, one may expect a quantum Hall effect in graphene at the unusual filling factors $\nu_G = 0, \pm 1$. Remember that these states do not belong to the series (3.22), $\nu_G = \pm 2, \pm 4, ...$ of the RQHE which may be explained by LL quantisation within the picture of non-interacting relativistic particles. In the same manner as for the spin quantum Hall ferromagnet, the gapless spin-density-wave modes, which reveal a higher degeneracy due to the larger SU(4) symmetry, do not imply that the charged modes are also gapless. Indeed, the elementary charged excitations of the SU(4) quantum Hall ferromagnet are generalised skyrmions [97, 99] which are separated by a gap from the ground state, which therefore describes an incompressible quantum liquid that displays the quantum Hall effect. A quantum Hall effect has indeed been observed at these unusual filling factors [22], in agreement with the formation of an SU(4) quantum Hall ferromagnet. However, there exist alternative scenarios to describe the appearance of a quantum Hall effect at these filling factors [100, 101, 102] and a clear indication of SU(4) quantum Hall ferromagnetism is yet lacking.

We finally emphasise that an SU(4) description is not restricted to graphene. Indeed, if one takes into account the electron spin, the bilayer quantum Hall system and its excitations may also be treated within the SU(4) framework [98, 103, 3, 99] although the interaction does not respect the full SU(4) symmetry because of the asymmetry in the layer pseudo-spin described above.

5.3 Multi-Component Wave Functions
多组分波函数

Until now, we have considered a multi-component quantum Hall effect at the integer filling factor $\nu = 1$ (or other integer fillings in the case of graphene) that is described in terms of the Vandermonde determinant (4.7) $\prod_{k<l}(z_k - z_l)$ regardless of whether the particle at the position z_k is in a state $\uparrow$ or $\downarrow$. The spin orientation has only been taken into account within a spin wave function that is multiplied to the Vandermonde determinant. One may naturally ask the question whether one may also describe other filling factors than $\nu = 1$.

A simple generalisation of the quantum Hall ferromagnetism to other filling factors consists of replacing the Vandermonde determinant by, e.g., the Laughlin (4.3) at $\nu = 1/(2s+1)$ or the Jain wave function (4.30) at $\nu = p/(2sp+1)$ and to multiply it again with a spin wave function that is naturally ferromagnetic because the orbital wave function remains anti-symmetric. There are, however, more general states for which the orbital wave function is not fully anti-symmetric, but only in the intra-component parts as it is required by the Pauli principle. These states are described in terms of wave functions proposed by Halperin in 1983 [84] that we present in this section, as well as a natural generalisation to systems with more components than $K = 2$.

5.3.1 Halperin's wave function
Halperin 波函数

Halperin's wave function for spin-1/2 electrons is a straight-forward generalisation of Laughlin's proposal (4.3). We consider the particle positions to be separated into two sets $\{z_1^{\uparrow}, z_2^{\uparrow}, ..., z_{N_\uparrow}^{\uparrow}\}$ for spin-$\uparrow$ particles

and $\{z_1^\downarrow, z_2^\downarrow, ..., z_{N_\downarrow}^\downarrow\}$ for spin-$\downarrow$ particles. If the particles with different spin orientation could be treated as independent from one another, i.e. in the absence of an interaction between spin-$\uparrow$ and spin-$\downarrow$ particles, one would simply write down a product ansatz

$$\psi^L_{\uparrow,m_1}(\{z_j^\uparrow\}) \times \psi^L_{\downarrow,m_2}(\{z_j^\downarrow\}) = \prod_{k<l}^{N_\uparrow} \left(z_k^\uparrow - z_l^\uparrow\right)^{m_1} \prod_{k<l}^{N_\downarrow} \left(z_k^\downarrow - z_l^\downarrow\right)^{m_2} \tag{5.7}$$

of two independent Laughlin wave functions that need not necessarily be described by the same exponent m. The total filling factor would then be simply the sum $\nu = \nu_\uparrow + \nu_\downarrow$ of the filling factors $\nu_\uparrow = 1/m_1$ and $\nu_\downarrow = 1/m_2$ for spin-$\uparrow$ and spin-$\downarrow$ particles, respectively.

Apart from the fact that this situation is not particularly interesting, it is also unphysical because the Coulomb interaction does not depend on the spin orientation of the particle pairs. In the wave function (5.7), two particles of opposite spin orientation may be at the same position, i.e. the wave function does not vanish in general for $z_k^\uparrow = z_l^\downarrow$. Remember that such a double occupancy of the same position would be penalised by an energy cost on the order of the short-range component v_0 in a pseudopotential expansion.

In order to account for these inter-component correlations, Halperin proposed to add a factor $\prod_{k=1}^{N_\uparrow} \prod_{l=1}^{N_\downarrow} (z_k^\uparrow - z_l^\downarrow)^n$ to the wave function (5.7) the exponent of which does not necessarily need to be odd because particles of opposite spin orientation are not constrained by the Pauli principle. Halperin's wave function

$$\psi^H_{m_1,m_2,n}(\{z_j^\uparrow, z_j^\downarrow\}) = \prod_{k<l}^{N_\uparrow} \left(z_k^\uparrow - z_l^\uparrow\right)^{m_1} \prod_{k<l}^{N_\downarrow} \left(z_k^\downarrow - z_l^\downarrow\right)^{m_2} \prod_{k=1}^{N_\uparrow} \prod_{l=1}^{N_\downarrow} \left(z_k^\uparrow - z_l^\downarrow\right)^{n} \tag{5.8}$$

is therefore characterised by the set (m_1, m_2, n) of three exponents.

In analogy with Laughlin's wave function, for which we have $\nu = 1/m$, the exponents fix the (component) filling factors, as one may see from the power-counting argument (see Sec. 4.2). According to this argument, the maximal exponent for a particular particle position cannot exceed the number of flux quanta N_B threading the area $\mathcal{A}$ of the 2D electron system. Apart from the shift that vanishes anyway in the thermodynamic limit, one obtains the two equations

$$N_B = m_1 N_\uparrow + n N_\downarrow \qquad \text{以及} \qquad N_B = m_2 N_\downarrow + n N_\uparrow. \tag{5.9}$$

This means that, contrary to the simpler case of Laughlin's wave function, the number of zeros in one component is not simply given by the corresponding exponent times the number of particles in this component (first term in the above expressions). Instead, it is also affected by the particles in the other component that contribute each a zero of order n (second term) due to the mixed term in Halperin's wave function (5.8). In terms of the component filling factors,

$$\nu_\sigma = \frac{N_\sigma}{N_B}\,, \tag{5.10}$$

Eq. (5.9) may be rewritten in matrix form

$$\begin{pmatrix} 1 \\ 1 \end{pmatrix} = \begin{pmatrix} m_1 & n \\ n & m_2 \end{pmatrix} \begin{pmatrix} \nu_\uparrow \\ \nu_\downarrow \end{pmatrix}, \tag{5.11}$$

from which one obtains the component filling factors by matrix inversion

$$\begin{pmatrix} \nu_\uparrow \\ \nu_\downarrow \end{pmatrix} = \frac{1}{m_1 m_2 - n^2} \begin{pmatrix} m_2 & -n \\ -n & m_1 \end{pmatrix} \begin{pmatrix} 1 \\ 1 \end{pmatrix}, \tag{5.12}$$

and one finds

$$\nu = \nu_\uparrow + \nu_\downarrow = \frac{m_1 + m_2 - 2n}{m_1 m_2 - n^2} \tag{5.13}$$

for the total filling factor.

One first notices that, in Eq. (5.12), not only the filling factors are fixed by the exponents but also, for a given magnetic field (i.e. a given number of flux quanta), the number of particles per component. Contrary

to what one could have expected from the expression of Halperin's wave function (5.8), the numbers N_σ, namely the ratio between them, cannot be chosen arbitrarily.

Furthermore, the above expressions (5.12) and (5.13) for the filling factors are ill-defined if the exponent matrix in Eq. (5.11) is not invertible, i.e. when its determinant is zero, $m_1 m_2 - n^2 = 0$. The only physically relevant situation arises when all exponents are equal odd integers $m_1 = m_2 = n$. However, this result should not surprise us: we are then confronted again with a completely anti-symmetric wave function, actually a Laughlin wave function, which requires a ferromagnetic spin wave function. As we have seen above, in the discussion of the quantum Hall ferromagnetism, the ground-state manifold comprises states with different polarisation along the z-axis: the state with $N_\uparrow = N$ and $N_\downarrow = 0$ is an equally valid ground state as a state with $N_\uparrow = N_\downarrow = N/2$ or $N_\uparrow = 0$ and $N_\downarrow = N$, where $N = N_\uparrow + N_\downarrow$ is the total number of particles. The component filling factor is therefore not well-defined and depends on the polarisation

$$p_z = \frac{N_\uparrow - N_\downarrow}{N} = \frac{\nu_\uparrow - \nu_\downarrow}{\nu}, \tag{5.14}$$

whereas the total filling factor is simply given by $\nu = 1/m$, in terms of the common odd exponent m. Notice that contrary to the quantum Hall ferromagnet, a state with an invertible exponent matrix has a polarisation that is completely fixed,

$$p_z = \frac{m_2 - m_1}{m_1 m_2 - n^2} \ . \tag{5.15}$$

We finally mention that not all states that can be written down in terms of Halperin's wave function are good candidates for the description of the ground state chosen by the system. One may show, e.g. within a generalisation of Laughlin's plasma analogy (presented in Sec. 4.2.5) to two or more components, that several of Halperin's wave functions do not describe a homogeneous liquid but a liquid in which the different components phase-separate [104]. For two components, the condition for a homogeneous state is simply that both the exponents m_1 and m_2, which describe the intra-component correlations, must be larger than n for the inter-component correlations. As an example, we may study the states $(3,3,1)$ and $(1,1,3)$, which would both be candidates for a possible two-component FQHE at $\nu = 1/2$ and which have indeed been investigated in the literature [105]. However, only the first one describes a homogeneous liquid, such that the second one may be discarded right from the beginning.

Furthermore, some of Halperin's wave functions, even if they satisfy the above-mentioned condition, turn out to be problematic if the interaction is SU(2) symmetric, such as for the true electron spin. In this case, one may show that (m,m,n) states are only eigenstates of the total-spin operator, which commutes with the interaction Hamiltonian, if $n = m$ (i.e. in the ferromagnetic state) or if $n = m - 1$ [1]. This restriction may be omitted though in bilayer quantum Hall systems or in wide quantum wells where the interaction Hamiltonian is not pseudo-spin SU(2)-symmetric.

Physical relevance of Halperin states
Halperin 态的物理对应

A physically relevant Halperin state is e.g. the unpolarised $(3,3,2)$ state which would occur at a filling factor $\nu = 2/5$. Remember from the discussion of CF theory in Sec. 4.4 that there is also a (naturally polarised) CF candidate, with $p = 2$ completely filled CF LLs, to describe the ground state at this filling factor. Which of them is now the better one? This question could be answered within exact-diagonalisation calculations, which showed that, in the absence of a Zeeman effect, the true ground state is described in terms of the unpolarised Halperin wave function $(3,3,2)$ [106]. Notice, however, that the energy difference between the two states is extremely small, as may be seen from variational calculations [76], such that the polarised CF state becomes the ground state above a critical value of the energy Δ_Z associated with the Zeeman effect. This critical value would therefore describe a phase transition between an unpolarised and a fully polarised FQHE state. Such transitions have indeed been observed in polarisation experiments, where the strength of the Zeeman effect was varied by a simultaneous change in the magnetic field and in the electronic density [107, 108].

5.3.2 Generalised Halperin wave functions
Halperin 波函数的推广

We would finally mention that Halperin's wave function may easily be generalised to describe possible FQHE states in systems with a larger number of components, such as the four spin-valley components in graphene. This generalised wave function for K-component quantum Hall systems may be written as a product

$$\psi^{SU(K)}_{m_1,...,m_K;n_{ij}}\left(\left\{z^{(1)}_{j_1}, z^{(2)}_{j_2}, ..., z^{(K)}_{j_K}\right\}\right) = \psi^{L}_{m_1,...,m_K} \times \psi^{inter}_{n_{ij}} \tag{5.16}$$

of a product of Laughlin wave functions

$$\psi^{L}_{m_1,...,m_K} = \prod_{j=1}^{K}\prod_{k_j<l_j}\left(z^{(j)}_{k_j} - z^{(j)}_{l_j}\right)^{m_j}$$

for each of the components and a term

$$\psi^{inter}_{n_{ij}} = \prod_{i<j}^{K}\prod_{k_i}^{N_i}\prod_{k_j}^{N_j}\left(z^{(i)}_{k_i} - z^{(j)}_{k_j}\right)^{n_{ij}}$$

that takes into account the correlations between particles in different components [109]. Here, the indices i and j denote the component, $i, j = 1, ..., K$, and $z^{(i)}_{k_i}$ is the complex position of the k_i-th particle in the component i.

Although the wave function (5.16) may seem scary at the first sight, it is as easily manipulated as Halperin's original wave function (5.8). The component filling factors $\nu_j = N_j/N_B$ may be determined, in the same manner as in the two-component case (5.11), with the help of the "exponent matrix" $\mathcal{M}$ the off-diagonal terms of which are the exponents $(\mathcal{M})_{ij} = n_{ij}$ (for $i \neq j$), whereas the diagonal terms are simply the exponents corresponding to the intra-component correlations, $(\mathcal{M})_{ii} = m_i$. The zero-counting argument yields the matrix equation

$$\begin{pmatrix} 1 \\ \vdots \\ 1 \end{pmatrix} = \mathcal{M}\begin{pmatrix} \nu_1 \\ \vdots \\ \nu_K \end{pmatrix} \tag{5.17}$$

relating the component filling factors to the exponents, and if $\mathcal{M}$ is invertible, all component filling factors are fixed by the inverse equation

$$\begin{pmatrix} \nu_1 \\ \vdots \\ \nu_K \end{pmatrix} = \mathcal{M}^{-1}\begin{pmatrix} 1 \\ \vdots \\ 1 \end{pmatrix}. \tag{5.18}$$

If the determinant $\det(\mathcal{M})$ is zero and the matrix thus not invertible, not all component filling factors can be determined. In analogy with the two-component case this hints at underlying ferromagnetic states. A perfect SU(K) ferromagnetic state is obtained when all components are equal odd integers, $m_i = n_{ij} = m$, in which case one obtains again a simple (fully anti-symmetric) Laughlin wave function for all particles regardless of to which component they belong. For $K = 4$ and $m = 1$, this is just the SU(4) ferromagnetic state at $\nu = 1$ which we have already discussed in the context of the quantum Hall effect at $\nu_G = \pm 1$ in graphene (Sec. 5.2.3).

Notice, however, that contrary to a two-component system, where one only needs to distinguish between an invertible and a non-invertible matrix, the situation is much richer for $K > 2$. One may indeed have different "degrees" of invertibility that are described by the *rank* of the matrix. Consider, e.g., the fully anti-symmetric wave function with $m_i = n_{ij} = m$. In this case, Eq. (5.17) actually consists only of one single equation relating the component filling factors, i.e. $1 = m(\nu_1 + ... + \nu_K) = m\nu$, and all other lines of the matrix equation are simply copies of the first one. The rank of this matrix is 1, i.e. only the total filling factor is fixed, $\nu = 1/m$ [SU(K) ferromagnet] whereas in the case of an invertible matrix the rank is K and the K lines in the matrix equation (5.17) represent (linearly) independent equations. If the rank of an exponent matrix is smaller than K but larger than 1, the resulting state is neither a full SU(K) ferromagnet

nor a state with completely fixed component filling factors (or polarisations) – it is rather a state with some intermediate ferromagnetic properties.

As for two-component Halperin wave functions (5.8), a generalisation of Laughlin's plasma analogy allows one to distinguish between physical (i.e. homogeneous) and unphysical states (which show a phase separation of at least some of the components). Indeed, the exponent matrix $\mathcal{M}$ must have only positive eigenvalues in order to describe a homogeneous state [104]. We finally mention that $\mathcal{M}$ encodes not only information concerning the filling factors (5.18), but fully describes the quantum Hall state (5.16), such as its topological degeneracy, the charges of its quasi-particle excitations as well as the statistical properties of the latter [110].

Appendix A

Electronic Band Structure of Graphene
石墨烯的电子能带结构

本节附录中我们用紧束缚近似计算石墨烯的能带 [111]，而结果我们已经在第1.2.3节呈现了。因为石墨烯的蜂巢晶格结构包含两种不同的子格子 A 和 B，电子波函数

$$\psi_{\mathbf{k}}(\mathbf{r}) = a_{\mathbf{k}}\psi_{\mathbf{k}}^{(A)}(\mathbf{r}) + b_{\mathbf{k}}\psi_{\mathbf{k}}^{(B)}(\mathbf{r}), \tag{A.1}$$

因此是 A 和 B 两种波函数波函数的叠加态，其中 $a_{\mathbf{k}}$，$b_{\mathbf{k}}$，是准动量 $\mathbf{k}$ 的复函数。$\psi_{\mathbf{k}}^{(A)}(\mathbf{r})$ 和 $\psi_{\mathbf{k}}^{(B)}(\mathbf{r})$ 都是 Bloch 函数

$$\psi_{\mathbf{k}}^{(j)}(\mathbf{r}) = \sum_{\mathbf{R}_l} e^{i\mathbf{k}\cdot\mathbf{R}_l}\phi^{(j)}(\mathbf{r}+\boldsymbol{\delta}_j-\mathbf{R}_l), \tag{A.2}$$

其中，原子波函数 $\phi^{(j)}(\mathbf{r}+\boldsymbol{\delta}_j-\mathbf{R}_l)$ 是中心位置在 $\mathbf{R}_l-\boldsymbol{\delta}_j$ 的函数，而 $\boldsymbol{\delta}_j$ 是格点 $\mathbf{R}_l$ 处 Bravais 格子中第 j 个原子的相对位置。通常来说，选取两个子格子中的一个，比如 A，作为 Bravais 晶格的原点，即 $\boldsymbol{\delta}_A = 0$。

有了这些波函数，我们可以来找 Schrödinger 方程

$$H\psi_{\mathbf{k}} = \epsilon_{\mathbf{k}}\psi_{\mathbf{k}},$$

的解，其中 H 是晶格上的电子的完整的 Hamiltonian，就是第2.1节中 (2.2) 那种。这里，我们不必选择在实空间中表示出来[1]。在 Schrödinger 方程上左乘 $\psi_{\mathbf{k}}^*$，得到 $\psi_{\mathbf{k}}^* H\psi_{\mathbf{k}} = \epsilon_{\mathbf{k}}\psi_{\mathbf{k}}^*\psi_{\mathbf{k}}$，利用 (A.1) 和 (A.2) 可以重写成

$$(a_{\mathbf{k}}^*, b_{\mathbf{k}}^*)\,\mathcal{H}_{\mathbf{k}}\begin{pmatrix} a_{\mathbf{k}} \\ b_{\mathbf{k}}\end{pmatrix} = \epsilon_{\mathbf{k}}\,(a_{\mathbf{k}}^*, b_{\mathbf{k}}^*)\,\mathcal{S}_{\mathbf{k}}\begin{pmatrix} a_{\mathbf{k}} \\ b_{\mathbf{k}}\end{pmatrix}. \tag{A.3}$$

Hamiltonian 的矩阵形式可以定义为

$$\mathcal{H}_{\mathbf{k}} \equiv \begin{pmatrix} \psi_{\mathbf{k}}^{(A)*}H\psi_{\mathbf{k}}^{(A)} & \psi_{\mathbf{k}}^{(A)*}H\psi_{\mathbf{k}}^{(B)} \\ \psi_{\mathbf{k}}^{(B)*}H\psi_{\mathbf{k}}^{(A)} & \psi_{\mathbf{k}}^{(B)*}H\psi_{\mathbf{k}}^{(B)}\end{pmatrix} = \mathcal{H}_{\mathbf{k}}^\dagger, \tag{A.4}$$

而交叠矩阵

$$\mathcal{S}_{\mathbf{k}} \equiv \begin{pmatrix} \psi_{\mathbf{k}}^{(A)*}\psi_{\mathbf{k}}^{(A)} & \psi_{\mathbf{k}}^{(A)*}\psi_{\mathbf{k}}^{(B)} \\ \psi_{\mathbf{k}}^{(B)*}\psi_{\mathbf{k}}^{(A)} & \psi_{\mathbf{k}}^{(B)*}\psi_{\mathbf{k}}^{(B)}\end{pmatrix} = \mathcal{S}_{\mathbf{k}}^\dagger \tag{A.5}$$

来描述使用的波函数的非正交性。可以从久期方程 Schrödinger 的本征值 $\epsilon_{\mathbf{k}}$ 得到能带：

$$\det\left[\mathcal{H}_{\mathbf{k}} - \epsilon_{\mathbf{k}}^{\lambda}\mathcal{S}_{\mathbf{k}}\right] = 0, \tag{A.6}$$

它需要有一个非零波函数的解，即 $a_{\mathbf{k}} \neq 0$ 且 $b_{\mathbf{k}} \neq 0$。λ 表示第几条能带，考虑到有与久期方程 (A.6) 的解一样多条能带，即，一个晶胞两个原子两条能带。

[1] 波函数 $\psi_{\mathbf{k}}(\mathbf{r})$ 是 Hilbert 矢量 $\psi_{\mathbf{k}}$ 的实空间表示

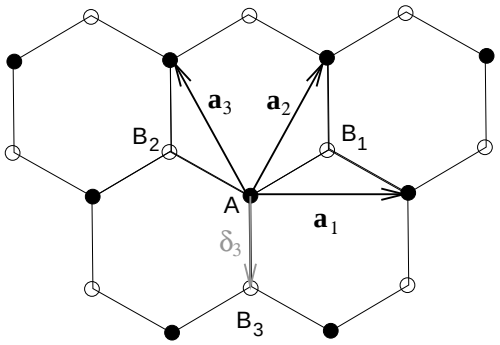

图 A.1: 蜂巢晶格的紧束缚模型。

接下来，我们忽略近邻格点的波函数交叠，因此交叠矩阵 (A.5)，考虑到对波函数的归一化，可以写成 $\mathbb{1}$ 乘以粒子数 N。久期方程告诉我们其实能带就是 Hamiltonian 矩阵 (A.4) 的本征值。不仅如此，由于两个子格子从化学角度来讲是完全一样的，我们实际上有 $\psi_{\mathbf{k}}^{(A)*} H \psi_{\mathbf{k}}^{(A)} = \psi_{\mathbf{k}}^{(B)*} H \psi_{\mathbf{k}}^{(B)}$，且对角元相当于只对能带贡献一个常数，我们可以取为 0。因此，(A.4) 式中唯一有用的项就是非对角项 $\mathcal{H}_{\mathbf{k}}^{AB} \equiv \psi_{\mathbf{k}}^{(A)*} H \psi_{\mathbf{k}}^{(B)} = N t_{\mathbf{k}}^{AB}$，其中*hopping 项*为

$$t_{\mathbf{k}}^{AB} \equiv \sum_{\mathbf{R}_l} e^{i\mathbf{k}\cdot\mathbf{R}_l} \int d^2 r \, \phi^{(A)*}(\mathbf{r} - \mathbf{R}_k) H \phi^B(\mathbf{r} + \boldsymbol{\delta}_{AB} - \mathbf{R}_m) \, , \tag{A.7}$$

而 $\boldsymbol{\delta}_{AB}$ 是连接 A 格点和 B 格点的矢量。

只考虑最近邻格点就足够得到石墨烯的能带结构了，因此其*hopping 强度*可以写为

$$t \equiv \int d^2 r \, \phi^{A*}(\mathbf{r}) H \phi^B(\mathbf{r} + \boldsymbol{\delta}_3), \tag{A.8}$$

其中取 $\boldsymbol{\delta}_{AB} = \boldsymbol{\delta}_3$ (见图. A.1)，注意其实也可以考虑远距离的 hopping，比如次近邻，这样会产生一些对角项。然而我们知道 $t \sim 3$ eV，比次近邻的 hopping 强度强十倍 [21]，而且它只影响低能下石墨烯电子的一些渐进性质[†]。

如果我们考虑任意一个 A 型子格子上的点 A(图. A.1)，我们可以看到 hopping 项 (A.7) 包含三个最近邻 B_1，B_2 和 B_3，每个都有相同的 hopping 强度 t。然而，格点 B_3 与格点 A 用相同的格矢，只不过平移了 $\boldsymbol{\delta}_3$ 而已，因此在 hopping 矩阵上并没有相位差；而 B_1 和 B_2 则分别有

$$\mathbf{a}_2 = \frac{\sqrt{3}a}{2}(\mathbf{e}_x + \sqrt{3}\mathbf{e}_y) \qquad \text{和} \qquad \mathbf{a}_3 \equiv \mathbf{a}_2 - \mathbf{a}_1 = \frac{\sqrt{3}a}{2}(-\mathbf{e}_x + \sqrt{3}\mathbf{e}_y),$$

其中最近邻碳原子间距 $a = |\boldsymbol{\delta}_3| = 0.142$ nm。因此，它们分别有相位因子 $\exp(i\mathbf{k}\cdot\mathbf{a}_2)$ 和 $\exp(i\mathbf{k}\cdot\mathbf{a}_3)$，而 hopping 项 (A.7) 就可以写为

$$t_{\mathbf{k}}^{AB} = t\gamma_{\mathbf{k}}^* = \left(t_{\mathbf{k}}^{BA}\right)^* ,$$

其中，我们对最近邻进行了相位求和

$$\gamma_{\mathbf{k}} \equiv 1 + e^{i\mathbf{k}\cdot\mathbf{a}_2} + e^{i\mathbf{k}\cdot\mathbf{a}_3}. \tag{A.9}$$

现在能带的色散就可以通过解久期方程 (A.6) 很容易的得到了

$$\epsilon_\lambda(\mathbf{k}) = \lambda \left| t_{\mathbf{k}}^{AB} \right| = \lambda t \left| \gamma_{\mathbf{k}} \right| , \tag{A.10}$$

如图. 2.2所示。能带色散显然是粒子-空穴对称的，而且价带 ($\lambda = -$) 与导带 ($\lambda = +$) 在两个点接触：

$$\pm\mathbf{K} = \pm\frac{4\pi}{3\sqrt{3}a}\mathbf{e}_x \, ,$$

其具体位置是通过 $\gamma_{\pm\mathbf{K}} = 0$ 来得到的，恰好与 BZ 的两个角 K 和 K' 一致。在第2.1节中我们讲过，未掺杂的石墨烯的能带结构是半满的，因此费米能恰好处在 K，K' 这些点上。

[†]译者注：会打开能隙，但是很小

Continuum Limit
连续极限

低能电子的特性可以通过在 K 和 K' 这样的点附近把能带中的相位因子 (A.9) 展开而得到

$$\begin{aligned}\gamma_{\mathbf{p}}^{\pm} \equiv \gamma_{\mathbf{k}=\pm\mathbf{K}+\mathbf{p}} &= 1 + e^{\pm i\mathbf{K}\cdot\mathbf{a}_2} e^{i\mathbf{p}\cdot\mathbf{a}_2} + e^{\pm i\mathbf{K}\cdot\mathbf{a}_3} e^{i\mathbf{p}\cdot\mathbf{a}_3} \\ &\simeq 1 + e^{\pm i2\pi/3}\left[1 + i\mathbf{p}\cdot\mathbf{a}_2\right] + e^{\mp i2\pi/3}\left[1 + i\mathbf{p}\cdot\mathbf{a}_3\right] \\ &= \gamma_{\mathbf{p}}^{\pm(0)} + \gamma_{\mathbf{p}}^{\pm(1)}\end{aligned}$$

根据 Dirac 点的定义和其处于第一 BZ 的角上 K 和 K' 处，我们有 $\gamma_{\mathbf{p}}^{\pm(0)} = \gamma_{\pm\mathbf{K}} = 0$。做 $|\mathbf{p}|a$ 为小量的一级展开；方便起见，假定 $\hbar = 1$，从而动量和波矢有相同的量纲。

一阶展开为

$$\begin{aligned}\gamma_{\mathbf{p}}^{\pm(1)} &= i\frac{\sqrt{3}a}{2}\left[(p_x + \sqrt{3}p_y)e^{\pm i2\pi/3} + (-p_x + \sqrt{3}p_y)e^{\mp i2\pi/3}\right] \\ &= \mp\frac{3a}{2}(p_x \pm ip_y),\end{aligned} \tag{A.11}$$

其中利用了 $\sin(\pm 2\pi/3) = \pm\sqrt{3}/2$，和 $\cos(\pm 2\pi/3) = -1/2$。这导致了有效低能 Hamiltonian

$$H_{\mathbf{p}}^{\xi} = \xi v(p_x\sigma^x + \xi p_y\sigma^y), \tag{A.12}$$

其中费米速度

$$v \equiv \frac{3ta}{2\hbar}\ . \tag{A.13}$$

其中 $\xi = \pm$ 指的是 K 和 K' 的区分；K 点的 Dirac Hamiltonian 可以通过 (2.4) 得到

$$H_D = v\mathbf{p}\cdot\boldsymbol{\sigma}\,, \tag{A.14}$$

而 K' 点的低能 Hamiltonian 为

$$H_D' = -v\mathbf{p}\cdot\boldsymbol{\sigma}^*\,, \tag{A.15}$$

而其中 $\boldsymbol{\sigma}^* = (\sigma^x, -\sigma^y)$。两种 Hamiltonian 都给出相同的能谱，因此是二重谷简并的。

注意到，如果为了避免 (A.15) 中 Hamiltonian 的共轭，可以通过交换 A 和 B 子格子，而在 K ($\xi = +$) 和 K' ($\xi = -$) 两个谷的时候 Hamiltonian 可以写成这种简略的形式

$$H_D^{\xi} = \xi H_D = \xi v\mathbf{p}\cdot\boldsymbol{\sigma}\,. \tag{A.16}$$

Appendix B

Landau Levels of Massive Dirac Particles
有质量的 Dirac 粒子的 Landau 能级

Mass Confinement of Dirac Fermions at $B = 0$
Dirac 费米子在 $B = 0$ 下的质量限制

即使不存在磁场的时候，石墨烯中对电子的约束也是很微妙的，因为构造一个简单的 $V_{\text{conf}} = V(y)\mathbb{1}$ 这样的束缚势能是不能束缚 Dirac 电子的。这是由于叫*Klein 悖论*的相对论性效应导致的，即一个 (无质量的) 相对论性粒子可以穿透势垒而不产生背向散射 [112]。这种效应可以这么理解：考虑入射的电子处于 $V = 0$ 状态，而电子的能量比费米能稍微高一点。在势垒处，Dirac 点被提高到了很高的能量，而这里的 Fermi 能处于价带。This effect may be understood in the following manner: consider an incident electron in the region with $V = 0$ the energy of which is slightly above the Fermi energy. In the potential barrier, the Dirac point is shifted to a higher energy that corresponds to the barrier height and the Fermi energy lies now in the valence band, where the electron may still find a quantum state (with the same wave-vector direction and the same velocity v) – instead of moving as an electron in the conduction band, it thus simply moves in the same direction as an electron in the valence band [图. B.1(a)]. This is in stark contrast with quantum mechanical tunneling of a non-relativistic particle, for which the transmission probability through a potential barrier is exponentially suppressed because of a lacking quantum state at the same energy as that of the incident electron.

The problem is circumvented by a so-called *mass confinement*

$$V_{\text{conf}} = V(y)\,\sigma^z = \begin{pmatrix} V(y) & 0 \\ 0 & -V(y) \end{pmatrix}, \tag{B.1}$$

and we discuss first the simpler case of a constant mass term $M\sigma^z$ that needs to be added to the Dirac Hamiltonian. That this term yields indeed a mass may be seen from the Dirac Hamiltonian at $B = 0$

$$H_D^m = v\mathbf{p}\cdot\boldsymbol{\sigma} + M\sigma^z = \begin{pmatrix} M & v(p_x - ip_y) \\ v(p_x + ip_y) & -M \end{pmatrix}, \tag{B.2}$$

the diagonalisation of which yields the energy spectrum

$$\epsilon_\lambda(\mathbf{p}) = \lambda\sqrt{v^2|\mathbf{p}|^2 + M^2},$$

which is gapped at zero momentum. This is nothing other than the dispersion relation of a relativistic particle[1] with mass m such that $M = mv^2$. Qualitatively one may see from 图. B.1(b) why a mass confinement is more efficient than a potential barrier. Indeed, when the particle approaches the edge with $M(y) \neq 0$ a

[1] The sign $\lambda = -$ corresponds to the anti-particle.

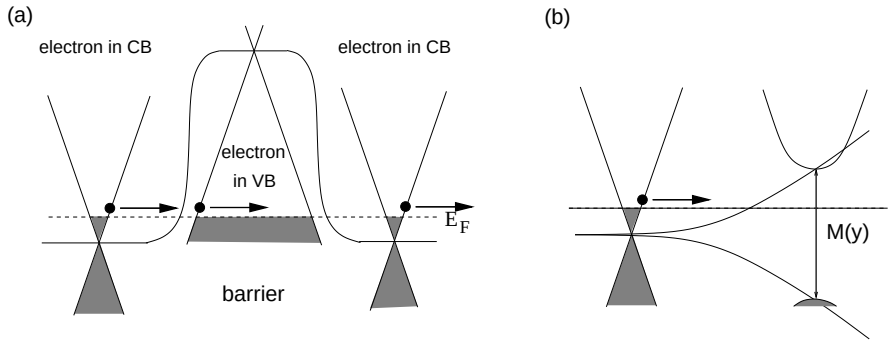

図 B.1: *(a)* Klein tunneling through a barrier. An incident electron in the conduction band (CB) above the Fermi energy, which is at the Dirac point before the barrier, transverses the barrier as en electron above the Fermi energy in the valence band (VB). The valence band is partially emptied because the Dirac point has shifted to a higher energy corresponding to the barrier height. *(b)* Mass confinement. A gap opens when the particle approaches the edge, which becomes a forbidden region where no quantum state can be found at the energy corresponding to that of the incident electron.

gap opens. An electron slightly above the Dirac point may then only propagate in the region with $M = 0$, whereas at the edge its energy lies in the gap which is a forbidden region, and the electron is thus confined.

Similarly to the $B = 0$ case, one may find the energy spectrum of the massive Dirac Hamiltonian (B.2) in a perpendicular magnetic field, which reads, in terms of the ladder operators a and $a^\dagger$,

$$H_D^B = \begin{pmatrix} M & v(\Pi_x - i\Pi_y) \\ v(\Pi_x + i\Pi_y) & -M \end{pmatrix} = \begin{pmatrix} M & \sqrt{2}\frac{\hbar v}{l_B} a \\ \sqrt{2}\frac{\hbar v}{l_B} a^\dagger & -M \end{pmatrix}. \tag{B.3}$$

Its eigenvalues may be obtained in the same manner as in the $M = 0$ case (c.f. Sec. 2.3.2), and one obtains

$$\epsilon_{\lambda n} = \lambda \sqrt{M^2 + 2\frac{\hbar^2 v^2}{l_B^2} n} \tag{B.4}$$

for the massive relativistic LLs, $n \neq 0$.

Special care needs to be taken in the discussion of the central LL $n = 0$, which necessarily shifts away from zero energy. The associated quantum state (2.24) is zero in the first component u_0, whereas the second component is given by $v_0 = |0\rangle$. In order to satisfy the second line in the eigenvalue equation

$$H_D^B \psi_0 = \epsilon_0 \psi_0 \qquad \Leftrightarrow \qquad \begin{pmatrix} M & \sqrt{2}\frac{\hbar v}{l_B} a \\ \sqrt{2}\frac{\hbar v}{l_B} a^\dagger & -M \end{pmatrix} \begin{pmatrix} 0 \\ |0\rangle \end{pmatrix} = \epsilon_0 \begin{pmatrix} 0 \\ |0\rangle \end{pmatrix},$$

one needs to fulfil

$$\sqrt{2}\frac{\hbar v}{l_B}\, a^\dagger\, u_0 = (\epsilon_0 + M) v_0 \qquad \Leftrightarrow \qquad 0 = (\epsilon_0 + M)|0\rangle, \tag{B.5}$$

such that the only solution is $\epsilon_0 = -M$. The relativistic $n = 0$ LL is therefore shifted to negative energies and does no longer satisfy particle-hole symmetry. This effect is called *parity anomaly* and depends on the *sign of the mass*.

In the case of graphene, we need to remember that there are two copies of the energy spectrum, one at the K point and one at the K' point. As we have disussed in Appendix A, the Hamiltonian (B.3) describes the low-energy properties at the K point whereas we need to interchange the A and B sublattices at the K' point and add a global sign in front of the off-diagonal terms [see Eq. (A.16)],

$$H_D^{B\prime} = \begin{pmatrix} -M & -\sqrt{2}\frac{\hbar v}{l_B} a \\ -\sqrt{2}\frac{\hbar v}{l_B} a^\dagger & M \end{pmatrix} = -H_D^{B\prime}. \tag{B.6}$$

Naturally, the eigenstates of this Hamiltonian are the same as those of the Hamiltonian (B.3) at the K point, but the eigenvalues change their sign. Due to the particle-hole symmetry of the levels (B.4), the global sign does not affect the energy spectrum for $n \neq 0$. However, the $n = 0$ LL, which does not respect particle-hole symmetry, must again be treated apart, and one finds in the same manner as for the K point the condition corresponding to Eq. (B.5),

$$-\sqrt{2}\frac{\hbar v}{l_B}\, a^\dagger\, u_0 = (\epsilon_0 - M)v_0 \qquad \Leftrightarrow \qquad 0 = (\epsilon_0 - M)|0\rangle. \tag{B.7}$$

One notices that the $n = 0$ LL level at the K' point shifts to positive energies as a function of the mass, such that the overall level spectrum for graphene, when one takes into account *both* valleys, is again particle-hole symmetric, but the valley degeneracy is lifted for $n = 0$.

The case of a mass term that varies in the y-direction, such as for the mass confinement potential, may finally be treated in the same manner as we have discussed in Sec. 3.1.2: the system remains translation-invariant in the x-direction, such that the Landau gauge is the appropriate gauge and the wave vector k in this direction is a good quantum number. Because this wave vector determines the position of the eigenstate in the y-direction, $y_0 = kl_B^2$, the energy spectrum is given by the expression (3.21),

$$\epsilon_{\lambda n, y_0;\xi} = \lambda\sqrt{M^2(y_0) + 2\frac{\hbar^2 v^2}{l_B^2}n}, \tag{B.8}$$

for $n \neq 0$ and both valleys $\xi = \pm$, whereas the $n = 0$ LL is found at

$$\epsilon_{n=0, y_0;\xi} = -\xi M(y_0). \tag{B.9}$$

Bibliography

[1] Prange, R. and Girvin, E., S. M. (1990) *The Quantum Hall Effect*. Springer.

[2] Yoshioka, D. (2002) *The Quantum Hall Effect*. Springer.

[3] Ezawa, Z. F. (2000) *Quantum Hall Effects – Field Theoretical Approach and Related Topics*. World Scientific.

[4] Girvin, S. M. (1999) *The Quantum Hall Effect: Novel Excitations and Broken Symmetries,* in A. Comptet, T. Jolicoeur, S. Ouvry and F. David (Eds.) *Topological Aspects of Low-Dimensional Systems – École d'Éte de Physique Théorique LXIX*. Springer.

[5] Murthy, G. and Shankar, R. (2003) *Rev. Mod. Phys.*, **75**, 1101.

[6] Novoselov, K. S., Geim, A. K., Morosov, S. V., Jiang, D., Katsnelson, M. I., Grigorieva, I. V., Dubonos, S. V., and Firsov, A. A. (2005) *Nature*, **438**, 197.

[7] Zhang, Y., Tan, Y.-W., Stormer, H. L., and Kim, P. (2005) *Nature*, **438**, 201.

[8] Akkermans, E. and Montambaux, G. (2008) *Mesoscopic Physics of Electrons and Photons*. Cambridge UP.

[9] Shubnikov, L. W. and de Haas, W. J. (1930) *Proceedings of the Royal Netherlands Society of Arts and Science*, **33**, 130 and 163.

[10] v. Klitzing, K., Dorda, G., and Pepper, M. (1980) *Phys. Rev. Lett.*, **45**, 494.

[11] Poirier, W. and Schopfer, F. (2009) *Eur. Phys. J. Special Topics*, **172**, 207.

[12] Poirier, W. and Schopfer, F. (2009) *Int. J. Mod. Phys. B*, **23**, 2779.

[13] Tsui, D. C., Störmer, H., and Gossard, A. C. (1983) *Phys. Rev. Lett.*, **48**, 1559.

[14] Laughlin, R. B. (1983) *Phys. Rev. Lett.*, **50**, 1395.

[15] Jain, J. K. (1989) *Phys. Rev. Lett.*, **63**, 199.

[16] Jain, J. K. (1990) *Phys. Rev. B*, **41**, 7653.

[17] Willett, R. L., Eisenstein, J. P., Stormer, H. L., Tsui, D. C., Gossard, A. C., and English, J. H. (1987) *Phys. Rev. Lett.*, **59**, 1776.

[18] Moore, G. and Read, N. (1991) *Nucl. Phys. B*, **360**, 362.

[19] Greiter, M., Wen, X.-G., and Wilczek, F. (1991) *Phys. Rev. Lett.*, **66**, 3205.

[20] Pan, W., Stormer, H. L., Tsui, D. C., Pfeiffer, L. N., Baldwin, K. W., and West, K. W. (2003) *Phys. Rev. Lett.*, **90**, 016801.

[21] Castro Neto, A. H., Guinea, F., Peres, N. M. R., Novoselov, K. S., and Geim, A. K. (2009) *Rev. Mod. Phys.*, **81**, 109.

[22] Zhang, Y., Jiang, Z., Small, J. P., Purewal, M. S., Tan, Y.-W., Fazlollahi, M., Chudow, J. D., Jaszczak, J. A., Stormer, H. L., and Kim, P. (2006) *Phys. Rev. Lett.*, **98**, 197403.

[23] Du, X., Skachko, I., Duerr, F., Luican, A., and Andrei, E. Y. (2009) *Nature*, p. doi:10.1038/nature08522.

[24] Bolotin, K. I., Ghahari, F., Shulman, M. D., Stormer, H. L., and Kim, P. (2009) *preprint*, p. arXiv:0910.2763.

[25] Ashcroft, N. W. and Mermin, N. D. (1976) *Solid State Physics*. Harcourt.

[26] Kittel, C. (2005) *Introduction to Solid State Physics*. Wiley, 8th Ed.

[27] Jackson, J. D. (1999) *Classical Electrondynamics*. Wiley, 3rd ed.

[28] Cohen-Tannoudji, C., Diu, B., and Laloë, F. (1973) *Quantum Mechanics*. Hermann.

[29] McClure, J. W. (1956) *Phys. Rev.*, **104**, 666.

[30] Berger, C., Song, Z., Li, T., Ogbazghi, A. Y., Feng, R., Dai, Z., Marchenkov, A. N., Conrad, E. H., First, P. N., and de Heer, W. A. (2004) *J. Phys. Chem.*, **108**, 19912.

[31] Sadowski, M. L., Martinez, G., Potemski, M., Berger, C., and de Heer, W. A. (2006) *Phys. Rev. Lett.*, **97**, 266405.

[32] Jiang, Z., Henriksen, E. A., L. C. Tung, Y.-J. W., Schwartz, M. E., Han, M. Y., Kim, P., and Stormer, H. L. (2007) *Phys. Rev. Lett.*, **98**, 197403.

[33] Champel, T. and Florens, S. (2007) *Phys. Rev. B*, **75**, 245326.

[34] Abrahams, E., Anderson, P. W., Licciardello, D. C., and Ramakrishnan, T. V. (1979) *Phys. Rev. Lett.*, **42**, 673.

[35] Büttiker, M. (1992) *The Quantum Hall Effect in Open Conductors,* in M. Reed (Ed.) *Nanostructured Systems (Semiconductors and Semimetals,* **35**, 191*)*. Academic Press.

[36] Büttiker, M., Imry, Y., Landauer, R., and Pinhas, S. (1985) *Phys. Rev. B*, **31**, 6207.

[37] Datta, S. (1995) *Electronic Transport in Mesoscopic Systems*. Cambridge UP.

[38] Klaß, U., Dietsche, W., v. Klitzing, K., and Ploog, K. (1991) *Z. Phys. B:Cond. Matt.*, **82**, 351.

[39] Büttiker, M. (1988) *Phys. Rev. B*, **38**, 9375.

[40] Hashimoto, K., Sohrmann, C., Wiebe, J., Inaoka, T., Meier, F., Hirayama, Y., Römer, R. A., Wiesendanger, R., and Morgenstern, M. (2008) *Phys. Rev. Lett.*, **101**, 256802.

[41] Sondhi, S. L., Girvin, S. M., Carini, J. P., and Shahar, D. (1997) *Rev. Mod. Phys.*, **69**, 315.

[42] Sachdev, S. (1999) *Quantum Phase Transitions*. Cambridge UP.

[43] Wei, H. P., Tsui, D. C., Paalanen, M. A., and Pruisken, A. M. M. (1988) *Phys. Rev. Lett.*, **61**, 1294.

[44] Wei, H. P., Engel, L. W., and Tsui, D. C. (1994) *Phys. Rev. B*, **50**, 14609.

[45] Li, W., Csathy, A., Tsui, D. C., Pfeiffer, L. N., and West, K. W. (2005) *Phys. Rev. Lett.*, **94**, 206807.

[46] Li, W., Vicente, C. L., Xia, J. S., Pan, W., Tsui, D. C., Pfeiffer, L. N., and West, K. W. (2009) *Phys. Rev. Lett.*, **102**, 216801.

[47] Chalker, J. T. and Coddington, P. D. (1988) *J. Phys. C*, **21**, 2665.

[48] Huckestein, B. (1995) *Rev. Mod. Phys.*, **67**, 357.

[49] Huckestein, B. and Backhaus, M. (1999) *Phys. Rev. Lett.*, **82**, 5100.

[50] Slevin, K. and Ohtsuki, T. (2009) *Phys. Rev. B*, **80**, 041304.

[51] Brey, L. and Fertig, H. (2006) *Phys. Rev. B*, **73**, 195408.

[52] Mahan, G. D. (1993) *Many-Particle Physics*. Plenum Press, 2nd Ed.

[53] Giuliani, G. F. and Vignale, G. (2005) *Quantum Theory of Electron Liquids*. Cambridge UP.

[54] Kallin, C. and Halperin, B. I. (1984) *Phys. Rev. B*, **30**, 5655.

[55] Iyengar, A., Wang, J., Fertig, H. A., and Brey, L. (2007) *Phys. Rev. B*, **75**, 125430.

[56] Roldán, R., Fuchs, J.-N., and Goerbig, M. O. (2009) *Phys. Rev. B*, **80**, 085408.

[57] Wigner, E. (1934) *Phys. Rev.*, **102**, 46.

[58] Fukuyama, H., Platzman, P. M., and Anderson, P. W. (1979) *Phys. Rev. B*, **19**, 5211.

[59] Andrei, E. Y., Deville, G., Glattli, D. C., Williams, F. I. B., Paris, E., and Etienne, B. (1988) *Phys. Rev. Lett.*, **60**, 2765.

[60] Gervais, G., Engel, L. W., Stormer, H. L., Tsui, D. C., Baldwin, K. W., West, K. W., and Pfeiffer, L. N. (2004) *Phys. Rev. Lett.*, **93**, 266804.

[61] Cooper, N. R. (2008) *Advances in Physics*, **57**, 539.

[62] Haldane, F. D. M. (1983) *Phys. Rev. Lett.*, **51**, 605.

[63] Haldane, F. D. M. and Rezayi, E. H. (1985) *Phys. Rev. Lett.*, **54**, 237.

[64] Fano, G., Ortolani, F., and Colombo, E. (1986) *Phys. Rev. B*, **34**, 2670.

[65] Girvin, S. M., MacDonald, A. H., and Platzman, P. M. (1986) *Phys. Rev. B*, **33**, 2481.

[66] Tinkham, M. (2004) *Introduction to Superconductivity*. Dover Publications, 2nd Ed.

[67] Girvin, S. M. and Jach, T. (1984) *Phys. Rev. B*, **29**, 5617.

[68] de Picciotto, R., Reznikov, M., Heidblum, M., Umansky, V., Bunin, G., and Mahalu, D. (1997) *Nature*, **389**, 162.

[69] Saminadayar, L., Glattli, D. C., Jin, Y., and Etienne, B. (1997) *Phys. Rev. Lett.*, **79**, 2526.

[70] Nayak, C., Simon, S. H., Stern, A., Friedman, M., and Das Sarma, S. (2008) *Rev. Mod. Phys.*, **80**, 1083.

[71] Mermin, N. D. (1979) *Rev. Mod. Phys.*, **51**, 591.

[72] Haldane, F. D. M. (1991) *Phys. Rev. Lett.*, **67**, 937.

[73] Luhman, D. R., Pan, W., Tsui, D. C., Pfeiffer, L. N., Baldwin, K. W., and West, K. W. (2008) *Phys. Rev. Lett.*, **101**, 266804.

[74] Shabani, J., Gokmen, T., and Shayegan, M. (2009) *Phys. Rev. Lett.*, **103**, 046805.

[75] Halperin, B. I. (1984) *Phys. Rev. Lett.*, **52**, 1583.

[76] Jain, J. K. (2007) *Composite Fermions*. Cambridge UP.

[77] Lopez, A. and Fradkin, E. (1991) *Phys. Rev. B*, **44**, 5246.

[78] Halperin, B. I., Lee, P. A., and Read, N. (1993) *Phys. Rev. B*, **47**, 7312.

[79] Heinonen, E., O. (1998) *Composite Fermions*. World Scientific.

[80] Rezayi, E. H. and Read, N. (1994) *Phys. Rev. Lett.*, **72**, 100.

[81] Papić, Z., Möller, G., Milovanović, M., Regnault, N., and Goerbig, M. O. (2009) *Phys. Rev. B*, **79**, 245327.

[82] Wójs, A. and Quinn, J. J. (2000) *Philos. Mag. B*, **80**, 1405.

[83] Kitaev, A. Y. (2003) *Ann. Phys. (N.Y.)*, **303**, 2.

[84] Halperin, B. I. (1983) *Helv. Phys. Acta*, **56**, 75.

[85] Abolfath, M., Belkhir, L., and Nafari, N. (1997) *Phys. Rev. B*, **55**, 10643.

[86] Sondhi, S. L., Karlhede, A., Kivelson, S. A., and Rezayi, E. H. (1993) *Phys. Rev. B*, **47**, 16419.

[87] Moon, K., Mori, H., Yang, K., Girvin, S. M., MacDonald, A. H., Zheng, I., Yoshioka, D., and Zhang, S.-C. (1995) *Phys. Rev. B*, **51**, 5143.

[88] Fertig, H. A. (1989) *Phys. Rev. B*, **40**, 1087.

[89] Wen, X.-G. and Zee, A. (1992) *Phys. Rev. Lett*, **69**, 1811.

[90] Ezawa, Z. F. and Iwazaki, A. (1993) *Phys. Rev. B*, **47**, 7295.

[91] Spielman, I. B., Eisenstein, J. P., Pfeiffer, L. N., and West, K. W. (2000) *Phys. Rev. Lett.*, **84**, 5808.

[92] Kellogg, M., Eisenstein, J. P., and an K. W. West, L. N. P. (2004) *Phys. Rev. Lett.*, **036801**.

[93] Tutuc, E., Shayegan, M., and Huse, D. A. (2004) *Phys. Rev. Lett*, **93**, 036802.

[94] Nomura, K. and MacDonald, A. H. (2006) *Phys. Rev. Lett.*, **96**, 256602.

[95] Goerbig, M. O., Douçot, B., and Moessner, R. (2006) *Phys. Rev. B*, **74**, 161407.

[96] Alicea, J. and Fisher, M. P. A. (2006) *Phys. Rev. B*, **74**, 075422.

[97] Yang, K., Das Sarma, S., and MacDonald, A. H. (2006) *Phys. Rev. B*, **74**, 075423.

[98] Arovas, D. P., Karlhede, A., and Lilliehöök, D. (1999) *Phys. Rev. B*, **59**, 13147.

[99] Douçot, B., Goerbig, M. O., Lederer, P., and Moessner, R. (2008) *Phys. Rev. B*, **78**, 195327.

[100] Gusynin, V. P., Miransky, V. A., Sharapov, S. G., and Shovkovy, I. A. (2006) *Phys. Rev. B*, **74**, 195429.

[101] Fuchs, J.-N. and Lederer, P. (2007) *Phys. Rev. Lett.*, **98**, 016803.

[102] Herbut, I. F. (2007) *Phys. Rev. B*, **75**, 165411.

[103] Ezawa, Z. F. (1999) *Phys. Rev. Lett.*, **82**, 3512.

[104] de Gail, R., Regnault, N., and Goerbig, M. O. (2008) *Phys. Rev. B*, **77**, 165310.

[105] MacDonald, A. H., Yoshioka, D., and Girvin, S. M. (1989) *Phys. Rev. B*, **39**, 8044.

[106] Chakraborty, T. and Zhang, F. C. (1984) *Phys. Rev. B*, **29**, 7032.

[107] Kang, W., Young, J. B., Hannahs, S. T., Palm, E., Campman, K. L., and Gossard, A. C. (1997) *Phys. Rev. B*, **56**, R12776.

[108] Kukushkin, I. K., v. Klitzing, K., and Eberl, K. (1999) *Phys. Rev. Lett.*, **82**, 3665.

[109] Goerbig, M. O. and Regnault, N. (2007) *Phys. Rev. B*, **75**, 241405.

[110] Wen, X.-G. and Zee, A. (1992) *Phys. Rev. B*, **46**, 2290.

[111] Wallace, P. R. (1947) *Phys. Rev.*, **71**, 622.

[112] Klein, O. (1929) *Z. Phys.*, **53**, 157.